13:59:13 OCA PAD AMENDMENT - PROJECT HEADER INFORMATION 05/01/92

Active

Project #: E-21-H03 Cost share #: Rev #: 1
Center # : 10/24-6-R7391-0A0 Center shr #: OCA file #:
Work type : RES
Contract#: STD AGREEMENT DATED 12/19/91 Mod #: 1 Document : AGR
Prime #: Contract entity: GTRC

Subprojects ? : N CFDA: N/A
Main project #: PE #: N/A

Project unit: ELEC ENGR Unit code: 02.010.118
Project director(s):
STUBER G L ELEC ENGR (404)894-2923

Sponsor/division names: BELLSOUTH ENTERPRISES /
Sponsor/division codes: 251 / 004

Award period: 920101 to 920630 (performance) 920630 (reports)

Sponsor amount	New this change	Total to date
Contract value	(66,802.00)	74,258.00
Funded	(66,802.00)	74,258.00
Cost sharing amount		0.00

Does subcontracting plan apply ?: N

Title: PERSONAL AND MOBILE COMMUNICATIONS

PROJECT ADMINISTRATION DATA

OCA contact: Ina R. Lashley 894-4820

Sponsor technical contact

(000)000-0000

Sponsor issuing office

MR NEALE C. HIGHTOWER
(404)249-4510

BELLSOUTH ENTERPRISES, INC.
1100 PEACHTREE STREET, N.E.,
SUITE 8F08
ATLANTA, GA 30309

Security class (U,C,S,TS) : U ONR resident rep. is ACO (Y/N): N
Defense priority rating : N/A N/A supplemental sheet
Equipment title vests with: Sponsor GIT
NONE PROPOSED.
Administrative comments -
AMENDMENT 1 DECREASES TOTAL ESTIMATED COST BY $66,802 AND PERIOD OF PERFORMANCE BY SIX MONTHS.

GEORGIA INSTITUTE OF TECHNOLOGY
OFFICE OF CONTRACT ADMINISTRATION

NOTICE OF PROJECT CLOSEOUT

Closeout Notice Date 08/26/92

Project No. E-21-H03_____ Center No. 10/24-6-R7391-0A0_

Project Director STUBER G L_____ School/Lab ELEC ENGR_____

Sponsor BELLSOUTH ENTERPRISES/_____

Contract/Grant No. STD AGREEMENT DATED 12/19/91__ Contract Entity GTRC

Prime Contract No. _____

Title PERSONAL AND MOBILE COMMUNICATIONS_____

Effective Completion Date 920630 (Performance) 920630 (Reports)

Closeout Actions Required:	Y/N	Date Submitted
Final Invoice or Copy of Final Invoice	Y	_____
Final Report of Inventions and/or Subcontracts	N	_____
Government Property Inventory & Related Certificate	N	_____
Classified Material Certificate	N	_____
Release and Assignment	N	_____
Other _____	N	_____

Comments_____

_____

Subproject Under Main Project No. _____

Continues Project No. _____

Distribution Required:

Project Director	Y
Administrative Network Representative	Y
GTRI Accounting/Grants and Contracts	Y
Procurement/Supply Services	Y
Research Property Managment	Y
Research Security Services	N
Reports Coordinator (OCA)	Y
GTRC	Y
Project File	Y
Other _____	N
_____	N

PERSONAL AND MOBILE COMMUNICATIONS

Final Report for
OCA Project No. E21-H03

Prepared for
BellSouth Enterprises, Inc.

prepared by

Gordon L. Stüber

School of Electrical Engineering
Georgia Institute of Technology
Atlanta, Georgia 30332

Sponsor Technical Contact

Melvin Frerking

BellSouth Enterprises, Inc.
1100 Peachtree Street, NE
Atlanta, Georgia 30309

June 1992

Acknowledgement

This research contained in this report was completed with the assistance of the following Ph.D. students. These Ph.D. students have been pursuing their degrees with funding from BellSouth Enterprises through June 30, 1992.

1. Kevin West
2. Mark Austin
3. Ming-Ju Ho
4. Ramzi Barghouthi

Abstract

The report addresses three main issues associated with personal and mobile communication systems. The first is radio resource allocation in microcellular networks that involves microcellular teletraffic modeling and dynamic channel allocation algorithms. In this report, new vehicular teletraffic model is developed for urban microcellular environments. Simulation results are also provided that compares fixed channel allocation with dynamic resource allocation for an active-dormant teletraffic model.

The second issue in the report is the characterization of co-channel interference in a microcellular environment. This report extends current literature by providing a new exact analytical method for estimating co-channel interference with shadowed Rician or Rayleigh or Nakagami faded interferers. Applications to the analysis of signal strength based microcellular hand-off algorithms is suggested.

The final issue in the report is the acquisition of pseudo-noise spreading sequences that are used in direct-sequence CDMA cellular systems. A tutorial section with some new results is included on the algebraic properties of Gold and Kasami sequences. A soft-decision based sequence acquisition scheme is proposed and analyzed for direct-sequence CDMA systems employing the small set of Kasami sequences.

Contents

List of Figures

List of Tables

1 Introduction

This report contains four sections that address three basic issues associated with personal and mobile telephone systems. These are i) radio resource management in microcellular systems, ii) characterization of co-channel interference in microcellular systems with hand-off applications, and iii) receiver sequence synchronization in direct-sequence CDMA systems. A further introduction of each of these topics is as follows.

Section 2 of this report is concerned with the issue of radio resource management in microcellular systems. The study of radio resource management requires two items: development of microcellular teletraffic models, and the specification of dynamic channel allocation strategies. A *new vehicular teletraffic model*, called the eight-zone model, is developed in this report that is particularly useful for studying radio resource management in urban microcellular environments. The model accounts for the dependency of vehicular teletraffic on traffic signals, average vehicle velocities, multiple traffic lanes, and vehicular flow. Several existing dynamic channel allocation strategies are reviewed. A sample simulation is provided that compares the performance of dynamic resource allocation and fixed channel assignment for an active-dormant teletraffic model. Future work is recommended that will compare the performance of existing dynamic channel allocation strategies by using our new eight-zone teletraffic model. These simulation studies can be performed very efficiently on a MasPar MP1 massively parallel processing machine that is presently available at Georgia Tech.

Section 3 of this report is concerned with the characterization of co-channel interference in a microcellular environment. Current literature on co-channel interference in microcells either limits the analysis to the case where the signals are affected by fading only (no shadowing), or makes the unrealistic assumption of coherently adding interferers. This report reviews this literature and extends current theory by presenting a *new exact analytical method for estimating co-channel interference* for shadowed Rician or Rayleigh or Nakagami faded interferers. It is concluded that

the Rice factor of the desired signal significantly effects the probability of co-channel interference; the Rice factors of the interferers have little effect, and for simplifying purposes the interferers can be safely assumed to be Rayleigh faded. Future research on the application of the co-channel interference methods developed in this report to the evaluation of carrier-to-interference ratio or signal strength based microcellular hand-off algorithms is recommended.

Section 4 is a tutorial chapter on the algebraic properties of pseudo-noise sequences for CDMA mobile communication systems. Motivated by the problem of sequence acquisition in spread spectrum receivers, the algebraic properties of Gold and Kasami sequences are studied. In particular, large sets of codewords with the minimum possible Hamming weight that are orthogonal to a set of Gold or Kasami sequences are to be characterized. *New insights on the structure of the codes are presented.* The number of codewords of weights 5 and 6 in the double-error-correcting BCH codes are also found for the first time in this report.

Estimation of the phase of a spreading sequence represents a major task for a spread-spectrum receiver. This process is called sequence acquisition. In Section 5, a *soft-decision based sequence acquisition* scheme is proposed and analyzed for direct-sequence CDMA systems employing Kasami sequences. The algebraic properties of Kasami sequences are exploited to provide a very reliable estimate of the PN phase before tracking is attempted. This estimate is obtained by generating and combining multiple estimates of each PN chip in the linear feedback shift register of the receiver. The proposed technique is effective for PN sequences having very long periods.

2 Radio Resource Allocation for Microcellular Networks

2.1 Introduction

Dense urban areas are characterized by large numbers of people. Some of these people may use wireline telephones, while others may rely on wireless links to provide telephone service. Each person that uses a wireless link occupies a portion of the available bandwidth resources for some amount of time. Unfortunately, the available spectrum is a limited resource. Once all of the available spectrum is allocated to users, additional users cannot be accommodated. This results in the undesirable effect of blocking new requests for a link.

Suppose that the available spectrum is divided into channels. A channel could be a frequency slot, as in frequency division multiple access (FDMA), or a time slot, as in time division multiple access (TDMA). The co-channel reuse factor, D/R, requires that two cells which are within a certain distance D of each other (relative to the radius of the cells R) cannot use the same channel simultaneously. New call arrivals within a cell and calls that are "handed-off" from another cell when a mobile crosses a cell boundary both require the acquisition of a new channel. The channels are a resource which must be used as efficiently as possible; therefore, FDMA and TDMA schemes require a channel allocation strategy. A good strategy attempts to optimize the performance based on some criterion such as probability of new call blocking, hand-off failure, or total capacity.

In order to evaluate the performance of any particular channel allocation algorithm, a suitable teletraffic model must be used. Different environments (such as large macrocells, highway microcells, or urban microcells) have different characteristic vehicular traffic flows, and therefore require different models. Of these three environments, the urban microcellular is the most difficult environment in which to allocate channels efficiently, because of the uneven and time-varying distribution of teletraffic.

In this report, it is important to realize the distinction between *vehicular traffic* and *vehicular teletraffic*. Vehicular traffic is the arrangement of vehicles (cars, busses, etc.) as a function of space and time. It does not depend on the calls being placed or received, nor the strategies being used to allocate channels. Vehicular teletraffic refers to the distribution of active calls, the rate at which they occur, and the rate at which they require hand-offs. Obviously, teletraffic depends greatly on vehicular traffic. If a large number of vehicles are in a particular area, there are likely to be a large number call arrivals and hand-offs in that area.

The remainder of this section is as follows. Section 2.2 discusses the microcellular environment and teletraffic models. One teletraffic model is the active-dormant model suggested by Nanda and Goodman [3]. A new model called the *eight-zone model* is presented that provides a much better characterization of vehicular teletraffic. Several dynamic channel allocation strategies are suggested in Section 2.3. A sample simulation is provided in Section 2.4 that compares the dynamic resource allocation and fixed channel allocation methods.

2.2 The Microcellular Environment

In a macrocellular system, the cells are large and contain a roughly constant number of users. The number of users may vary throughout the day, but the short-term variations in traffic are small relative to the average traffic. This is because a large cell tends to average out local variations in traffic density. Consequently, the call arrival rate in each cell may be modeled as being constant. Teletraffic can be modeled as a Markov process with reasonable accuracy, that is, call arrivals, completions, and hand-off attempts can be modeled as having exponentially distributed interarrival times.

In dense urban areas, capacity may be a problem because of the large number of users. Consequently, the service may be poor, and the actual traffic may be well below the offered traffic. If the cells are made smaller, there is a corresponding increase in capacity. This is due to the fact that smaller cells contain fewer potential users. This means that there are more available channels per user, and the performance increases,

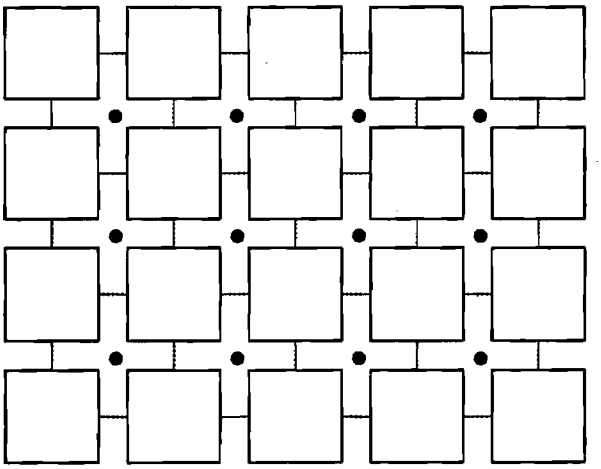

Figure 2.1: Possible arrangement of urban microcells

since the probability of new call blocking or a hand-off failure is reduced. However, when cells are reduced, the short-term variations in traffic are no longer small relative to the average traffic. The number of mobiles in a cell may vary greatly with time. Furthermore, the rate of flow of vehicles into or out of each cell may vary greatly, due to vehicle interactions, jamming, and traffic signals, all of which are characteristic of an urban environment. The call arrival rate for small cells is therefore time-varying.

Cell model Many different types of arrangements are possible for the cell boundaries and base-station locations with respect to the streets and buildings. One possible arrangement has a base station located at the center of each intersection, as illustrated in fig. 2.1.

Propagation model In an urban microcellular environment in which the base-stations are at street-lamp heights, the propagation characteristics become sensitive to the structure of the buildings. A distinction must be made between line-of-sight (LOS) and non-line-of-sight (NLOS) propagation. In the case of a base-station at every intersection, the LOS propagation loss is of greater importance, since a mobile will always have a direct LOS path to its serving base-station. One possible propagation path loss model is [4]:

$$S(d) = -20\log(d^a(1+\frac{d}{g})^b) + c \tag{2.1}$$

where the variables are defined as follows:

$S(d)$ = the signal level (dB or μv)

d = distance from the transmitting antenna (m)

a = basic attenuation rates for short distances (approx. 1)

b = additional attenuation rate for distances greater than 100 to 200 m

g = the break point of the attenuation curve

c = offset (dB)

Teletraffic model Analytic treatment of urban vehicular traffic is very difficult, if not impossible. Vehicle interactions, jamming, and traffic signals make the vehicular traffic non-Markovian. Markov processes are easy to simulate in an event-driven fashion. Non-Markovian processes are not. The following two teletraffic models attempt to model non-Markovian urban teletraffic as being Markovian, but with time-varying parameters.

2.2.1 Active-dormant Microcellular Teletraffic Model

A microcellular environment is expected to have a non-uniform distribution of teletraffic and have dynamic variations that are unpredictable. One possible model is that used in [3]. Because it uses two different call arrival rates, one for an "active" cell and another for a "dormant" cell, it will be referred to as the active-dormant model. The active-dormant model characterizes the non-uniform distribution of vehicular traffic by allowing each cell to be in one of two possible modes: active or dormant. Cells which are in the active mode have a higher call arrival rate than the dormant cells. From time to time, each cell transitions from one mode to another, thus reflecting the temporal variation in vehicular traffic. The model only considers call arrivals, call completions, and call hand-offs.

The active-dormant model has a small number of parameters, which are listed below:

D_{HI}	Duration of the active mode (seconds)
D_{LO}	Duration of the dormant mode (seconds)
T_{HI}	Traffic intensity in the active mode (Erlangs)
T_{LO}	Traffic intensity in the dormant mode (Erlangs)
μ	Individual call completion rate (seconds^{-1})
h	Average number of hand-offs per call

Call arrivals Call arrivals are calls which originate within a cell rather than those resulting from a hand-off. Call arrivals are characterized by a call arrival rate, which is the reciprocal of the average time between two arrivals. The interarrival times are considered to be exponentially distributed, and all cells are assumed to have independent arrivals. The traffic intensity of a cell is the product of the call arrival rate and the average duration of a single call. This average time is the reciprocal of μ, which is one of the parameters given above. Two traffic intensities, T_{HI} and T_{LO}, are listed as parameters. The corresponding call arrival rates can be derived from these values. λ_{HI} is the call arrival rate in an active cell. λ_{LO} is the call arrival rate in a dormant cell. λ is the call arrival rate in the whole system.

$$\lambda_{HI} = \mu T_{HI} \tag{2.2}$$

$$\lambda_{LO} = \mu T_{LO} \tag{2.3}$$

$$\lambda = A\lambda_{HI} + D\lambda_{LO} \tag{2.4}$$

where A is the instantaneous number of active cells in the system, and D is the instantaneous number of dormant cells in the system. Call arrival rates are additive, because the interarrival times are exponentially distributed and the arrivals in different cells are considered to be independent.

Call completions Call completions occur similarly to call arrivals. The call completion rate in the i_{th} cell is $M_i\mu$, where M_i is the instantaneous number of active calls in cell i. The call completion rate for the whole system is the sum of all of the completion rates. This is equal to $M\mu$, where $M = \sum_i M_i$.

Call hand-offs Calls are assumed to last, on the average, long enough to encounter h hand-offs. Since the are an average of h hand-offs per call, hand-offs occur h times as often as call completions. Therefore, the hand-off generation rate in the i_{th} cell is $M_i h\mu$, and the system hand-off generation rate is $Mh\mu$.

Event generation A simulation of the active-dormant model involves generating a random time until the next event, performing that event, and repeating the process. Each type of event occurs with exponential interarrival times. The three types of events are considered to occur independently of each other, so the total system event rate is $\lambda + M\mu + Mh\mu$. Now, due to the memoryless property of the exponential distribution, at any epoch the expected duration until the occurrence of the next event is a constant. So, if three random times are generated, one being the time until the next call arrival, one being the time until the next call completion, and the last being the time until the next call hand-off, the least of these times corresponds to the next event which will occur. Once that event occurs, the expected time until the next event is still the same as always. So, event generation is implemented by generating three random times and choosing the event with the smallest time. Once this event is performed, the process is repeated. Thus the event generation process can be described by an imbedded Markov chain with the following probabilities:

$$\begin{aligned}
\Pr(\text{Next event is a call arrival}) &= \frac{\lambda}{\lambda+M\mu+Mh\mu} \\
\Pr(\text{Next event is a call completion}) &= \frac{M\mu}{\lambda+M\mu+Mh\mu} \\
\Pr(\text{Next event is a call hand-off}) &= \frac{Mh\mu}{\lambda+M\mu+Mh\mu}
\end{aligned}$$

Given that one of these events occur in the system, the probability that it occurs in cell i is given by the following formulas:

$$\begin{aligned}
\Pr(\text{Arrival in cell } i\text{, given an arrival}) &= \frac{\lambda_i}{\lambda} \\
\Pr(\text{Completion in cell } i\text{, given a completion}) &= \frac{M_i}{M} \\
\Pr(\text{Hand-off from cell } i\text{, given a hand-off}) &= \frac{M_i}{M}
\end{aligned}$$

Mode transitions Calls arrive in the i_{th} cell at a rate of λ_i, which is equal to λ_{HI} if the cell is active or λ_{LO} if the cell is dormant. The average number of calls which

arrive during each mode is the product of the arrival rate and the duration of that mode.

$$N_{HI} = \lambda_{HI} D_{HI} \tag{2.5}$$

$$N_{LO} = \lambda_{LO} D_{LO} \tag{2.6}$$

If a cell is in active mode, then the number of calls which will arrive in that cell before it transitions to dormant mode is a random variable whose mean is N_{HI}. Likewise, a cell remains in dormant mode for an average of N_{LO} call arrivals before transitioning to active mode. Each time a cell transitions from one mode to another, a random threshold is generated. A call arrival counter is maintained. When the call arrival counter exceeds the threshold, the cell transitions.

2.2.2 A New Eight-zone Microcellular Teletraffic Model

The active-dormant model assumes that variations in vehicular traffic are unpredictable; however, the variations are in fact predictable because of the cyclic nature of traffic signals, which are characteristic of a urban microcellular environment. The active-dormant model is very simple in that it only assumes two possible call arrival rates per cell: λ_{HI} and λ_{LO}. In actuality, the call arrival rate in a cell is proportional to the number of inactive mobiles in the cell.

The eight-zone model, so named because each cell is divided into eight zones, attempts to take the finite vehicular population of the individual cells into consideration. It also uses the state of the individual traffic signals to determine the flow of mobiles among the zones of each cell.

Suppose that each cell is divided into four quadrants, corresponding to each one of the four approaches of the intersection, and also suppose that each quadrant is divided into two zones; one for entering mobiles and another for exiting mobiles. Fig. 2.2 shows these eight zones as well as the three flows that are associated the south quadrant which assumes no left turns. These flows are in mobiles per second. The *right flow* (*left flow*) of a quadrant is the flow of mobiles out of its entering zone that make a right turn (left turn). The *straight flow* of a quadrant is the flow of

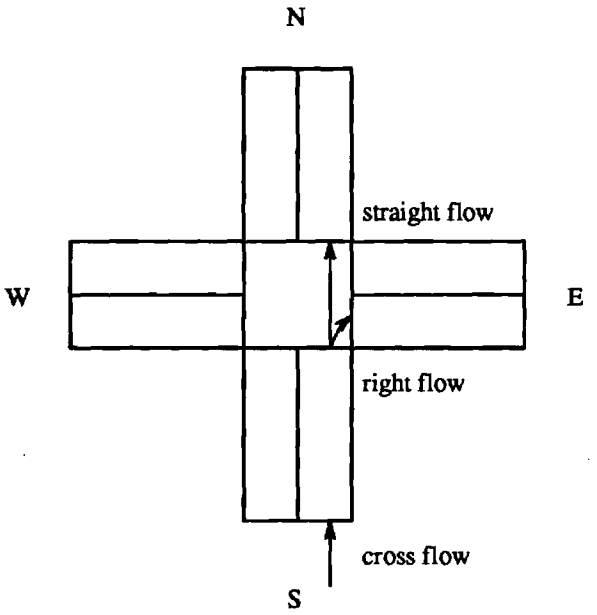

Figure 2.2: The zones of a single cell and the flows associated with the south quadrant.

mobiles out of its entering zone which go straight. The *cross flow* of a quadrant is the flow of mobiles into its entering zone from the adjacent cell. These three flows have the following symbols:

$q_{i,right}$	Right flow out of the i_{th} quadrant
$q_{i,left}$	Left flow out of the i_{th} quadrant
$q_{i,straight}$	Straight flow out of the i_{th} quadrant
$q_{i,cross}$	Cross flow into of the i_{th} quadrant

Additionally, let the following symbols represent the number of mobiles in each zone at any particular time:

$N_{active,i}$	Number of active mobiles in zone i
$N_{inactive,i}$	Number of inactive mobiles in zone i
N_i	Total number of mobiles in zone i ($N_{active,i} + N_{inactive,i}$)

The model has the following parameters:

λ	Call arrival rate for a single mobile
μ	Call completion rate for a single call
L_Q	The length of a single quadrant of a cell
L_M	The average effective length of a single mobile in jam conditions
$\overline{v}$	The average velocity of a moving mobile
N_{lanes}	The number of lanes
$P_{straight}$	The probability of a mobile going straight at an intersection
P_{right}	The probability of a mobile turning right at an intersection
P_{left}	The probability of a mobile turning left at an intersection

Call arrivals The call arrival rate in each zone is simply the product of the single mobile call arrival rate times the number of inactive mobiles in that zone. The system call arrival rate is the sum of all zone arrival rates.

$$\Lambda_i = \lambda N_{inactive,i} \tag{2.7}$$

$$\Lambda = \sum_i \Lambda_i \tag{2.8}$$

Call completions The call completion rate in each zone is the product of the single call completion rate times the number of active mobiles in that zone. The system call completion rate is the sum of all zone completion rates.

$$M_i = \mu N_{active,i} \tag{2.9}$$

$$M = \sum_i M_i \tag{2.10}$$

Mobile flow The flow of mobiles from one zone to another is not dependent on whether the individual mobiles are active or inactive. In general, the flow of mobiles is dependent on a great number of parameters such as vehicular concentration, number of lanes, width of lanes, weather conditions, traffic signals, etc. Obviously, a practical model cannot account for all of these factors. Some simplifications must be made. Our model will assume that flow is determined by exponentially distributed zone inter-crossing times, with the mean zone inter-crossing time determined as follows.

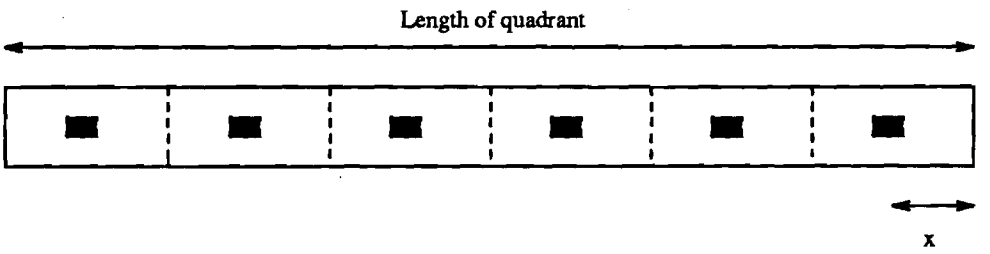

Figure 2.3: Even spacing of mobiles within a single lane.

Let T_C be the time it takes a mobile to cross from one zone to another. Assume for the moment that the number of lanes is one. Then,

$$T_C = \frac{x}{v} \tag{2.11}$$

where x is the distance to the zone boundary and v is the velocity of the mobile. If the mobiles are evenly distributed throughout the zone as in Fig. 2.3, then

$$x = \frac{L_Q}{2N} \tag{2.12}$$

The instantaneous flow rate q is simply the reciprocal of T_C. Substituting the expression for x into the reciprocal of T_C gives:

$$q = \frac{2vN}{L_Q} \tag{2.13}$$

Assuming that all moving mobiles are moving with a velocity equal to the average velocity of $\overline{v}$ gives:

$$q = \frac{2\overline{v}N}{L_Q} \tag{2.14}$$

Now, assume that there are N_{lanes} lanes. Then, the number of mobiles per lane is, on the average, $\frac{N}{N_{lanes}}$. But, there are now N_{lanes} lanes, each with its own flow. Assuming that the flow in the lanes are equal and independent of each other, the total flow is:

$$q = \frac{2N_{lanes}\overline{v}\frac{N}{N_{lanes}}}{L_Q} \tag{2.15}$$

which reduces to Eq. (2.14).

Eq. (2.14) is the flow for moving mobiles which are unimpeded; however, there are two conditions which could make the flow zero, regardless of the number of mobiles

in the zone. If mobiles are stopped at a red light in a zone which enters an intersection, then the flow is zero. If the number of vehicles in the zone into which the mobiles enter is the maximum number of mobiles, then the flow is also zero. The maximum number of mobiles which can fit in a zone is

$$N_{max} = \frac{N_{lanes} L_Q}{L_M} \tag{2.16}$$

Therefore, the flow from zone i to zone j is given by the following rule:

$$q_{i,j} = \begin{cases} \frac{2\bar{v}N}{L_Q} & \text{if green light and } N_j < N_{max} \\ 0 & \text{otherwise} \end{cases} \tag{2.17}$$

Right flow, left flow and straight flow are affected by a traffic signal; cross flow is not. Also, the right flow and straight flow are subject to driver inclinations, i.e., each mobile will turn right with probability P_{right}, make a left turn with probability P_{left}, and go straight with a probability of $P_{straight}$, assuming that the flow in these directions is not zero due to a red traffic signal or full destination zone. Notice that cross flow is defined going into a particular zone. That is why $q_{i,cross}$ depends on the mobiles in zone j, which is the zone providing the cross flow into zone i.

$$q_{i,right} = \begin{cases} \frac{2P_{right}\bar{v}N_i}{L_Q} & \text{if green light and } N_j < N_{max} \\ 0 & \text{otherwise} \end{cases} \tag{2.18}$$

$$q_{i,left} = \begin{cases} \frac{2P_{left}\bar{v}N_i}{L_Q} & \text{if green light and } N_j < N_{max} \\ 0 & \text{otherwise} \end{cases} \tag{2.19}$$

$$q_{i,straight} = \begin{cases} \frac{2P_{straight}\bar{v}N_i}{L_Q} & \text{if green light and } N_j < N_{max} \\ 0 & \text{otherwise} \end{cases} \tag{2.20}$$

$$q_{i,cross} = \begin{cases} \frac{2\bar{v}N_j}{L_Q} & \text{if } N_i < N_{max} \\ 0 & \text{otherwise} \end{cases} \tag{2.21}$$

Each cell has four quadrants, each of which has four flows. There are then sixteen flows per cell. Each of these are considered to be independent of all other flows. Since the time until the next mobile crossing at the i^{th} location is exponentially distributed

with parameter q_i, the interarrival times of any mobile crossing in the whole system is the sum of all of the individual zone crossing rates.

$$Q = \sum_i q_i \tag{2.22}$$

Event generation The generation of events in this model is similar to the event generation in the active-dormant model. There are three types of events: call arrivals, call completions, and mobile crossovers. Each type of event is considered to have exponentially distributed interarrival times, and they are independent of each other. Therefore,

$$\begin{aligned}
\Pr(\text{Next event is a call arrival}) &= \frac{\Lambda}{\Lambda+M+Q} \\
\Pr(\text{Next event is a call completion}) &= \frac{M}{\Lambda+M+Q} \\
\Pr(\text{Next event is a mobile crossover}) &= \frac{Q}{\Lambda+M+Q}
\end{aligned}$$

Given that one of these events occur in the the system, the probability that it occurs in zone i is given by the following:

$$\begin{aligned}
\Pr(\text{Arrival in zone } i, \text{ given an arrival}) &= \frac{\Lambda_i}{\Lambda} \\
\Pr(\text{Completion in zone } i, \text{ given a completion}) &= \frac{M_i}{M} \\
\Pr(\text{Crossover of type } \textit{type} \text{ in zone } i, \text{ given a crossover}) &= \frac{q_{i,type}}{Q}
\end{aligned}$$

Call hand-offs In this model, it is important to distinguish between a *mobile crossover* and a *call hand-off*. A mobile crossover occurs when any mobile, whether active or inactive, crosses from one zone into another. A call hand-off is a type of mobile crossover in which an active mobile crosses a cell boundary. An active mobile which crosses from one zone into another (as in the case of right flow and straight flow) does not cause a hand-off attempt; an active mobile which crosses a cell boundary does. This hand-off attempt may fail, depending on the channel allocation in the destination cell. A call hand-off can only happen in the case of cross flow.

Traffic signals Traffic signals can be random, coordinated, or vehicle actuated. For each cell the following items are stored: the state of its traffic signal (the signal color that each approaching vehicle sees at a particular time), a timer which stores the

elapsed time since the last signal transition, and a threshold time. When the timer exceeds the threshold time, the traffic signal transitions from one state to another. In the case of fixed and random traffic signals, the threshold time is constant. The cycle length is therefore also constant. In the case of vehicle actuated traffic signals, there is a fixed range of possible threshold times. The actual threshold time depends on whether or not there are mobiles waiting at a red signal and whether or not there is a flow of mobiles on the approach which see a green signal.

Each time an event occurs anywhere in the system, each traffic signal timer is incremented by the event arrival time (which is an exponentially distributed random variable). The transitions of the traffic signals are not themselves event generated, i.e., each time an event occurs, the traffic signals are checked, and it may be that several (or no) traffic signals may transition at once. When the signal timer is incremented, it will likely exceed the threshold by a non-zero amount. This creates a slight error, since the traffic signal is effectively delayed by that particular amount; however, since the event interarrival times will likely be very small relative to the cycle time of a traffic signal, the error introduced by this will likely be negligible. After transition, the traffic signal timers can be initialized to the amount of the error so that the effect is not cumulative.

2.3 Some Dynamic Channel Allocation Strategies

A channel allocation strategy coordinates the use of channels among the cells so that the channels are reused far enough apart to keep co-channel interference at an acceptable level. The simplest type of channel allocation strategy is fixed channel allocation (FCA). In FCA, each cell is assigned a subset of the available channels. Any mobile within a cell can use only those channels which are assigned to that cell. Once all of the channels are occupied, the cell can no longer accommodate new calls or accept hand-offs from adjacent cells. It may be that a new call can not be accommodated without violating the co-channel reuse constraint if the nearby cells are not using all of the available channels. In FCA, this property is not exploited.

FCA is not efficient when there is an uneven distribution of teletraffic which

varies with time. Since the number of channels which are assigned to each cell is fixed, the strategy as a whole does not account for variations in demand for channels. A more efficient strategy allows cells that require many channels to use any channel provided the channel is not currently being used in a nearby cell. *Channel borrowing* is such a strategy. In channel borrowing, all of the cells are still assigned a fixed subset of the total available channels; however, if a particular cell is using all of its pre-assigned channels and another is needed, it can borrow a channel from its neighbors. While it is using that particular channel, its neighbors are deprived of its use.

One simple way of adapting to varying demands for channels is a method called *directed retry* [5]. In directed retry, if a call is blocked, then it is permitted to try to make a connection with a base station in a nearby cell, subject to channel availability and sufficient signal power. Unfortunately, this has the effect of effectively increasing the size of the cells and thus increasing the global interference level within the network [6]. Therefore, it is preferred that hand-offs be executed as close as possible to predetermined cell boundaries.

Channel allocation strategies which do not assign any channels to any cells are known as *dynamic channel allocation* (DCA) strategies. Any cell can use any channel, provided that its use does not violate the co-channel reuse constraint. Cells aquire and release channels depending on their demand for channels. Of course, this must be done in an organized manner; uncoordinated acquiring and releasing of channels with no clear strategy would produce poor results, particularly in heavy traffic. There are many possible dynamic channel allocation strategies.

2.3.1 Maximum Packing

Maximum packing [7] is, in a sense, an optimum dynamic channel assignment strategy. When the demand in a particular network changes, i.e., a new call arrives or a hand-off is attempted, it is possible that the new demand could be met through the simple acquisition of a new channel. However, in the event that there are no channels immediately available to the new base station, it may still be possible to accommodate

the new call by a rearrangement of existing calls. This means that certain calls already in progress might be assigned to a new channel even though the call is not being handed-off to a new base station. This is called an *intra-cell hand-off*. A call arrival in one particular location may affect calls far away, because the system as a whole will rearrange all of the calls.

Maximum packing is centralized control in the extreme sense. It is too computationally intensive to be used for dynamic channel allocation. In a linear environment, such as a highway microcellular system, maximum packing can be implemented without ever having to do more than two reassignments per call arrival; however, in a more general, two dimensional system, such as an urban microcellular environment, the number of reassignments needed per call arrival grows without bound as a function of the number of cells in the system [8]. In an urban microcellular system, mobiles do not spend very much time in each cell. Fast channel acquisition for call arrivals and hand-offs is necessary. Maximum packing is simply not an option.

Maximum packing, while not a feasible strategy to implement, does provide an upper bound on performance. Feasible dynamic channel allocation strategies are necessarily sub-optimum, but if a feasible strategy is shown to perform nearly as well as maximum packing (through analysis or simulation), then that strategy is a indeed a very good strategy.

2.3.2 Maxavail

Feasible channel allocation algorithms in a microcellular environment must be able to react to short-term variations in teletraffic intensity. One way of speeding up the channel allocation process is to decentralize it, i.e., each base station manages its own channel assignment rather than referring to a central controller. Each base station accomplishes this through the use of a decentralized channel allocation strategy and limited or no communication with nearby base stations. The *Maxavail* algorithm [9] is such a strategy.

The Maxavail algorithm is a dynamic channel allocation strategy which assigns channels to calls as they arrive. When a call arrives, it is assigned the channel which

maximizes the total number of channels available in the entire system. The entire system does not actually have to be examined; maximizing the channel availability in a sufficiently large neighborhood of the cell in which a call arrives will produce the same result. The total number of channels available in the system is the sum of the total number of channels available in each cell. A channel is not available in a given cell if it is already being used in that cell or in another cell close enough to violate the channel reuse constraint. Maxavail can be simply described by the following algorithm, which describes the sequence of events when a new call arrives in a given cell:

1. For each channel that is available for use, compute the system wide channel availability, assuming that particular channel is the one which will be assigned.
2. Choose the channel which maximizes the sum.
3. In case of a tie, choose the least channel, assuming that the channels are arbitrarily ordered.
4. If no channel is available, then the call is blocked.

Remax1 A variation of Maxavail is an algorithm called *Remax1* [9]. It permits one call reassignment. A call reassignment is the transfer of a call already in progress to another channel. Remax1 can be simply described by the following algorithm, which describes the sequence of events when a new call arrives in a given cell:

1. Attempt to obtain a channel using the Maxavail algorithm.
2. If all of the channels are unavailable, go to step 3. Otherwise, assign the channel obtained using the Maxavail algorithm.
3. Make a list of all of the channels that are unavailable in the given cell because of exactly one call that is in progress.
4. Apply the Maxavail algorithm to each of the interfering calls.

5. For each of the calls which are not determined as being blocked by the Maxavail algorithm, calculate the systemwide channel availability, assuming that the call is reassigned to the channel determined by the Maxavail algorithm, and that the new incoming call is assigned to the newly freed channel.

6. Choose the call to be reassigned as the call which maximizes the systemwide channel availability.

7. If no channel can be assigned by a single reassignment, then the call is blocked.

Remax2 Yet another variation of Maxavail is *Remax2* [9]. Remax2 allows two call reassignments when a new call arrives. Remax2 is a recursive application of Remax1. The algorithm can be simply described by replacing the "Maxavail" in the Remax1 algorithm with "Remax1."

Another approach for increasing capacity is to allow call reassignments when a channel is released. In this case, when a channel is to be released due to a call completion or a hand-off to another cell, a reassignment is made such that the systemwide channel availability is maximized. The Dynamic Resource Acquisition (DRA) algorithm, described in the next section, does exactly this.

2.3.3 Dynamic Resource Aquistion

Dynamic Resource Acquisition (DRA) [3] is a channel allocation strategy in which base stations acquire and release channels according to a reward/cost function. The reward/cost function depends on the channels currently being used in nearby cells.

The *interference neighbourhood* of a cell is the set surrounding cells such that, if a channel is being used by a any member in this set, the cell cannot use that channel. The interference neighbourhood is determined by the propagation characteristics of the microcellular environment, which can be modeled using Eq. 2.1. For example, the set of all cells adjacent to a particular cell might comprise its interference neighbourhood. Or, the interference neighbourhood might be determined by interference power levels that result when the cells try to reuse the same channel. In this case,

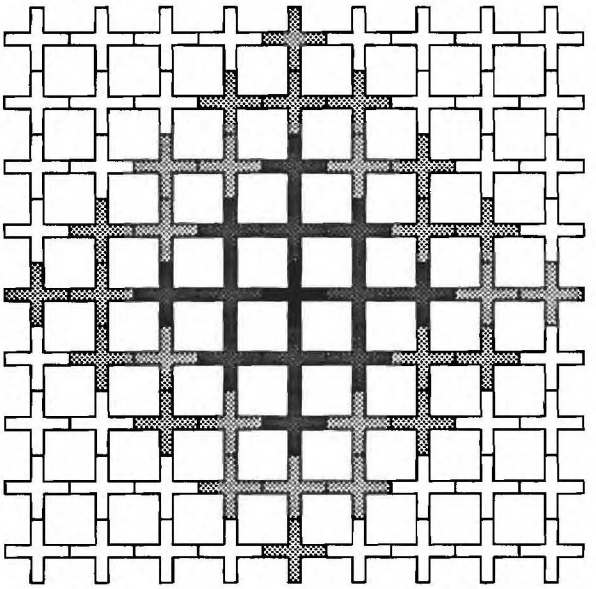

Figure 2.4: Example interference and DRA neighbourhoods of an urban microcell.

different cells could have interference neighbourhoods of varying shapes and sizes, depending on the propagation characteristics in a particular geographic area.

The *DRA neighbourhood* of a cell is the set of all cells whose interference neighbourhoods overlap the interference neighbourhood of the given cell. Fig. 2.4 shows an example of an interference neighbourhood and a DRA neighbourhood of an urban microcell.

Upon a call arrival or hand-off attempt, the base station of the given cell must acquire a channel. If there are no channels available, i.e., every channel is either in use in that cell or in its interference neighbourhood, then the call is blocked. If there are channels available, then a channel is selected which minimizes the cost of acquiring that channel. The cost associated with acquiring a new channel is the number of cells which are deprived of using that channel if the base station in the given cell acquires it. Suppose that a base station is calculating the cost function of a particular channel. It asks each base station in its interference neigbourhood whether or not that base station's interference neigbourhood includes any cells currently using that channel. For every cell for which this is true, the cost function is not incremented, since these base stations are already deprived from using that channel, and acquiring it will not

affect them. However, for every cell for which this is not true, the cost function is incremented, since acquiring the channel will deprive these cells of its use, while not acquiring it will permit them to use it. The cost function of all of the available channels are compared, and the channel with the least cost function is selected for use.

Upon a call termination or hand-off to another cell, the base station of the given cell must release a channel. In order to maximize efficiency, call reassignments are permitted in this case. In this way, the base station can choose which channel gets released rather than being forced to release the one being used by the terminating call. It selects the channel to be released by choosing the one which maximizes a reward function associated with releasing that channel. Suppose that a call using a channel with a low reward function terminates. The base station calculates the reward function of all of its active calls, and chooses the one with the highest reward function. It then reassigns this call to the now-available channel with the low reward function and releases the channel with the high reward function. The reward function is calculated in exactly the same way as the cost function in the case of acquiring a channel. The difference is that, when releasing a channel the cost function is maximized, while when acquiring a channel the cost function is minimized.

The implementation described in [3] uses carrier acquisition instead of channel acquisition. Each carrier is a particular frequency band which has a certain number of TDMA slots. A base station cannot acquire a particular carrier if a cell in its interference neighbourhood is currently using any time slot in that carrier, although a single cell can use all the slots of a given carrier. In this way, channels are allocated in groups rather than individually. This reduces the amount of communication between base stations. Carriers are only acquired when a new channel is needed and all previously acquired carriers have all their time slots filled up. Carriers are only released when all of the time slots of a carrier are unused. Of course, since call reassignments are permitted, the active calls are packed so that, at any given time, there is at most one carrier which does not have all of its time slots filled.

2.3.4 Channel Segregation

Channel Segregation [10] is a decentralized channel allocation strategy in which each base station acquires channels based upon its past history of channel acquisition successes and failures. Each base station maintains a table of priority functions (defined below). Each priority function is a value which corresponds to a channel. When a new call arrives or a hand-off is attempted, the base station selects a channel based on these priority functions and updates them accordingly. The procedure is as follows:

1. When a new call arrives or a hand-off is attempted, the base station selects the unused channel which has the highest priority function. Note that the frequency reuse constraint is not considered at this point; the only channels which are forbidden to be selected are those which are in use by that particular base station.

2. The base station listens to the channel and decides whether or not the channel has too much interference from surrounding cells.

3. If the interference power is sufficiently low, then the channel is sensed idle. It is selected for use, and its priority function is increased.

4. If the interference power is too high, then the channel is sensed busy. It is not selected for use, and its priority function is decreased. Then, the unused channel with the next highest priority is selected. The process continues from step 2.

5. If all of the channels are busy, then the call is blocked.

The priority function of each channel can be defined in different ways. One definition is the probability of successful acquisition of the corresponding channel. Each priority function is the ratio of the number of successful acquisitions of that channel to the total number of attempts.

Channel Segregation is similar to DRA. However, while DRA requires communication between nearby base stations, Channel Segregation requires no direct communication between base stations. Decisions are made solely on sensing the interference present on each channel. This interference may be co-channel or adjacent channel interference. It may be possible that the propagation characteristics of the microcellular environment may cause a large variation in co-channel reuse distances. In one particular region, cells that are very close to each other might not interfere with each other, while another region may require that the co-channel cells be much farther apart.

Channel Segregation does not allow for the possibility of call reassignments. In DRA, call reassignments are used in order to maximize the reward function when a channel (or carrier) is released. Such a policy may be beneficial in Channel Segregation. Consider what happens when a call terminates or is handed-off to another cell. If a channel is released, then it becomes available for use by nearby base stations. If a nearby base station successfully acquires the channel, then it is "encouraged" to use it again because the priority function for that particular channel is increased. In other words, not using a channel "encourages" nearby base stations to use it. If a base station's "favorite" channels are those with the highest priority, then it would want to occupy those for as long as possible so that surrounding base stations are "discouraged" from using them. Therefore, if a channel with a high priority function becomes idle, then a reassignment strategy would reassign the call whose channel has the lowest priority function to the now idle channel with the highest priority function, and the channel with the lowest priority function is then released.

2.4 A Sample Simulation of DRA versus FCA

The DRA and FCA channel algorithms were simulated over a range of different call arrival rates, and the results were compared.

Teletraffic model The active-dormant teletraffic model was used for this simulation. The simulation was run on a twelve by twelve array of cells. The array was

connected as a torus, i.e., the cells along the top edge were made adjacent to the cells along the bottom edge, and the cells along the left edge were made adjacent to the right edge. This has the effect of eliminating edges and edge effects altogether. The following parameters were held constant for the duration of the simulation:

$$\begin{aligned} D_{HI} &= 60 \text{ seconds} \\ D_{LO} &= 240 \text{ seconds} \\ \mu &= 0.01 \text{ calls/second} \\ h &= 2 \text{ handoffs per call} \end{aligned}$$

The total average traffic intensity, T_{AV}, was varied from 10 to 50. The ratio between T_{HI} and T_{LO} was held at a constant:

$$\frac{T_{HI}}{T_{LO}} = 10$$

Total average traffic intensity is:

$$T_{AV} = P_{HI}T_{HI} + P_{LO}T_{LO}$$

where P_{HI} and P_{LO} are the probabilities of any given cell being active or dormant.

$$\begin{aligned} P_{HI} &= \frac{D_{HI}}{D_{HI} + D_{LO}} \\ P_{LO} &= \frac{D_{LO}}{D_{HI} + D_{LO}} \end{aligned}$$

Given these equations, T_{HI} and T_{LO} can be expressed as a function of T_{AV}:

$$\begin{aligned} T_{HI} &= 10T_{AV}\frac{D_{HI} + D_{LO}}{10D_{HI} + D_{LO}} \\ T_{LO} &= T_{AV}\frac{D_{HI} + D_{LO}}{10D_{HI} + D_{LO}} \end{aligned}$$

This reduces to:

$$\begin{aligned} T_{HI} &= 3.5714T_{AV} \\ T_{LO} &= 0.3571T_{AV} \end{aligned}$$

Co-channel reuse constraint The simulation assumes that adjacent cells are not permitted to use the same channel. However, cells which are diagonally adjacent are not truly adjacent, as can be seen from Fig. 2.4 and are assumed not to violate the co-channel reuse constraint.

Initialization At the beginning of each simulation, the cells in the array were randomly made active or dormant according to the probabilities P_{HI} and P_{LO}. The transition threshold of each cell was assigned a random number with mean N_{HI} or N_{LO}, depending on whether or not the cell is active or dormant. The carriers were divided into two disjoint subsets, and the cells were assigned carriers in "checkerboard" fashion. The simulation was permitted to run for a simulated period of one hour before any information was gathered concerning the success or failure of call arrivals or hand-off attempts.

Dynamic resource acquisition The DRA algorithm was simulated using the interference and DRA neighbourhoods shown in Fig. 2.5, which correspond to the given co-channel reuse constraint. Since there are four cells in the interference neighbourhood, the DRA reward-cost function for a particular carrier can take on six values: 0-4, and, if a cell in the interference neighbourhood is using that particular carrier, the reward-cost function is considered to be infinite. If upon request for a carrier (either on a call arrival or hand-off) all the carriers have infinite costs, then the call is blocked (in the case of a call arrival) or forced to terminate (in the case of a hand-off attempt). The reward function for releasing a particular carrier will never be infinite. After initialization, the cells are free to acquire or release carriers according to current demand.

Fixed channel allocation For the sake of comparison, a simulation was run using the same teletraffic model, but using a fixed channel allocation strategy instead of DRA. The "checkerboard" pattern described in the initialization is assumed to satisfy the co-channel reuse constraint; therefore, the fixed allocation strategy has a cluster size of two. Since there are 20 carriers each with four slots, there are a total of 80

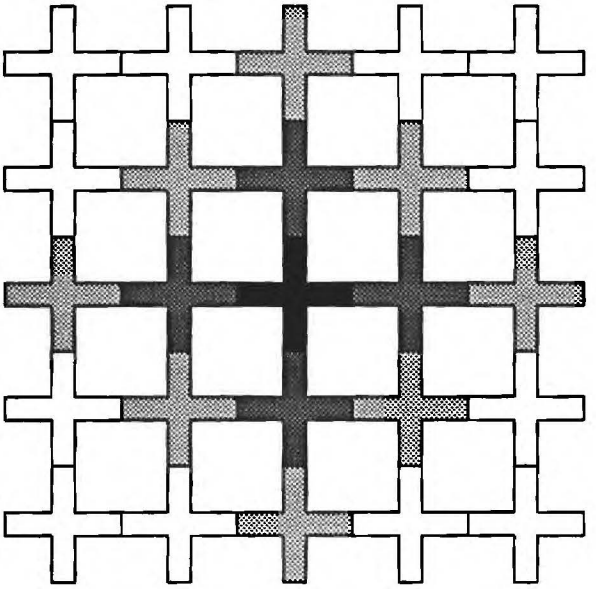

Figure 2.5: Interference and DRA neighborhoods used in simulation

channels. Hence, each cell has 40 channels available for use. Since the strategy is fixed, this amount does not change.

Simulation results The simulations were run for simulated periods of three hours, which started after the one hour initialization period. During these periods, the number of call arrivals, call blocks, hand-off attempts, and hand-off attempt failures were counted, and the ratios were used to estimate the probability of call blocking, shown in Fig. 2.6, and the probability of hand-off attempt failure, shown in Fig. 2.7.

As can be seen from the results, the DRA strategy has a lower probability of call blocking than the FCA strategy over the entire range of the simulation. As the offered traffic becomes very large, the improvement decreases. The DRA strategy also has a lower probability of hand-off failure over most of the range; however, as the offered traffic becomes very large, the improvement decreases, and the probability of hand-off failure actually becomes slightly greater for DRA.

Finally, we note that Nanda and Goodman [3] have compared the performance of DRA and FCA for highway microcells. They concluded that DRA provided a large improvement over FCA. In contrast, our comparison of DRA and FCA for urban Manhattan microcells does not show a significant improvement. One possible reason

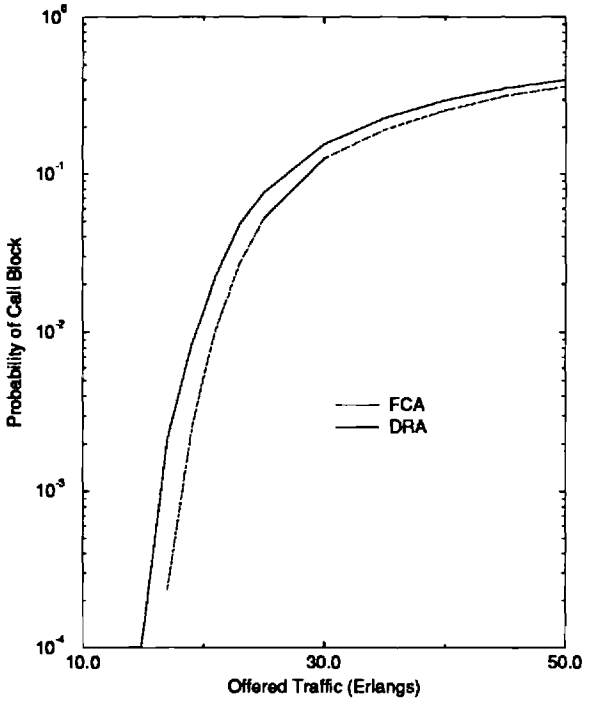

Figure 2.6: Probability of call block for FCA and DRA

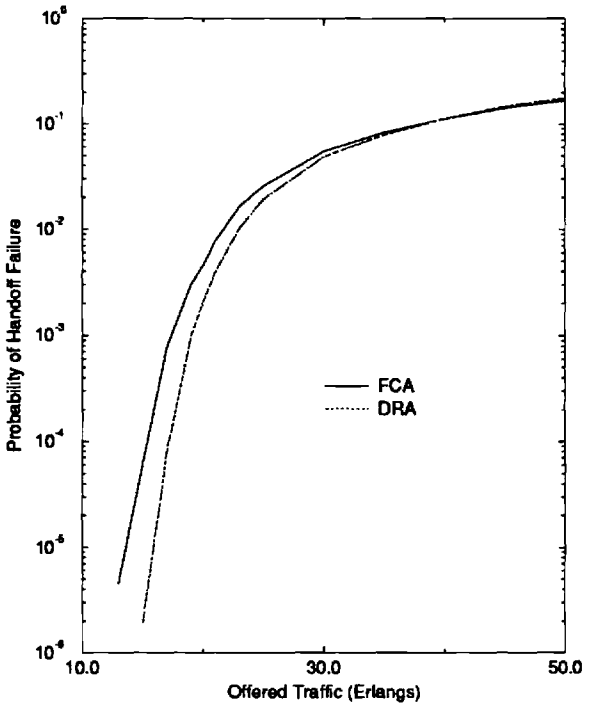

Figure 2.7: Probability of handoff failure for FCA and DRA

is that the interference neighbourhood in our results is smaller. Another possible reason is that the duration of the active mode in Nanda and Goodman's study is 15 minutes, whereas we chose a value of 60 seconds to provide a more realistic model of the bursty nature of urban vehicular traffic.

3 Analysis of Co-channel Interference for Micro-cellular Systems with Hand-off Applications

3.1 Introduction

In the early years of mobile radio there were only a small number of users and capacity was not an issue. As new users entered the network, extra channels were added by consuming additional bandwidth resources. Co-channel interference, which is the interference between channels with the same carrier frequency, was virtually non-existent due to the large *co-channel reuse factor.*[1] Eventually, user demand increased and limitations in available bandwidth were reached, forcing mobile communication engineers to devise new schemes for greater spectral efficiency. Without considering the improvements derived from bandwidth efficient modulation and trunking, the primary solution for increased spectral efficiency is to reduce the co-channel reuse distance.[2] Consequently, in modern mobile radio systems with high traffic loads, the distance between cells is small and spectral efficiency is limited by co-channel interference. The reuse distance is usually chosen as the minimum distance that users can communicate within a tolerable amount of co-channel interference. This limit is related to the *protection ratio* (δ), which defines the tolerable ratio of the power of the desired signal (ψ_0), to the total interference ($\sum_i \psi_i$).

$$P_{\text{out}} \triangleq \Pr(\text{Unacceptable Co-channel Interference}) = \Pr\left(\frac{\psi_0}{\sum_i \psi_i} < \delta\right) \qquad (3.1)$$

The protection ratio δ is dependent on the type of modulation employed and the characteristics of the receiver [11]. The definition in CCIR recommendation for determining the appropriate protection ratio ratio is as follows: "A degradation of the initial S/N of 20 dB to a $(S+N)/I$ of 14 dB is taken as the criterion to correspond with the minimum acceptance grade of service." [11]. Some typical values are listed in Table 3.1. High capacity systems with many channels per carrier tend to require

[1]The co-channel reuse factor is defined as the ratio of spatial separation between cells using a common set of carrier frequencies and the radius of the cells.

[2]The reuse distance is the distance between cells with the same carrier frequency.

modulation type	protection ratio	reference
analog FM (25 kHz spacing)	8 dB	[12, 11]
GMSK (GSM system)	9.5 dB	[13]
analog FM (12.5 kHz spacing)	12 dB	[12]
SSB (8.34 kHz spacing)	20 dB	[14]

Table 3.1: Typical protection ratio values for different modulation schemes.

a greater protection ratio.

Given the current trend towards smaller cell sizes, the probability that a mobile will cross a cell boundary during a call increases. In fact, Labedz [15] has shown that the number of cell boundary crossings per call is inversely proportional to the cell radius. This means that more *hand-off* or call transfers to neighbouring cells must take place to maintain call continuity. The central issue when designing microcellular systems is to devise a good hand-off algorithm. A good hand-off algorithm executes a hand-off as close as possible to the established cell boundaries, performs the hand-off as quickly as possible, maintains the best speech quality for the mobile subscriber at any instant, and relieves undesired network congestion. Good hand-off algorithms are a crucial part of a mobile radio system because they keep the cell boundaries intact and keep the co-channel interference at the planned level. This results in greater spectral efficiency.

A variety of methods have been presented in the literature for monitoring the link quality to determine when a hand-off should be performed. Such methods use bit error rate [16], signal-to-interference ratio [17], signal strength measurements [18, 19, 20, 21, 22], distance measurements [22, 23] or various combinations of these fundamental schemes. Of these methods, signal strength based hand-off techniques have received the most attention. However, hand-off algorithms that are based only on signal strength have known deficiencies. For example, if many strong interferers are present, a signal strength based hand-off algorithm may be fooled into thinking that it has an acceptable link quality due to a large signal strength even though the

carrier-to-interference (CIR) ratio is unacceptable. Thus, other link quality measurement techniques, in particular CIR measurements, provide very useful information for making hand-off decisions. In order to evaluate CIR based hand-off algorithms, an accurate characterization of co-channel interference analysis is required.

This chapter summarizes various models for estimating co-channel interference in microcellular systems. Section 3.2 provides an overview of hand-off algorithms along with a discussion of the similarities between the analysis of hand-off algorithms and the characterization of co-channel interference. Section 3.3 describes common probability distributions that are used to describe the faded and shadowed envelope of a received signal. Section 3.4 outlines current methods, and new results for co-channel interference calculations. Section 3.5 discusses how the theory in Section 3.4 can be applied to the evaluation of hand-off algorithms. Concluding remarks are presented in Section 3.6.

3.2 Hand-off Algorithms in Microcellular Systems

As previously mentioned, a variety of hand-off algorithms have been presented in the literature. It is immediately apparent that an analysis of co-channel interference analysis will be useful for predicting how well a CIR based hand-off algorithm will perform. We now show below that the mathematical formulation for co-channel interference analysis will also allow the analysis of signal strength based hand-off algorithms.

For a signal strength based hand-off algorithm, the mobile or base station must make an estimate of the *local mean*[3], which in a low interference situation, is related to the distance from the base station and to some extent the link quality. It is useful to define the following variables:

$\psi(n) \triangleq$ sample of received signal power with fading and shadowing

$\Psi(n) \triangleq$ received signal power without fading but with shadowing

$m_\Psi \triangleq$ received signal power without fading or shadowing

[3]The local mean is the average strength of the signal over a local area.

where

$$\Psi(n) = \mathrm{E}[\psi(n)], \tag{3.2}$$

The hand-off algorithm makes a hand-off decision based on the estimate of the local mean. In cases where the received signal is low-pass filtered before sampling, one can assume that the multipath variation has been completely filtered out leaving only shadowed samples [19]. However, a more accurate analysis assumes that sampled signals experience both multipath and shadowing. Thus, the basic comparison that a hand-off algorithm makes is :

$$\Pr\left(\overline{\psi_0(\cdot)} < \delta\overline{\psi_1(\cdot)}\right) \tag{3.3}$$

where $\bar{x}$ is the average value of x, the subscripts denote base stations 0 and 1 respectively, and δ represents the protection ratio or *hand-off hysteresis.* The comparison in (3.3) has the same form as the co-channel interference equation (3.1). Therefore, under the proper perspective, the analysis of co-channel interference can be applied to the analysis of signal strength based hand-off algorithms. Obviously, if the average in (3.3) is over one sample then (3.3) has the exact form as in (3.1), where ψ_1 assumes the role of the interferer in (3.1). Likewise, if running sums are used for the averages in (3.3), then the transfer of all but one sample to the right hand side of (3.3) also transforms (3.3) into the form of (3.1). Note that the running sum signal strength average is used in the TIA 45.3 North American TDMA cellular standard [24]. In this standard, the hand-off decision is based on a window average of the signal strength over 25 frames, i.e.,

$$\overline{\psi(\cdot)} = \frac{1}{25}\sum_{i=1}^{25}\psi(i) \tag{3.4}$$

Samples of the signal strength are taken every 40 ms for an effective window length of 1 second. Samples of the current base station and alternate base stations are not taken simultaneously, but rather 6.67 ms apart which is the slot duration within a frame. All of the analysis of signal strength averaging hand-off algorithms in the literature have chosen to neglect this fact and have assumed that signal strength samples are taken simultaneously.

Another signal strength averaging method that can be viewed in the form of equation (3.1) is the one related to GSM recommendation 05.08[23]. This method uses an M-of-N criteria, where N samples are collected and the hand-off algorithm checks to determine whether M of the N $\overline{\psi(\cdot)}$ are less than the protection ratio. In terms of the variables defined above, an alternative hand-off algorithm could determine whether M out the N $\frac{\psi_0(\cdot)}{\psi_1(\cdot)}$ are less than the protection ratio. In this case, each of the N decision statistics has the form of (3.1).

In summary, the analysis of co-channel interference provides a method predicting the performance of signal strength based hand-off algorithms under two possible forms of averaging, running sum and M-of-N averaging. More discussion on this topic will follow the general co-channel interference analysis in the next section.

3.3 Probability Distributions used in Co-channel Interference Analysis

The probability of co-channel interference can be calculated once the probability distribution functions (*pdf's*) of the desired and interfering signals are specified. In order to provide a unified discussion throughout the remainder of Section 3, an overview of the various forms cited in the literature is presented here. This preliminary discussion will provide a handy reference to the dialogue that follows.

The desired and interference distributions are most often based on the *pdf* of the signal envelope or squared signal envelope, which can be characterized by three disjoint phenomena: envelope fading, shadowing or local mean variation, and path loss [25, 26]. These phenomena are related, since the expected value of the faded envelope is the shadow random variable, and the expected value of the shadow random variable is the path loss.

3.3.1 Envelope Fading

Any bandpass signal centered on a carrier with angular frequency w_c, can be represented by using inphase $x_I(t)$ and quadrature $x_Q(t)$ notation [27].

$$r(t) = \Re\{(x_I(t) + jx_Q(t))e^{-jw_c t}\} \tag{3.5}$$

Hence, at any time instant t, the magnitude of the envelope of $r(t)$ is

$$\mathbf{r} = \sqrt{x_I^2 + x_Q^2}. \tag{3.6}$$

Here, x_I and x_Q are safely assumed to be Gaussian distributed.[4] If the means of x_I and x_Q are zero, then $\mathbf{r}$ is Rayleigh distributed; otherwise, $\mathbf{r}$ is Rician distributed.

Rayleigh Fading: When $\mathbf{r}$ has a Rayleigh distribution,

$$\begin{aligned}
p_{\mathbf{r}}(r) &= \frac{r}{\sigma_r^2}\exp\left\{-\frac{r^2}{2\sigma_r^2}\right\} \\
\mathrm{E}[\mathbf{r}^k] &= (2\sigma_r^2)^{\frac{k}{2}}\Gamma\left[1+\frac{k}{2}\right], \\
\mathrm{E}[\mathbf{r}] &= \overline{r} = \frac{\sqrt{\pi}}{2}\sqrt{2\sigma_r^2} \\
\mathrm{E}[\mathbf{r}^2] &= \overline{r^2} = 2\sigma_r^2 \\
\overline{r^2} &= \frac{4}{\pi}\overline{r}^2 \\
p_{\mathbf{r}}(r) &= \frac{\pi r}{2\overline{r}^2}\exp\left\{-\frac{\pi r^2}{4\overline{r}^2}.\right\}
\end{aligned} \tag{3.7}$$

Here, $\overline{r}$ is called the local mean of the signal, and has been shown to follow a log-normal distribution in both macro- and microcells [28, 29, 30]. Often, it is easier to work with of the envelope power, $\mathbf{y} = \mathbf{r}^2$, which gives rise to the exponential distribution

$$p_{\mathbf{y}}(y) = \frac{1}{\overline{r^2}}\exp\left\{-\frac{y}{\overline{r^2}}.\right\} \tag{3.8}$$

[4]The assumption that x_I and x_Q are Gaussian distributed is physically justified in the mobile radio environment, since the vector sum of a large number of plane waves that are arriving with random phase tends towards a Gaussian distribution by application of the Central Limit Theorem.

Rician fading: The Rician distribution arises when x_I and x_Q do not have zero mean. This occurs when a specular component or Line Of Sight (LOS) path exists between the mobile and base station. If the envelope is Rician distributed, then

$$p_{\mathbf{r}}(r) = \frac{r}{\sigma_r^2}\exp\left\{-\frac{(s^2+r^2)}{2\sigma_r^2}\right\} I_0\left(\frac{rs}{\sigma_r^2}\right), \tag{3.9}$$

and the envelope power $\mathbf{y} = \mathbf{r}^2$, and instantaneous envelope power $\mathbf{z} = \frac{1}{2}\mathbf{r}^2$ have the non-central chi-square distributions

$$p_{\mathbf{y}}(y) = \frac{1}{2\sigma_r^2}\exp\left\{-\frac{(s^2+y)}{2\sigma_r^2}\right\} I_0\left(\sqrt{y}\frac{s}{\sigma_r^2}\right) \tag{3.10}$$

$$p_{\mathbf{z}}(z) = \frac{1}{\sigma_r^2}\exp\left\{-\frac{(s^2+2z)}{2\sigma_r^2}\right\} I_0\left(\sqrt{2z}\frac{s}{\sigma_r^2}\right) \tag{3.11}$$

where (3.11) is the most popular form in the literature [31, 32, 2]. Quite often it is useful to write the Rician and non-central chi-square distributions in terms of the Rice factor K which represents the ratio of the power in the specular to scattered component. Writing the distributions in terms of the Rice factor gives:

$$\begin{aligned}
K &= \frac{s^2}{2\sigma_r^2} \\
K_{\text{dB}} &= 10\log_{10}\left(\frac{s^2}{2\sigma_r^2}\right) \\
\text{E}[r^2] &= \overline{r^2} = s^2 + 2\sigma_r^2 \\
s^2 &= \frac{K\overline{r^2}}{K+1} \\
2\sigma_r^2 &= \frac{\overline{r^2}}{K+1} \\
p_{\mathbf{r}}(r) &= \frac{2r(K+1)}{\overline{r^2}}\exp\left\{-K-\frac{(K+1)r^2}{\overline{r^2}}\right\} I_0\left(2r\sqrt{\frac{K(K+1)}{\overline{r^2}}}\right) \\
p_{\mathbf{y}}(y) &= \frac{K+1}{\overline{r^2}}\exp\left\{-K-\frac{(K+1)y}{\overline{r^2}}\right\} I_0\left(2\sqrt{y}\sqrt{\frac{K(K+1)}{\overline{r^2}}}\right).
\end{aligned} \tag{3.12}$$

When $K = 0$ there is no LOS path and Rician distribution reduces to the Rayleigh distribution. When $K \longrightarrow \infty$ the Rician distribution reduces to a Gaussian distribution. Bultitude [33] chose $K = 7 \sim 12$ dB. Green [34] used the range $K = 0$ to 32 for microcells. The value of K is dependent on the carrier frequency [35]. Due to more the favorable specular condition K increases at higher frequencies. In general, channels with a larger K require a smaller fade margin than Rayleigh fading channels.

Nakagami-m fading: Some publications [36] use the Nakagami-m distribution to describe the faded envelope, because it is a flexible and general distribution that can model different fading environments. The Nakagami-m distribution is described by the density function

$$p_{\mathbf{r}}(r) = \frac{2m^m r^{2m-1}}{\Gamma(m)\Omega^m} e^{-\frac{mr^2}{\Omega}} \qquad m \geq \frac{1}{2} \tag{3.13}$$

where

$$m = \frac{\Omega^2}{\mathrm{Var}(r^2)} \tag{3.14}$$

$$\Omega = \mathrm{E}[r^2] \tag{3.15}$$

When $m = 1$, the Nakagami-m distribution reduces to a Rayleigh distribution. The Nakagami-m distribution can be used to approximate a Rician distribution by using the following expression for the K factor

$$K = \frac{\sqrt{m^2 - m}}{m - \sqrt{m^2 - m}} \qquad m \geq 1 \tag{3.16}$$

The envelope power $\mathbf{y} = \mathbf{r}^2$ has the density

$$p_{\mathbf{y}}(y) = (\frac{m}{\Omega})^m \frac{y^{m-1}}{\Gamma(m)} \exp\left\{-\frac{my}{\Omega}\right\} \tag{3.17}$$

3.3.2 Log-normal Shadowing of the Local Mean

Shadowing is a function of scattering loss which depends upon the nature of terrain. Topographical variations in the propagation path, such as buildings cause scattering losses, and terrain variations such as hills cause diffraction losses. The effect is a slow variation in the local mean as the receiver moves from one spatial location to the next. In macrocellular systems shadowing is often described by a log-normal distribution with a standard deviation that is related to the morphological structure in the vicinity of the receivers [37, 25, 14, 38].

Confusion may arise when using the log-normal distribution for co-channel interference analysis, since some authors [14, 39, 12] assume that the mean ($\overline{r}$) is log-normally distributed with a standard deviation of $\sigma = 6 - 12$ dB, while others [40, 31, 41, 42] assume that the mean power ($\overline{r^2}$) is lognormally distributed with the

same value of σ. Clearly, these are two different measurements, since one measures voltage and the other measures power. However, because the envelope distribution is single-sided (*the pdf is only defined for positive values*), σ happens to be the same in either case. The following presentation clearly describes the relation between log-normal shadowing assuming voltage, or power measurements [43].

If the average power is assumed to follow a log-normal distribution then,

$$p(\overline{r^2}) = \frac{1}{\overline{r^2}\sigma\sqrt{2\pi}} \exp\left\{-\frac{(\ln\overline{r^2} - m)^2}{2\sigma^2}\right\} \tag{3.18}$$

where

$\sigma \triangleq$ standard deviation of slow fading measured in natural units (nats)

$m \triangleq$ mean of the slow fading measured in nats.

If a transformation is made into the more common decibel form then,

$$\begin{aligned} \sigma_p &= 10 \cdot \log_{10} e \cdot \sigma \\ m_p &= 10 \cdot \log_{10} e \cdot m \end{aligned}$$

so that,

$$p(\overline{r^2}) = \frac{10}{\overline{r^2}\sigma_p \ln 10\sqrt{2\pi}} \exp\left\{-\frac{(10\log_{10}\overline{r^2} - m_p)^2}{2\sigma_p^2}\right\} \tag{3.19}$$

where,

$\sigma_p \triangleq$ standard deviation of shadowing in decibels

$m_p \triangleq$ mean of shadowing in decibels

$\overline{r^2} \triangleq$ mean of envelope fading power.

Likewise, if voltage is measured then

$$p(\overline{r}) = \frac{20}{\overline{r}\sigma_v \ln 10\sqrt{2\pi}} \exp\left\{-\frac{(10\log_{10}\overline{r}^2 - m_v)^2}{2\sigma_v^2}\right\} \tag{3.20}$$

where,

$\sigma_v =$ standard deviation of shadowing in decibels

$m_v =$ mean of shadowing in decibels

$\overline{r} =$ mean of envelope fading voltage.

For Rician envelope fading ($K = 0$ for Rayleigh envelope fading),

$$\overline{r^2} = C(K)\overline{r}^2 \tag{3.21}$$

where

$$\begin{aligned} C(K) &= \frac{4e^{2K}(K+1)}{\pi_1 F_1^2(3/2, 1; K)} \\ K &\triangleq \text{Rice factor} \\ C(0) &= \frac{4}{\pi} \text{ if } \overline{r} \text{ is Rayleigh.} \end{aligned} \tag{3.22}$$

Then,

$$p(\overline{r^2}) = \frac{p_{\overline{r}}\left(\sqrt{\frac{\overline{r^2}}{C(K)}}\right)}{2C(K)\sqrt{\frac{\overline{r^2}}{C(K)}}}. \tag{3.23}$$

so that,

$$p_{\overline{r^2}}(\overline{r^2}) = \frac{10}{\overline{r^2}\sigma_p \ln 10\ \sqrt{2\pi}} \exp\left\{-\frac{(10\log_{10}\overline{r^2} - (m_v + 10\log_{10}C(K)))^2}{2\sigma_v^2}\right\} \tag{3.24}$$

Consequently,

$$\begin{aligned} m_p &= m_v + 10\log_{10}C(K) \\ \sigma_p &= \sigma_v. \end{aligned} \tag{3.25}$$

For $C(0)$ (when $\overline{r}$ is Rayleigh) we have,

$$\begin{aligned} m_p &= m_v - 10\log_{10}\frac{\pi}{4} \\ \sigma_p &= \sigma_v \end{aligned} \tag{3.26}$$

Therefore, the standard deviation is the same for both voltage or power measurements, but the mean changes.

At present there is no consensus on the shadow distribution for microcells. For microcellular systems, Bultitude [33] and Muammar [32] believe that the shadowing is not log-normal. However, some authors [32, 30, 29] still use a log-normal distribution to model microcellular shadowing by changing the value of σ_p (or σ_v). Regarding the latter approach, there are some general comments that can be made about the value of σ_p in microcells.

- σ_p should be increased in microcells because there are few obstacles [44, 45].
- higher frequencies are more sensitive to shadowing than lower frequencies [25, 4]. Therefore, higher frequencies should have a larger σ_p.
- shadowing is insensitive to the base station antenna height [30].

For macrocellular systems a value of $\sigma_p = 8$ dB is commonly used. For microcellular systems a value of $\sigma_p = 12$ dB is more appropriate, because of the small cell size and expected higher transmitted frequency in microcells.

Finally, a log-normal distribution with small σ_p can be approximated by a Nakagami-m-distribution over the interval $(e^{m_p - 1/4}, e^{m_p + 1/4})$ where m_p is the log-normal mean [36].

3.3.3 Superimposed Envelope Fading and Shadowing Distributions

It has been found, at least in macrocellular systems [46], that superimposing the envelope fading distribution on top of the shadow distribution is a better characterization of the overall distribution of the envelope. Various equivalent forms for Rayleigh, Rician, and Nakgami envelope fading superimposed on log-normal shadowing are summarized in this section.

Rayleigh fading: When voltage samples are used and the shadowing is log-normal, the result is sometimes called the Susuki distribution.

$$\begin{aligned} p_{\mathbf{r}}(r) &= \int_0^\infty \frac{\pi r}{2\overline{r}^2} \exp\left\{-\frac{\pi r^2}{4\overline{r}^2}\right\} \frac{20}{\overline{r}\sigma \ln 10\ \sqrt{2\pi}} \exp\left\{-\frac{(10\log_{10}\overline{r} - m_v)^2}{2\sigma}\right\} d\overline{r} \\ &= \sqrt{\frac{\pi}{8\sigma^2}} \int_{-\infty}^\infty \frac{r}{10^{\overline{r}/10}} \exp\left\{-\frac{\pi r^2}{4 \cdot 10^{\overline{r}/10}}\right\} \exp\left\{-\frac{(\overline{r} - m_v)^2}{2\sigma}\right\} d\overline{r}, \quad \overline{r} \text{ in dB.} \end{aligned} \tag{3.27}$$

Likewise, with power samples, the density of $\mathbf{y} = \mathbf{r}^2$ is

$$\begin{aligned} p_{\mathbf{y}}(y) &= \int_0^\infty \frac{1}{\overline{r^2}} \exp\left\{-\frac{y}{\overline{r^2}}\right\} \frac{10}{\overline{r^2} \ln 10\ \sigma\sqrt{2\pi}} \exp\left\{-\frac{(10\log_{10}\overline{r^2} - m_p)^2}{2\sigma}\right\} d\overline{r^2}, \\ &= \frac{1}{\sigma\sqrt{2\pi}} \int_{-\infty}^\infty \frac{1}{10^{\overline{r^2}/10}} \exp\left\{-\frac{y}{10^{\overline{r^2}/10}}\right\} \exp\left\{-\frac{(\overline{r^2} - m_p)^2}{2\sigma}\right\} d\overline{r^2}, \quad \overline{r^2} \text{ in dB.} \end{aligned} \tag{3.28}$$

Rician fading: With Rician fading, the envelope power distribution is most commonly used, where

$$\begin{aligned} p_{\mathbf{y}}(y) &= \int_0^\infty \frac{K+1}{\overline{r^2}} \exp\left\{-K - \frac{(K+1)y}{\overline{r^2}}\right\} I_0\left(2\sqrt{y}\sqrt{\frac{K(K+1)}{\overline{r^2}}}\right) \\ &\quad \times \frac{1}{\overline{r^2}\sigma_{nats}\sqrt{2\pi}} \exp\left\{-\frac{(\ln\overline{r^2} - m)^2}{2\sigma_{nats}}\right\} d\overline{r^2}. \\ &= \int_0^\infty \frac{K+1}{\overline{r^2}} \exp\left\{-K - \frac{(K+1)y}{\overline{r^2}}\right\} I_0\left(2\sqrt{r^2}\sqrt{\frac{K(K+1)}{\overline{r^2}}}\right) \\ &\quad \times \frac{10}{\overline{r^2}\ln 10\ \sigma\sqrt{2\pi}} \exp\left\{-\frac{(10\log_{10}\overline{r^2} - m_p)^2}{2\sigma}\right\} d\overline{r^2}, \\ &= \frac{1}{\sigma\sqrt{2\pi}} \int_{-\infty}^\infty \frac{K+1}{10^{\overline{r^2}/10}} \exp\left\{-K - \frac{(K+1)y}{10^{\overline{r^2}/10}}\right\} I_0\left(2\sqrt{r^2}\sqrt{\frac{K(K+1)}{10^{\overline{r^2}/10}}}\right) \\ &\quad \times \exp\left\{-\frac{(\overline{r^2} - m_p)^2}{2\sigma}\right\} d\overline{r^2}, \quad \overline{r^2} \text{ in dB.} \end{aligned} \tag{3.29}$$

3.3.4 Path Loss

Empirical path loss prediction methods have been proposed by Okumura, Hata, Ibrahim, Lee, and others. Okumura's model has been adopted by the CCIR for path loss prediction in macrocellular systems. Hata's model is a simplification of Okumura's model and is easy to use. Since Hata's model has some limitations[5], Okumura and Hata's model cannot be used for microcellular systems [4]. Mogensen [30] has proposed a modification to Hata's model for small cell sizes.

Path loss in macrocells is often modeled as being inversely proportional to the α^{th} power of the radio path length d, i.e.,

$$\text{PL}(d) \propto 1/d^\alpha \tag{3.30}$$

In free space $\alpha = 2$, while in macrocellular systems $\alpha \approx 4$. For microcellular systems the presence of LOS could result in a path loss exponent of $\alpha = 2 \sim 3$. Many authors

[5]Hata's model is good only over quasi-smooth terrain. The ranges of the input parameters are: frequency 150-1500 MHz, cell size 1-20 km, base station antenna height 30-200 m, mobile station antenna height 1-10 m

[4, 34, 47] suggest the following two-slope path loss model for for microcells:

$$\mathrm{PL}(d) \propto \frac{1}{d^a(1+d/g)^b} \tag{3.31}$$

This model is good for cell sizes ranging from 200 m to 1 km where $a \simeq 2$, $b = 3.5 \sim 4$. The *break point* g ranges from 150 to 300 m. The break point has been shown to be proportional to the transmitted frequency [21]. In general, path loss increases with higher frequencies. It has been shown that $\mathrm{PL}_{1.8GHZ} = \mathrm{PL}_{900MHZ} + 10$ dB [30]. In the sequel, the parameters used in the two-slope model are: $a = 2$, $b = 3.5$, and $g = 150$ m.

3.4 Downlink Co-channel Interference Analysis for Microcellular Systems

3.4.1 Likely Scenarios and Literature Review

In traditional macrocells (radius greater than 2km), the envelope distribution can be characterized as Rayleigh with log-normal shadowing [26, 25]. Conversely, in microcellular systems, the envelope fading is generally considered Rician [34]. Abu-Dayya [48] also used the Nakagami distribution to describe the envelope distribution.

Both the Rayleigh and Rician (or Nakagami) distributions are needed in microcellular co-channel interference calculations. The following cases for the envelope fading distributions are likely to occur in a microcellular environment.

1. The desired signal is Rician faded and the interferers are Rayleigh faded.

2. The desired signal is Rayleigh faded and the interferers are either Rayleigh or Rician faded. This generally happens when the mobile has moved far enough away from the serving base station so that the desired signal is Rayleigh faded, and some interferers become Rician faded. This may also happen when a mobile rounds the corner of an obstacle, sometimes referred to as the *corner effect.*

3. Both the desired and interfering signals are Rician faded. This case has only been treated in the literature in the absence of shadowing [32].

4. The desired signal is Rayleigh faded, while the co-channel interferers are Nakagami faded.

Tables 3.2 and 3.4.1 summarize the most recent literature for the above cases:

Desired Signal	Single Interferer	Multiple Interferers	Reference
Rice	Rayleigh	Rayleigh	Yao and Sheikh [1]
Rice	Rice	Rice	Muammar [32]
Rice	Nakagami	Nakagami	this report

Table 3.2: Envelope Fading Only

Desired Signal	Single Interferer	Multiple Interferers	Coherent Addition	Reference
Rayleigh	Rayleigh	Rayleigh	No	Linnartz [40]
Rice	Rayleigh	Rayleigh	Yes	Prasad [2]
Rice	Rayleigh	1-Rayleigh, others Rice	No	this report
Rayleigh	Rice	Rayleigh or Rice	No	this report
Rice	Nakagami	Nakagami	No	this report

Table 3.3: Envelope Fading and Shadowing

General Methods for Calculating Co-channel Interference: In general, the probability of co-channel interference with N interferers can be written as [49]:[6]

$$\Pr\left(x_0 < \delta \sum_{i=1}^{N} x_i\right) = 1 - \int_{\beta}^{\infty} p(x_0)dx_0 \int_0^{x_0/\delta} p(x_i)dx_i \cdots \int_0^{\left(x_0/\delta - \sum^{N-1} x_i\right)} p(x_N)dx_N \tag{3.32}$$

where,

$x_0 \triangleq$ desired signal voltage (or power)

$x_i \triangleq i^{th}$ interferer voltage (or power)

[6]The probability of co-channel interference is is also the *outage* at a specified distance from the serving base-station

$$\begin{aligned} \beta &\triangleq \text{minimum signal voltage (or power) required for communication} \\ \delta &\triangleq \text{protection ratio} \\ N &\triangleq \text{number of interferers.} \end{aligned} \tag{3.33}$$

Here, x_0, x_i can be measured in voltage or power. If $\beta = 0$, then the following method used by Linnartz [40] can be used to calculate co-channel interference probability. Let,

$$\begin{aligned} X &= \frac{x_0}{W} \\ Y &= W \end{aligned} \tag{3.34}$$

where

$$W = \sum_{i=1}^{N} x_i \tag{3.35}$$

Then

$$p_{X,Y}(x,y) = \frac{p_{x_0,W}(xy,y)}{J(x_0,W)} \tag{3.36}$$

where $J(x_0, W) = 1/y$ denotes the Jacobian of x_0 and W, so that

$$p_X(x) = \int_0^\infty p_{x_0}(xy) p_W(y) y dy. \tag{3.37}$$

Therefore,

$$P_{\text{out}} \triangleq \Pr\left(\frac{x_0}{W} < \delta\right) = 1 - \int_\delta^\infty p_X(x) dx. \tag{3.38}$$

Alternatively,

$$\begin{aligned} P_{\text{out}} &= \Pr\left(W \geq \frac{x_0}{\delta}\right) \\ &= \int_0^\infty p_{x_0}(x) \int_{x_0/\delta}^\infty p_W(y) dy dx \end{aligned} \tag{3.39}$$

The authors in Table 3.2 have considered the effect of envelope fading for their co-channel interference calculations. A brief review of the envelope fading only case will be discussed in the next section.

3.4.2 Envelope Fading Only

Rayleigh Fading with Rayleigh Interferers: Yao and Sheikh [1] considered a Rician faded desired signal and Rayleigh faded interferers and have derived closed form solutions for the probability of co-channel interference. By using (3.11) for the distribution of the desired signal and (3.8) for the distribution of the interfering signal with

$$\begin{aligned} \overline{r_i^2} &= \overline{r^2} \text{ in (3.8)} \\ \delta &\triangleq \text{protection ratio} \\ b &= \frac{\overline{r_i^2}}{\sigma_r^2} \text{ ratio of scattered powers} \\ K &= \frac{s^2}{2\sigma_r^2} \text{ Rice factor,} \end{aligned}$$

the probability of co-channel interference (which equals the outage probability) for a single interferer is easily found using (3.38) as

$$\mathrm{P_{out}} = \frac{\delta}{\delta + b} \exp\left\{-\frac{Kb}{\delta + b}\right\}. \tag{3.40}$$

The single interferer co-channel interference probability is plotted in Figure 3.8. It is apparent from the graph that the Rice factor K of the desired signal has a significant effect on the outage probability. This result will also be true when shadowing is added in the sequel.

If multiple interferers with independent powers ($\overline{r_i^2}$) are present, then the distribution of co-channel interference can be written as

$$p_y(y) = \sum_{i=1}^{N} \overline{r_i^2} \exp\left(-\frac{y}{\overline{r_i^2}}\right) \prod_{\substack{j=1 \\ j \neq i}}^{N} \frac{1}{\overline{r_i^2} - \overline{r_j^2}}, \tag{3.41}$$

so that using (3.38) for $\Pr(x_0 < \delta \sum_i x_i)$ yields,

$$\mathrm{P_{out}} = 1 - \sum_{i=1}^{N} \left\{1 - \frac{\delta}{\delta + b_i} \exp\left(-\frac{Kb_i}{\delta + b_i}\right)\right\} \prod_{\substack{j=1 \\ j \neq i}}^{N} \frac{b_j}{\overline{b_i^2} - \overline{b_j^2}} \tag{3.42}$$

where, $b_i = \sigma_r^2 / \overline{r_i^2}$. Since b_i is different for each interferer (3.42) cannot be plotted unless some further assumptions are made. Yao makes the simplifying assumption

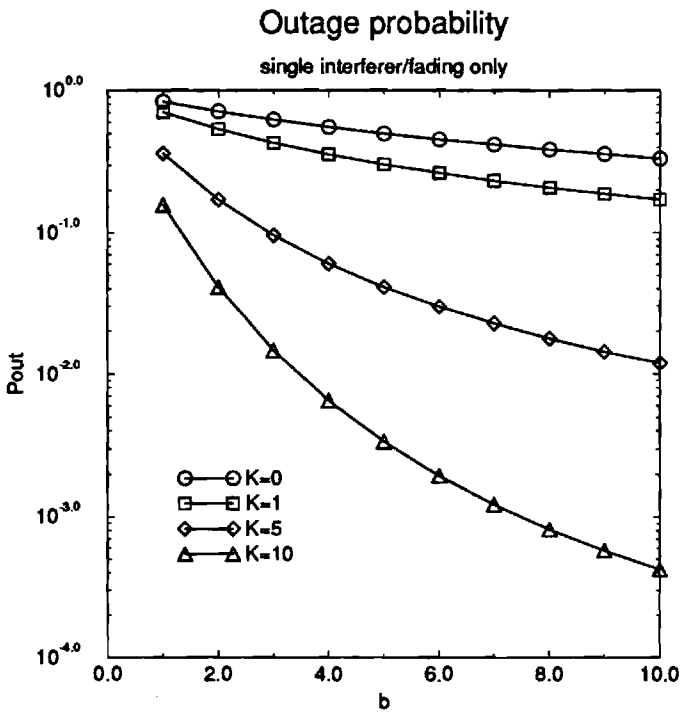

Figure 3.8: Probability of co-channel interference (outage P_{out}) with a single interferer

that the powers ($\overline{r_i^2}$) are all equal and numerical results for this case are shown in Figure 3.9.

In summary, Yao and Sheikh showed that the Rice factor K of the desired signal has a large effect on the outage probability for the single interferer case. They further conclude that additional interferers have little additional effect under the assumption that they all have equal powers ($\overline{r_i^2}$).

Rician fading with Rician interferers: Muammar [32] has examined the case where both the desired signal and the interfering signals are Rician faded. He claims to have a closed form solution for the probability of co-channel interference. However, the closed form solution is derived in terms of three infinite summations.[7] Therefore, only his conclusions without any specific equations are reported here.

Muammar was able to show that the system capacity in microcells should be higher, since, for a given protection ratio and reuse distance, the co-channel inter-

[7]Very often an infinite summation can be replaced by an integral.

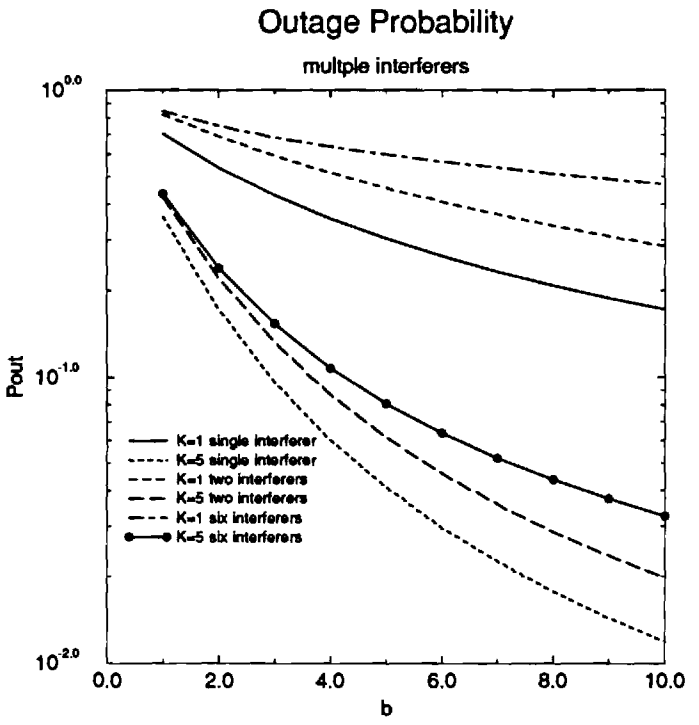

Figure 3.9: Probability of co-channel interference (outage P_{out}) with a multiple interferers, from [1].

ference is smaller. This was also seen in Yao and Sheikh's work. Furthermore, he was able to give lower and upper bounds on the probability of co-channel interference for particular values of the Rice factor. Contrary to intuition, he also observed a high level of co-channel interference near the serving base station. In addition, as the Rice factors of the interferers increased, the co-channel interference increased. For instance, if the difference in the power levels between desired and interfering signal is 35 dB, and the protection ratio is 10 dB, then the probability of co-channel interference is $P_{\text{out}} = 0.07$, for $K = -7$ dB, $K_i = -15$dB, and $P_{\text{out}} = 0.02$ for $K = -11$ dB and $K_i = -4$ dB. Unfortunately, Muammar did not consider shadowing at the time, but mentions it as future research.

Rician fading with Nakagami interferers: By using the distribution for the interferer power $\mathbf{y}$ in (3.17) and assuming that all interferer powers are independent

and identically distributed, the density of $W = \sum_{i=1}^{N} y_i$ is

$$p_W(y) = \left(\frac{m}{\Omega_I}\right)^{mN} \frac{y^{mN-1}}{\Gamma(mN)} \exp\left\{-\frac{my}{\Omega_I}\right\} \tag{3.43}$$

Using equation (3.39)

$$\int_{x_0/\delta}^{\infty} p_W(y)dy = \sum_{h=0}^{mN-1} (\frac{m}{\Omega_I \delta})^h \frac{x_0^h}{h!} \exp\left\{-\frac{mx_0}{\Omega_I \delta}\right\} \tag{3.44}$$

Then

$$\begin{aligned} P_{\text{out}} &= \int_0^{\infty} \frac{1}{2\sigma_r^2} \exp\left\{-\frac{y+s^2}{2\sigma_r^2}\right\} I_0\left(\frac{\sqrt{ys^2}}{2\sigma_r^2}\right) \sum_{h=0}^{mN-1} \left(\frac{m}{\Omega\delta}\right)^h \frac{y^h}{h!} \exp\left\{-\frac{my}{\Omega\delta}\right\} dy \\ &= \sum_{t=0}^{\infty} \sum_{h=0}^{mN-1} \frac{e^{-k}}{(t!)^2} \frac{(h+t)!}{h!} \left(\frac{k}{1+A}\right)^t \frac{A^h}{(1+A)^{h+1}} \end{aligned} \tag{3.45}$$

where

$$A = \frac{m\text{CIR}}{\delta(k+1)} \tag{3.46}$$

and

$$\text{CIR} = \frac{(K+1)2\sigma_r^2}{\Omega_I} \tag{3.47}$$

Here CIR is the ratio of the average desired signal power and the average power of an individual interferer. Figures 3.10-3.12 plot P_{out} as a function of CIR while varying the Rice factor K of the desired signal, the m values of the interfering signals, the protection ratio δ, and the number of interferers N. The outage P_{out} is sensitive to all of the above parameters, except for the m values of the interfering signals as seen in Figure 3.12. The reason is that outages are largely due to the fading of the desired signal rather than the fading of the interference signals. Figure 3.13 shows the required CIR to achieve an outage of 10^{-3} as a function of the Rice factor when $N = 6$ interfering signals are present.

3.4.3 Shadowing Only

The effects of fading can be mitigated by using microscopic diversity techniques such as antenna diversity [25]. If enough diversity branches are used, the fading will be effectively eliminated leaving a shadowed signal. In practice this would require a prohibitively large number of diversity branches so that some residual fading will always

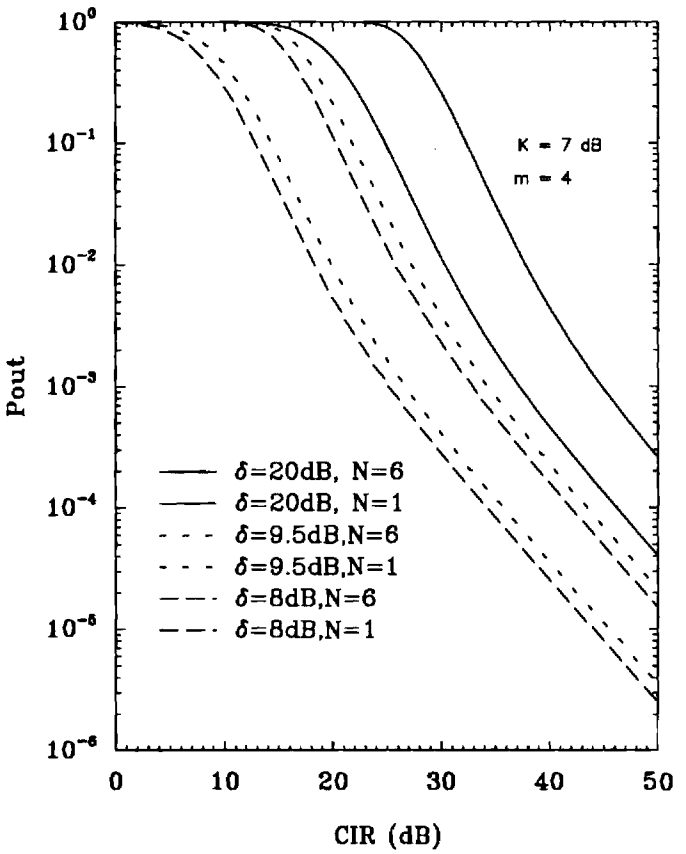

Figure 3.10: Probability of co-channel interference for different protection ratios and different numbers of interferers

remain. However, the analysis of the shadowing only case is useful for determining the effect of fading on the probability of co-channel interference. Usually, the shadowing of the desired signal and co-channel interferers is partially correlated [50]. However, uncorrelated shadowing will give worst case results, so our treatment is restricted to this case. Define the following:

$$\begin{aligned} y_{d\,\mathrm{dB}} &= 10\log_{10} y_d \\ y_{I\,\mathrm{dB}} &= 10\log_{10} y_I \\ \delta_{\mathrm{dB}} &= 10\log_{10}\delta \end{aligned}$$

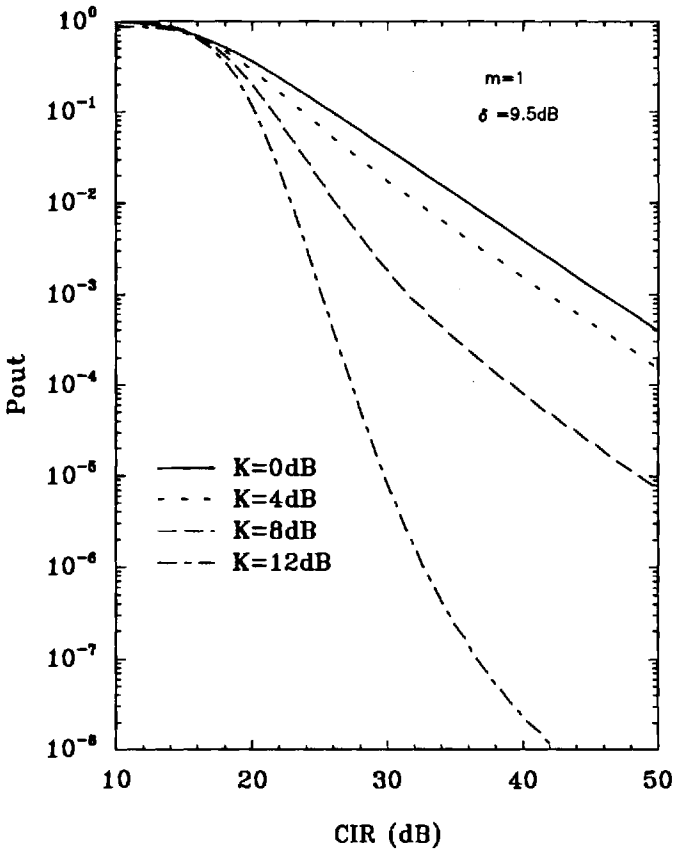

Figure 3.11: Probability of co-channel interference for different K factors

where $\mathbf{y}_d$ and $\mathbf{y}_I$ are the squared envelopes of the desired and interfering signals, respectively. It follows from Section 3.3.2 that with log-normal shadowing

$$p(\mathbf{y}_{\mathrm{dB}}) = \frac{1}{\sqrt{2\pi}\sigma_p}\exp\left\{-\frac{\mathbf{y}_{\mathrm{dB}} - m_{p\ \mathrm{dB}})^2}{2\sigma_p^2}\right\} \tag{3.48}$$

Since shadowing is primarily a function of the topography near to the mobile [12, 14, 38], the same dB spread has been assumed for the desired and interfering signals. A shadow standard deviation of 12 dB is appropriate for microcells.

Using an analysis similar to that in [37, 12] the following expression can be obtained for the probability of co-channel interference:

$$\begin{aligned} P_{\mathrm{out}} = \Pr(\mathbf{y}_{d\ \mathrm{dB}} - \mathbf{y}_{I\ \mathrm{dB}} < \delta_{\mathrm{dB}}) &= \frac{1}{\sqrt{2\pi}}\int_{-\infty}^{-V} e^{-z^2/2}dz \\ &\triangleq Q(V) \end{aligned} \tag{3.49}$$

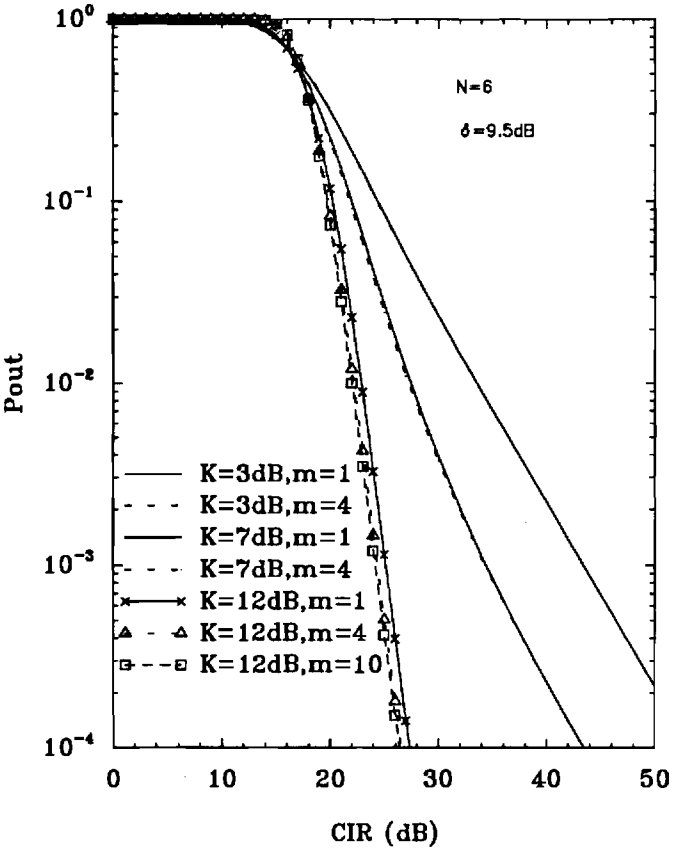

Figure 3.12: Probability of co-channel interference for different K factors and m values in the Nakgami-m distribution.

where

$$V = \frac{m_{d\ \mathrm{dB}} - m_{I\ \mathrm{dB}} - \delta_{dB}}{\sqrt{2\sigma_p^2}}$$
$$m_{d\ \mathrm{dB}} - m_{I\ \mathrm{dB}} = 10\log_{10}\left(\frac{m_d}{m_I}\right) \tag{3.50}$$

If a single interferer is present and the path loss is described by the two-slope model in (3.31), then

$$\frac{m_d}{m_I} = \frac{d_I^a(1+\frac{d_I}{g})^b}{d_d^a(1+\frac{d_d}{g})^b} \tag{3.51}$$

where d_d and d_I are the radio path lengths to the serving and interfering base stations, respectively. The co-channel interference can be expressed as a function of co-channel re-use factor D/R. Here we consider the worst case single interferer situation, where

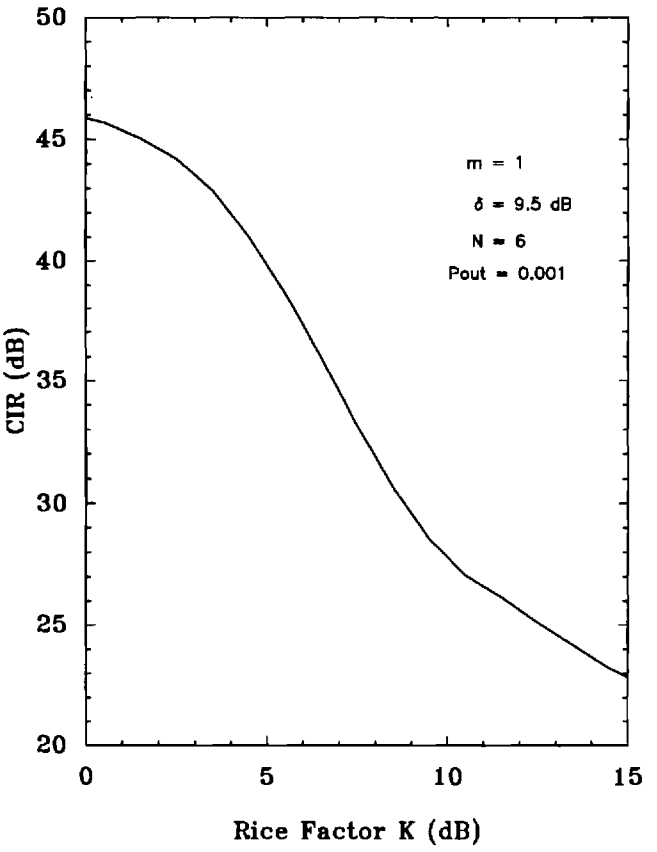

Figure 3.13: CIR against the Rice factor for $P_{\text{out}} = 10^{-3}$.

the mobile is located at the egde or corner of the cell so that $d = R$ and $d_I = D - R = R(q-1)$. Suppose that $\sigma_p = 12$ dB. Then Fig. 3.14 shows the probability of co-channel interference for different protection ratios. Fig. 3.15 plots the probability of co-channel interference for a protection ratio of 9.5 dB and different cell sizes.

For multiple interferers we can use the method suggested by Schwartz and Yeh [51, 13] to find an approximate log-normal distribution for the sum of multiple log-normal interferers. The first tier of six co-channel interferers will contribute most of the co-channel interference. Therefore, only the first tier interferers is considered, and it is assumed that the shadowing of these interferers is mutually uncorrelated and that they are all equidistant. By using Schwartz and Yeh's method the mean and standard deviation of the approximate log-normal distribution is calculated iteratively from the individual means and standard deviations of the interferers. The resulting

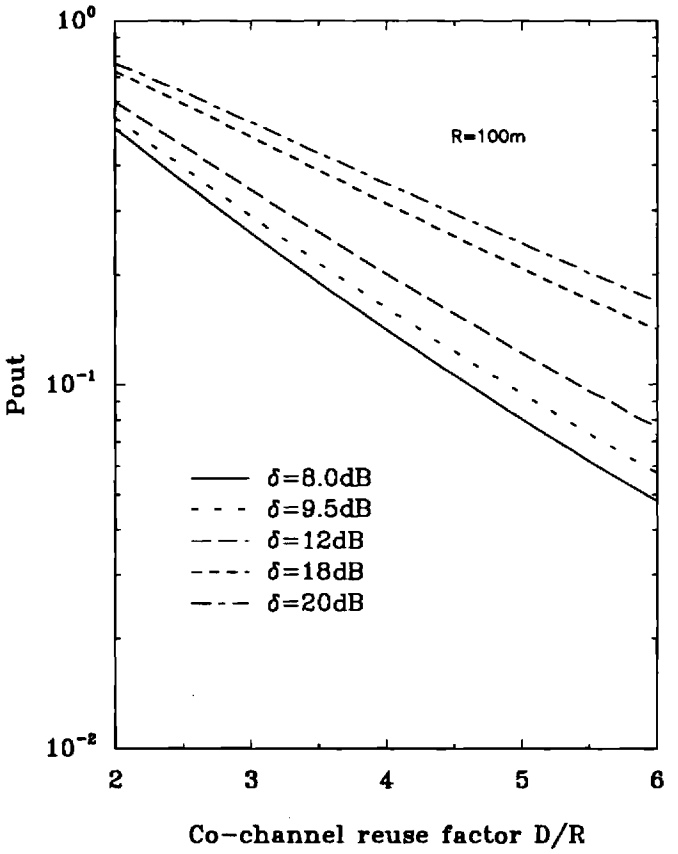

Figure 3.14: Probability of co-channel interference against the co-channel reuse factor for different protection ratios; $a = 2,\ b = 3.5,\ R = 100$ m.

parameters for the log-normal distribution are shown in Table 3.4.3 if the interferer means $m_{I\ \mathrm{dB}}$ are normalized to 0 dB. The values in Table 3.4.3 include the mean $\tilde{m}_I$ and standard deviation $\tilde{\sigma}_p$ of new approximate log-normal distribution.

When the number of interferers increasers, the mean of the sum increases while the variance of the sum decreases. Fig. 3.16 plots the probability of co-channel interference against $m_d - m_I - \delta_{dB}$. For more interferers m_I increases, resulting in a larger probability of co-channel interference.

3.4.4 Shadowing with Rician or Rayleigh Fading

A variety of papers are available which cover Rayleigh fading and log-normal shadowing in the macrocell environment [40, 49, 39, 12]. However, the only literature to

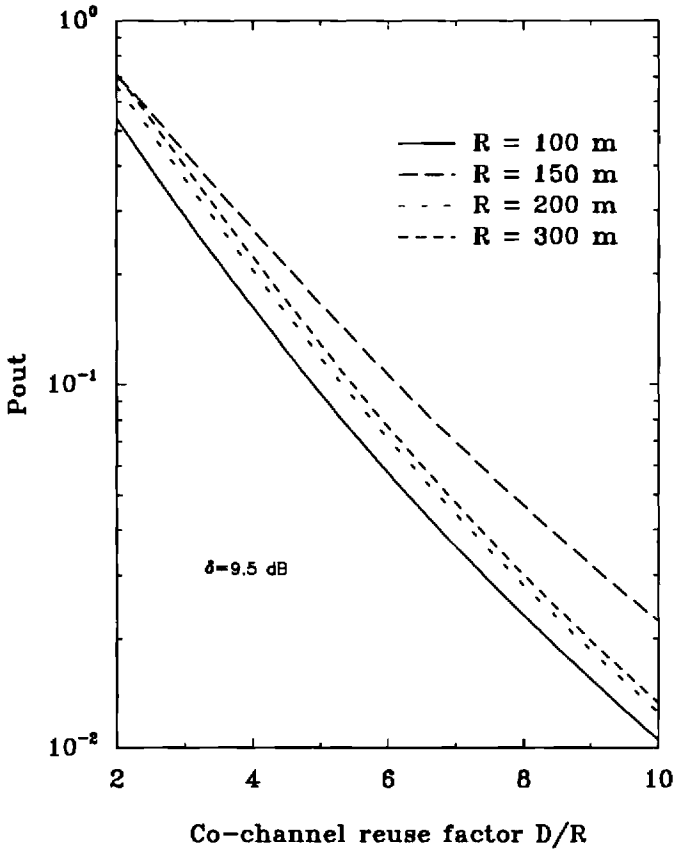

Figure 3.15: Probability of co-channel interference against the co-channel reuse factor for different cell sizes; $a = 2, b = 3.5$.

include both Rician fading and log-normal shadowing has been due to Prasad [2]. This may attributed to the fact that microcellular propagation characterized by Rician fading superimposed on log-normal shadowing is not very clearly portrayed in literature. Nevertheless, we will assume that this is a valid characterization.

Coherently Adding Interferers: Prasad [2], makes a simplifying assumption that the interferers add coherently so that if each x_i is Rayleigh faded with log-normal shadowing then the sum

$$\sum_{i=1}^{N} x_i \tag{3.52}$$

is also Rayleigh faded and shadowed. The distribution of shadowing in this case is the convolution of the N independent log-normal random variables. Schwartz and Yeh

n	1	2	3	4	5	6
$\tilde{m}_I$ (dB)	0.0000	7.4525	11.2003	13.6173	15.3723	16.7385
$\tilde{\sigma}_p$ (dB)	12.0000	9.5817	8.3972	7.6570	7.1342	6.7376

Table 3.4: Mean and standard deviation of the approximate log-normal distribution for the sum of N log-normal interferers. The interferers have a means of zero dB [2].

[38] have shown that the convolution of N independent log-normal random variables can be approximated by another log-normal random variable for values of σ that are typically found in cellular radio applications; see Table 3.4.3. Hence, the overall signal distribution of the sum of the interfering signals can be represented in the same form as a single interferer.

Coherent addition of the interfering signals rarely occurs in a mobile radio environment, because the multipath-fading channel characteristics cause the signals to arrive with random and rapidly time-variant phases. Hence, it is more realistic to assume that signals will add incoherently. The single interferer case, along with a new method for evaluating the probability of co-channel interference for incoherently adding interferers is presented in the next section.

Noncoherently Adding Interferers: This section derives the new results mentioned in Table 3.4.1. If the x_i are Rician or Rayleigh random variables then writing

$$x_0 < \delta \sum_{i=1}^{N} x_i \tag{3.53}$$

in terms of power samples $\lambda_i = x_i^2$ yields,

$$\lambda_0 < \delta \sum_{i=1}^{N} \lambda_i \tag{3.54}$$

where each of the λ_i are either exponential or non-central chi-square random variables with log-normally distributed means. Given that the $\{\lambda_i\}_{i=0}^{N}$ denote envelope power samples, (3.54) can be manipulated to assure that an exponentially distributed random variable ψ_0 is on the left hand side and all the rest of the random variables

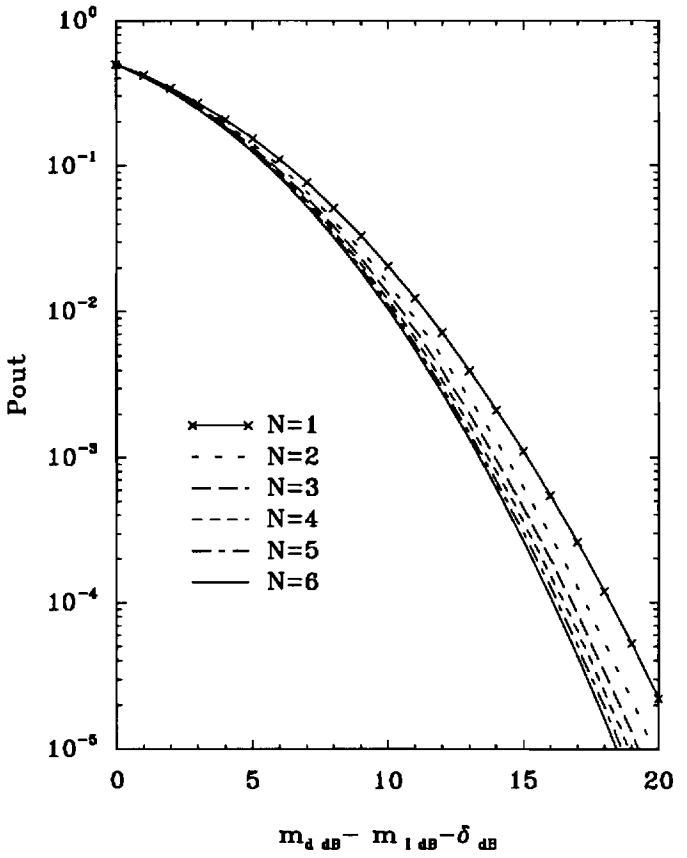

Figure 3.16: Probability of co-channel interference for different numbers of interferers.

are on the right hand side. Hence[8]

$$\psi_0 < \sum_{i=1}^{N} \alpha_i \psi_i \tag{3.55}$$

where ψ_0 is exponentially distributed and the $\{\psi_i\}_{i=1}^{N}$ are either exponentially or non-central chi-square distributed. Furthermore, $\alpha_i \in \{\delta, -1/\delta\}$ are appropriate constants.

Define the random variables X and Y as

$$X = \frac{\psi_0}{W} \tag{3.56}$$

$$Y = W \tag{3.57}$$

[8]Here $\psi_0 \ldots \psi_N$ are simply a convenient re-ordering of $\lambda_0 \ldots \lambda_N$.

where

$$W = \sum_{i=1}^{N} \alpha_i \psi_i. \tag{3.58}$$

Then the joint probability density function of X and Y is

$$p_{X,Y}(x,y) = \frac{p_{\psi_0,W}(xy,y)}{J(\psi_0,W)} \tag{3.59}$$

where $J(\psi_0,W) = 1/y$ denotes the Jacobian of ψ_0 and W, so that

$$p_X(x) = \int_{-\infty}^{\infty} p_{\psi_0}(xy) p_W(y) y dy. \tag{3.60}$$

Therefore,

$$\Pr\left(\frac{\psi_0}{W} < 1\right) = 1 - \int_1^{\infty} dx \int_{-\infty}^{\infty} p_{\psi_0}(xy) p_W(y) y dy. \tag{3.61}$$

After substituting the probability density function for $p_{\psi_0}(xy)$ and integrating with respect to x, the conditional probability that $\frac{\psi_0}{W} < 1$ given $\Psi_0 = \mathrm{E}[\psi_0]$ is

$$\Pr\left(\frac{\psi_0}{W} < 1 | \Psi_0\right) = 1 - \int_{-\infty}^{\infty} \exp\left\{-\frac{y}{\Psi_0}\right\} p_W(y) dy. \tag{3.62}$$

Using the novel method described by Linnartz [40], (3.62) can be simplified by using Laplace transform techniques. Given that the $\{\psi_i\}_{i=1}^N$ are independent, $p_W(y)$ in (3.62) is simply the convolution of the densities of the random variables $\{\alpha_i \psi_i\}_{i=1}^N$. Therefore, the integral in (3.62) becomes

$$\int_{-\infty}^{\infty} \left\{ \frac{p_{\psi_1}(y/\alpha_i)}{|\alpha_1|} * \cdots * \frac{p_{\psi_n}(y/\alpha_n)}{|\alpha_n|} \right\} e^{-vy} dy \tag{3.63}$$

where $*$ denotes convolution, and $v = \frac{1}{\Psi_0}$. If

$$F_{\psi_i}(v) = \mathcal{L}\left\{p_{\psi_i}(y)\right\} \tag{3.64}$$

where $\mathcal{L}\{\cdot\}$ denotes the Laplace transform, then after some algebra (3.63) can be written as,

$$\prod_{i=1}^{n} F_{\psi_i}(\alpha_i v). \tag{3.65}$$

Hence, (3.62) reduces to

$$\Pr\left(\frac{\psi_0}{W} < 1 | \Psi_0\right) = 1 - \prod_{i=1}^{n} F_{\psi_i}(\alpha_i v), \tag{3.66}$$

where

$$\begin{aligned} F_{\psi_i}(v) &= \mathcal{L}\{p_{\psi_i}(y)\} \\ &= \int_{-\infty}^{\infty} e^{-vy} \int_0^{\infty} p_{\psi_i}(y)dy \\ &= \int_{-\infty}^{\infty} e^{-vy} \int_0^{\infty} \frac{K_i+1}{\Psi_i} \exp\left\{-K_i - \frac{y(K_i+1)}{\Psi_i}\right\} \\ &\qquad \times I_0\left(2\sqrt{\frac{yK_i(K_i+1)}{\Psi_i}}\right) p_{\Psi}(\Psi_i)\mathrm{d}\Psi_i\mathrm{d}y \\ &= \int_0^{\infty} \frac{K_i+1}{K_i+1+v\Psi_i} \exp\left\{-\frac{v\Psi_i K_i}{K_i+1+v\Psi_i}\right\} p_{\Psi}(\Psi_i)d\Psi_i, \end{aligned} \tag{3.67}$$

with $p_{\Psi}(\Psi_i)$ given by (3.18) with $\overline{r^2} = \Psi$. Averaging over Ψ_0 yields the final result:

$$\Pr\left(\frac{\psi_0}{W} < 1\right) = 1 - \int_0^{\infty} \frac{1}{\sqrt{2\pi}\sigma_0\Psi_0} \exp\left\{-\frac{(\ln(\Psi_0) - m_0)^2}{2\sigma_0^2}\right\} \left(\prod_{i=1}^{n} F_{\psi_i}(v\alpha_i)\right) d\Psi_0 \tag{3.68}$$

Equation (3.68) can be computed using the numerical method of Gauss-Hermite Quadrature integration. A brief summary of this integration method is provided in Appendix 3A.

The single interferer case: Two possible scenarios are examined in this case. The first scenario occurs when the desired signal power is non-central chi-square distributed (3.12) (Rician fading) and the interfering signal power is exponentially distributed (3.8) (Rayleigh fading). In this case (3.68) can be used since

$$\Pr\left(\frac{\psi_0}{\delta\psi_1} < 1\right) = \Pr\left(\frac{\psi_1}{\frac{\psi_0}{\delta}} > 1\right). \tag{3.69}$$

Swapping the role of ψ_0 and ψ_1 in (3.68), along with $\alpha_i = \frac{1}{\delta}$, gives the probability of co-channel interference as:

$$P_{\text{out}} = \Pr\left(\frac{\psi_1}{\frac{\psi_0}{\delta}} < 1\right) = \int_0^{\infty} \frac{1}{\sqrt{2\pi}\sigma_1\Psi_1} \exp\left\{-\frac{(\ln(\Psi_1) - m_1)^2}{2\sigma_1^2}\right\} F_{\psi_0}(\frac{1}{\Psi_1\delta})d\Psi_1. \tag{3.70}$$

A plot of the co-channel interference probability for various values of the Rice factor of the desired signal is shown in Figure 3.17. It is apparent from Figure 3.17 that the Rice factor of the desired signal has a significant effect on the probability of co-channel interference (outage).

In the second scenario, the desired signal is Rayleigh faded while the interfering signal is Rician faded. In this case, (3.68) can be used directly with $n = 1$, $\alpha_i = \delta$. Figure 3.18 summarizes the results for this case and shows that the Rice factor of the interfering signal has little effect on the probability of co-channel interference.

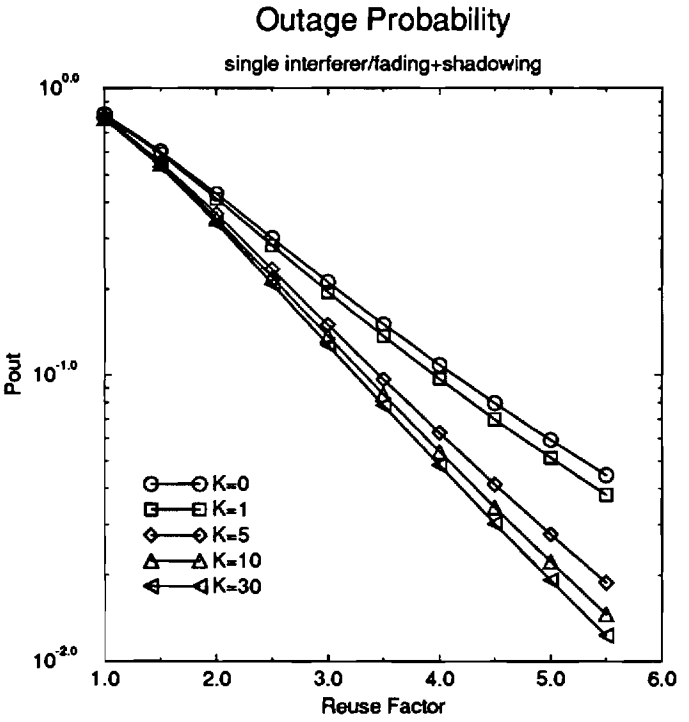

Figure 3.17: Probability of co-channel interference for a Rician faded desired signal with a Rayleigh faded interferer.

Multiple Interferers: In this case, (3.68) can be used directly if the desired signal is Rayleigh faded. Linnartz [40] examined the special case when all of the interferers are also Rayleigh faded. The last section showed that the Rice factor of the interfering signals had little effect on the probability of co-channel interference; hence, interfering signals that are either Rayleigh or Rician faded, can be approximated as Rayleigh faded interferers. With this assumption, the outage with n Rayleigh faded interferers is shown in Figure 3.19. This plot shows the obvious result that the number of interferers has a significant effect on the outage.

When the desired signal is Rician faded and interferers are either Rayleigh or

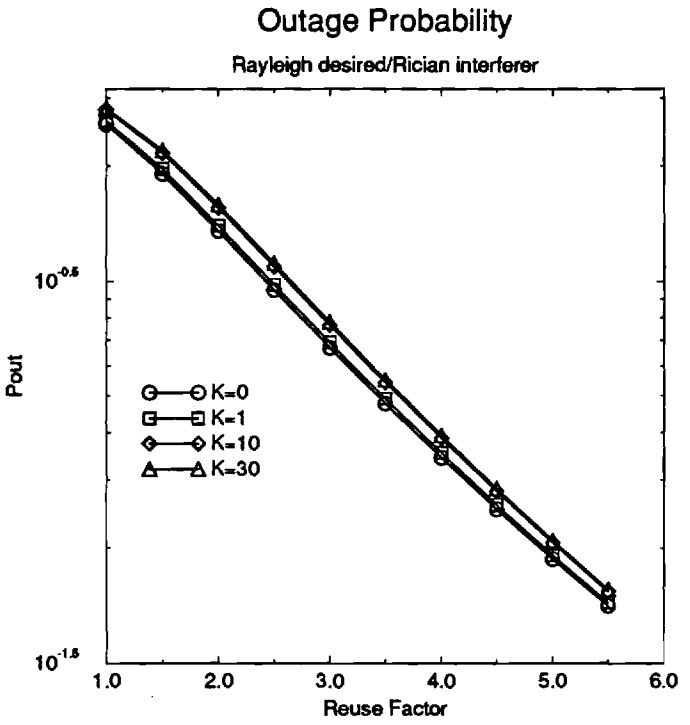

Figure 3.18: Probability of co-channel interference for a Rayleigh faded desired signal with a Rician faded interferer.

Rician faded a difficulty arises in obtaining numerical results for (3.68). Although (3.68) obviously exists, numerical imprecision arises because some of the α_i's are negative. Under this condition, one part of the integrand increases exponentially while the other part decreases exponentially, thereby creating the precision problem. This computational difficulty was surpassed by using a software package from the University of Waterloo, Canada, called **Maple**, which allows arbitrary precision arithmetic. Forty significant digits were sufficient for two interferers. However, time considerations precluded results for more than two interferers. The preliminary results for $n = 2$ are shown in Figure 3.20. As in the single interferer case, the Rice factor of the desired signal has a significant effect on the outage probability.

3.4.5 Shadowing with Rician and Nakagami Fading

Suppose that 60° cell sectoring is used so that there is just one predominant co-channel interferer. The probability of co-channel interference for this case has been

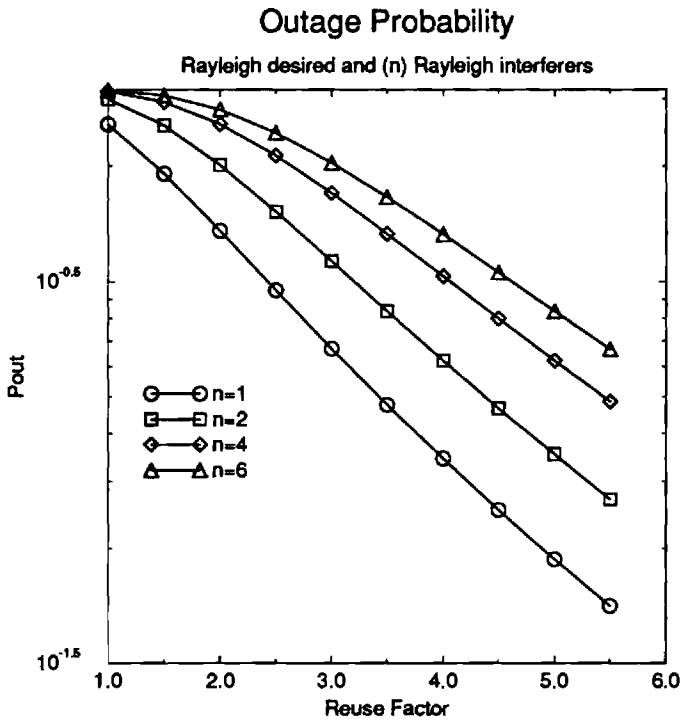

Figure 3.19: Outage for Rayleigh faded desired signal and n Rayleigh interferers.

derived in Appendix 3B and is:

$$P_{\text{out}} = \sum_{t=0}^{\infty} \sum_{h=0}^{m-1} \frac{e^{-k}}{(t!)^2} \frac{(h+t)!}{h!} \frac{k^t b}{\sqrt{\pi} c^{t+1}} \int_0^{\infty} \frac{u^{h-1}}{(\frac{1}{c}+u)^{h+t+1}} e^{-(b \ln u)^2} du \tag{3.71}$$

where

$$\begin{aligned} b &= \frac{5}{\sigma \ln 10} \\ c &= \frac{mf}{(k+1)\delta} \\ f &= = \frac{d_I^a (1+\frac{d_I}{g})^b}{d_d^a (1+\frac{d_d}{g})^b} \end{aligned}$$

Fig 3.21 compares the cases of log-normal shadowing only and Nakagami fading plus log-normal shadowing. It is apparent that fading contributes significantly to the probability of co-channel interference.

3.5 Future Research on Hand-off Problems

As suggested in Section 3.2, the mathematical framework for hand-off analysis is very similar to that for co-channel interference analysis. This section states some

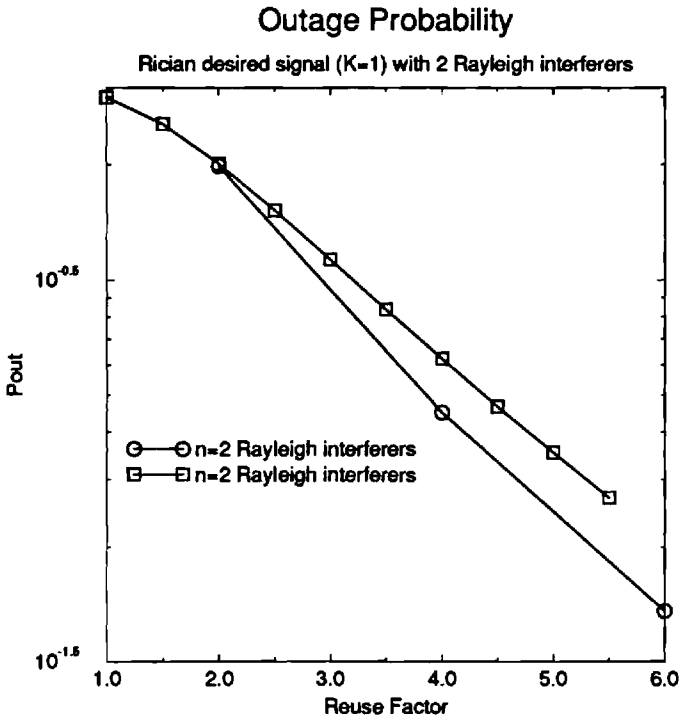

Figure 3.20: Probability of co-channel interference for a Rician faded desired signal with two Rayleigh faded interferers.

preliminary ideas on how carrier-to-interference ratio (CIR), and signal strength based hand-off algorithms could be analyzed with the aid of the co-channel interference analysis that has been presented.

Assuming that a mobile can measure the CIR of at least the serving base station, a hand-off decision is determined by the comparison of this measurement to the protection ratio. Analysis of a hand-off algorithm based on this method can be made directly by using the co-channel interference analysis that has been presented.

Because of fading, it is likely that a CIR based hand-off algorithm will employ some sort of average CIR statistic for the hand-off decisions. Analysis of a running sum average is not possible using the co-channel interference methodology that is suggested in this report, because using (3.68) will require the transfer of some samples from one side of the equation to the other, resulting in the aforementioned numerical precision difficulties. However, an M-of-N averaging method may be analytically feasible under the following simplifying assumptions.

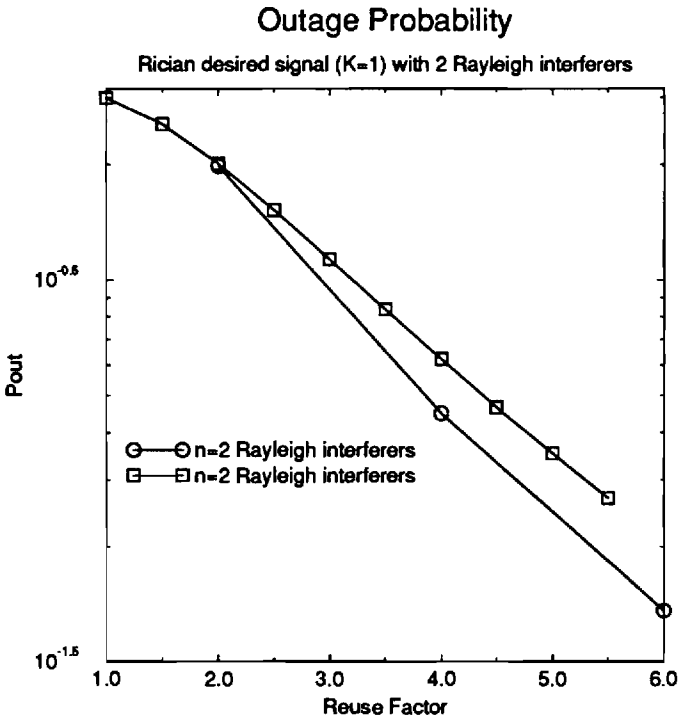

Figure 3.21: Comparison of the probability of co-channel interference for the cases of log-normal shadowing only and Nakagami fading superimposed on log-normal shadowing.

1. the envelope samples are affected by independent fading

2. the interferers have independent shadowing with respect to each other and over each of the N samples

3. the desired signal Ψ_0 has constant shadowing over the N samples.

Under these assumptions, the probability that M out of N samples are below the protection ratio is,

$$\binom{N}{M} \int_{R_{\Psi_0}} \Big(\Pr(CIR < \delta)\Big)^M \times \Big(1 - \Pr(\text{CIR} < \delta)\Big)^{M-N} p_{\Psi}(\Psi_0) d\Psi_0. \qquad (3.72)$$

An M-of-N signal strength based averaging hand-off algorithm can also be analyzed by using a similar approach.

3.6 Conclusions

In this section, methods for predicting co-channel interference in microcells were presented. Models for the signal envelope and the squared envelope distributions were discussed that accounted for the effects of fading and shadowing separately, and fading superimposed on top of shadowing.

This section extended the current theory in this area by presenting a new exact analytical method for calculating the co-channel interference under shadowed Rician/Rayleigh/Nakagami faded signals. Results were presented for the single interferer case, which showed that the Rice factor of the interferers had little effect on the probability of co-channel interference, whereas the Rice factor of the desired signal had a significant effect on the probability of co-channel interference. The same behavior was noticed in the case of two interferers. There are many problems that require further work, such as a study to determine the number of tiers of interferers that we should consider in microcellular systems, the probability of co-channel interference for indoor microcells, and the characterization of co-channel interference in special microcell structures such as lineal microcells.

A short discussion on the similarities between the analysis of co-channel interference and the analysis of hand-off algorithms was discussed. Future research on the application of co-channel interference methods to the evaluation of CIR or signal strength based averaging hand-off algorithms is recommended.

3.7 Appendices

Appendix 3A

HERMITE-GAUSS QUADRATURE INTEGRATION

The Hermite-Gauss Quadrature method of integration uses the following approximation

$$\int_{-\infty}^{\infty} f(x)e^{-x^2}dx \approx \sum_{i=1}^{m} H_i f(x_i) + E \tag{3A.1}$$

where,

$$x_i \triangleq \text{ the } i^{th} \text{ zero of } H_m(x)$$

$$H_m(x) \triangleq \text{the } m^{th} \text{ Hermite polynomial}$$
$$E \triangleq \text{approximation error}$$
$$H_i = \frac{2^{m+1}m!\pi}{H_{m+1}^2(x_i)} \tag{3A. 2}$$

$H_m(x)$ can be calculated from the recursion

$$H_0(x) = 1 \tag{3A. 3}$$
$$H_{m+1}(x) = 2xH_m(x) - 2mH_{m-1}(x). \tag{3A. 4}$$

Appendix 3B

Derivation of Equation (3.71)

For just single interfer affected by Nakagami fading only, the probability of co-channel interference is given by Eq. (3.45):

$$P_{\text{out}} = \sum_{t=0}^{\infty}\sum_{h=0}^{m-1}\frac{e^{-k}}{(t!)^2}\frac{(h+t)!}{h!}\left(\frac{k}{1+A}\right)^t\frac{A^h}{(1+A)^{h+1}} \tag{3B.1}$$

If the Nakagami fading is superimposed on log-normal shadowing, then

$$\begin{aligned} P_{\text{out}} &= \int_{-\infty}^{\infty}\int_{-\infty}^{\infty}\sum_{t=0}^{\infty}\sum_{h=0}^{m-1}\frac{e^{-k}}{(t!)^2}\frac{(h+t)!}{h!}\left(\frac{k}{1+A}\right)^t\frac{A^h}{(1+A)^{h+1}} \\ &\quad \frac{1}{2\pi\sigma_p^2}e^{-\frac{(\mathbf{y}_{d\ \mathrm{dB}}-m_{d\ rmdB})^2+(\mathbf{y}_{I\ \mathrm{dB}}-m_{I\ rmdB})^2}{2\sigma_p^2}}d\mathbf{y}_{d\ \mathrm{dB}}d\mathbf{y}_{I\ \mathrm{dB}} \\ &= \sum_{t=0}^{\infty}\sum_{h=0}^{m-1}\frac{e^{-k}}{(t!)^2}\frac{(h+t)!}{h!}\frac{k^t}{2\pi\sigma_p^2} \\ &\quad \int_{-\infty}^{\infty}\int_{-\infty}^{\infty}\frac{A^h}{(1+A)^{h+t+1}}e^{-\frac{(\mathbf{y}_{d\ \mathrm{dB}}-m_{d\ rmdB})^2+(\mathbf{y}_{I\ \mathrm{dB}}-m_{I\ rmdB})^2}{2\sigma_p^2}}d\mathbf{y}_{d\ \mathrm{dB}}d\mathbf{y}_{I\ \mathrm{dB}} \end{aligned} \tag{3B. 2}$$

where

$$A = \frac{mf}{\delta(k+1)}$$
$$f \triangleq 10^{\frac{m_{d\ \mathrm{dB}}-m_{I\ \mathrm{dB}}}{10}} = \frac{d_I^a(1+\frac{d_I}{g})^b}{d_d^a(1+\frac{d_d}{g})^b}$$

Let $\mathbf{y}_{d\ \mathrm{dB}} - m_{d\ rmdB}$, $\mathbf{y}_{I\ \mathrm{dB}} - m_{I\ rmdB}$. Then the double integral in the above equation is:

$$\begin{aligned}
\mathrm{DI} &= \int_{-\infty}^{\infty}\int_{-\infty}^{\infty} \frac{(\frac{m}{(k+1)\beta}10^{\frac{Y_1+m_{d\ \mathrm{dB}}-Y_2-m_{I\ \mathrm{dB}}}{10}})^h}{(1+\frac{m}{(k+1)\beta}10^{\frac{Y_1+m_{d\ \mathrm{dB}}-Y_2-m_{I\ \mathrm{dB}}}{10}})^{h+t+1}} e^{-\frac{Y_1^2+Y_2^2}{2\sigma_p^2}} dY_1 dY_2 \\
&= \int_{-\infty}^{\infty}\int_{-\infty}^{\infty} \frac{(\frac{mf}{(k+1)\beta}10^{\frac{Y_1-Y_2}{10}})^h}{(1+\frac{mf}{(k+1)\beta}10^{\frac{Y_1-Y_2}{10}})^{h+t+1}} e^{-\frac{Y_1^2+Y_2^2}{2\sigma_p^2}} dY_1 dY_2
\end{aligned}$$

Let

$$\begin{aligned}
Y_1 &= \frac{x+z}{\sqrt{2}},\ \ Y_2 = \frac{x-z}{\sqrt{2}} \\
u &= 10^{\frac{\sqrt{2}z}{10}} = e^{\frac{\sqrt{2}z}{10}(\ln 10)} \\
c &= \frac{mf}{(k+1)\beta}
\end{aligned}$$

Then

$$\begin{aligned}
\mathrm{DI} &= \int_{-\infty}^{\infty}\int_{-\infty}^{\infty} \frac{(\frac{mf}{(k+1)\beta}10^{\frac{\sqrt{2}z}{10}})^h}{(1+\frac{mf}{(k+1)\beta}10^{\frac{\sqrt{2}z}{10}})^{h+t+1}} e^{-\frac{x^2+z^2}{2\sigma_p^2}} dx dz \\
&= \sqrt{2\pi}\sigma_p \int_{-\infty}^{\infty} \frac{(\frac{mf}{(k+1)\beta}10^{\frac{\sqrt{2}z}{10}})^h}{(1+\frac{mf}{(k+1)\beta}10^{\frac{\sqrt{2}z}{10}})^{h+t+1}} e^{-\frac{z^2}{2\sigma_p^2}} dz \\
&= \sqrt{2\pi}\sigma_p \int_0^{\infty} \frac{(cu)^h}{(1+cu)^{h+t+1}} e^{-\frac{50(\ln u)^2}{2\sigma_p^2(\ln 10)^2}} \frac{10}{u\sqrt{2}\ln 10} du \\
&= \frac{\sigma_p\sqrt{\pi}10}{\ln 10 c^{t+1}} \int_0^{\infty} \frac{u^{h-1}}{(\frac{1}{c}+u)^{h+t+1}} e^{-(\frac{5\ln u}{\sigma_p \ln 10})^2} du
\end{aligned}$$

Finally,

$$\begin{aligned}
P_{\mathrm{out}} &= \sum_{t=0}^{\infty}\sum_{h=0}^{m-1} \frac{e^{-k}}{(t!)^2}\frac{(h+t)!}{h!}\frac{k^t 5}{\sqrt{\pi}\sigma_p \ln 10 c^{t+1}} \int_0^{\infty} \frac{u^{h-1}}{(\frac{1}{c}+u)^{h+t+1}} e^{-(\frac{5\ln u}{\sigma_p \ln 10})^2} du \\
&= \sum_{t=0}^{\infty}\sum_{h=0}^{m-1} \frac{e^{-k}}{(t!)^2}\frac{(h+t)!}{h!}\frac{k^t b}{\sqrt{\pi}c^{t+1}} \int_0^{\infty} \frac{u^{h-1}}{(\frac{1}{c}+u)^{h+t+1}} e^{-(b\ln u)^2} du \qquad \text{(3B. 3)}
\end{aligned}$$

4 Algebraic Properties of Gold and Kasami Sequences

4.1 Introduction

This section is mainly concerned with the algebraic properties of Gold and Kasami sequences. In Section 5, these properties will be exploited to provide rapid *sequence acquisition* for CDMA systems employing Kasami sequences in spreading their signals. Sequence acquisition is the process of synchronization between the transmitter and receiver sequence generators. It is necessary so that the receiver can despread the received signal.

The sequence acquisition technique that is described in Section 5 requires large sets of codewords that are orthogonal to the employed spreading sequence set with the minimum possible Hamming weight and with a one in their first bit position. These codewords are referred to as the parity-check polynomials of the spreading code and they represent a subset of the code dual to the spreading code. As described in Section 5, each of these polynomials can be used to generate an estimate of a received chip in the spreading sequence. It is desirable that the set of parity-check polynomials do not overlap so that the estimates are uncorrelated. Correlation is expected to reduce the performance of, and complicate the analysis of, the acquisition technique proposed in Section 5.

The auto- and cross-correlation functions of binary sequences are defined as follows:

$\Theta_{x,y}$ = Number of Agreements (A) - Number of Disagreements (D)
of the two compared sequences $\{x\}$ and $\{y\}$.

Let $\{z\} = \{x\} + \{y\}$, then

$$\begin{aligned} D &= wt\{z\} \\ A &= n - wt\{z\} \end{aligned}$$

where

$$\begin{aligned} n &= \text{length of } \{z\} \\ wt\{z\} &= \text{Hamming weight of } \{z\}. \end{aligned}$$

This leads to

$$\Theta_{x,y} = n - 2\,wt\{z\}. \tag{4.4}$$

4.1.1 Gold Sequences

A set of Gold sequences [52, 53] consists of $2^m + 1$ sequences each with a period $n = 2^m - 1$. These sequences can be generated by using preferred pairs of m-sequences as discussed below. The following Definition includes results originally obtained by Gold [53], Sarwate and Pursley [54, 55], and Komo [56]. This Definition will play a major rule in the decisions to be made throughout this study regarding the optimum set of sequences to be used in the application at hand.

Definition *Let $GF(2^m)$ represent the extension Galois field of the binary field $GF(2)$, where m is a positive integer. Let α be a primitive nth root of unity in the field, where $n = 2^m - 1$. Let $f_1(x)$ and $f_2(x)$ be a pair of primitive polynomials over $GF(2)$ each with degree m such that :*

$$f_1(\alpha) = 0$$

and

$$f_2(\alpha^d) = 0 \quad \textit{for some integer } d.$$

There are two cases:

Case 1. $m \neq 0$ mod-4: *If $d = 2^h + 1$ or $d = 2^{2h} - 2^h + 1$ and if $e = \gcd(m,\ h)$ is such that m/e is odd, then $f_1(x)$ and $f_2(x)$ constitute a preferred pair of polynomials. The two m-sequences, $\{u\}$ and $\{v\}$ that are generated by using $f_1(x)$ and $f_2(x)$, are referred to as a preferred pair of m-sequences. Their cross-correlation function is three-valued with possible values*

$$\Theta \in \{-1,\ -t(m),\ t(m) - 2\} \tag{4.5}$$

where

$$t(m) = 2^{\frac{m+e}{2}} + 1, \qquad e > 0.$$

It is desirable that e be as small as possible. $e = 1$ is possible as long as m is odd in order that $\frac{m}{e}$ be odd. $e = 2$ is also possible if m is even and $m \neq 0$ mod-4. This leads to the following upper bounds on Θ:

$$\Theta \leq \begin{cases} 2^{\frac{m+1}{2}} + 1 & m \text{ odd} \\ 2^{\frac{m+2}{2}} + 1 & m \text{ even} \end{cases}$$

Gold proved that if m is odd, then $d = 2^h + 1$, provided that $\gcd(m,\ h) = 1$. In general, a simple way to find a preferred pair of m-sequences is to let

$$d = 2^{\lfloor \frac{m+2}{2} \rfloor} + 1$$

where $\lfloor x \rfloor$ is the floor functions of x. This case represent what is usually referred to in the literature as the set of Gold sequences.

Case 2. $m = 0$ mod-4: *In this case, preferred pairs of m-sequences with the three-valued cross-correlation function given in (2) do not exist. However, pairs with a four-valued cross-correlation function can be obtained by letting*

$$d = 2^{\frac{m+2}{2}} - 1.$$

Notice that, $f_2(x)$ in this case is not necessarily primitive. The cross-correlation function can assume the values

$$\Theta \in \{-1,\ r(m),\ -r(m),\ 2r(m) + 1\},$$

where

$$r(m) = 2^{\frac{m}{2}} - 1.$$

This leads to the following upper bound on Θ:

$$\Theta \leq 2r(m) + 1 = 2^{\frac{m+2}{2}} - 1.$$

Also, pairs with a five-valued cross-correlation function can be obtained by letting

$$d = 2^{\frac{m+2}{2}} + 1.$$

In this case, the cross-correlation function can assume the values

$$\Theta \in \{-1,\ -s(m),\ -u(m),\ s(m)-2,\ u(m)-2\},$$

where

$$s(m) = 2^{\frac{m}{2}} + 1,$$

and

$$u(m) = 2^{\frac{m+2}{2}} + 1.$$

This leads to the following upper bound on Θ*:*

$$\Theta \leq u(m) = 2^{\frac{m+2}{2}} + 1.$$

In summary, the lowest cross-correlation is obtained for sets of Gold sequences for odd m. In fact, these sets satisfy Sidlinikov's bound on the absolute periodic correlation

$$\Theta_{max} \geq 2^{\frac{m+1}{2}} + 1$$

with equality, leading to an optimal set of sequences from the viewpoint of minimizing Θ_{max} [57]. For most of this section, attention will be restricted to Gold sequences for odd m, where $d = 2^{\frac{m+1}{2}} + 1$. Later, sequences for even m will be considered leading to Kasami sequences which possess better cross-correlation properties than the sets considered so far for even m.

A set of Gold sequences, G$[u, v]$, is generated by using two m-stage LFSR's as shown in Fig. 4.22 such that the feedback patterns of the two generators correspond to a preferred pair of polynomials. It consists of the two m-sequences $\{u\}$ and $\{v\}$, and the mod-2 sum of $\{u\}$ with all $2^m - 1$ cyclic shifts of $\{v\}$. That is

$$G[u, v] = \{u,\ v,\ u + T^p v;\quad p = 0, 1, ..., 2^m - 2\},$$

where $T^p v$ is the sequence $\{v\}$ delayed by p bits. Gold proved that the cross-correlation function between any two sequences, or the out-of-phase auto-correlation function of any sequence in the set, takes on the three values given in (2). Later, this result will be derived by applying (1) to a linear cyclic code, a subcode of which are the Gold sequences.

According to PN sequence theory [58, 59], a Gold sequence that is generated by adding two PN sequences generated from the two polynomials $f_1(x)$ and $f_2(x)$ can also be generated by a single LFSR with a feedback pattern corresponding to the polynomial

$$f(x) = \text{lcm}(f_1(x), f_2(x)),$$

and a length that is equal to the degree of $f(x)$. Since $f_1(x)$ and $f_2(x)$ are distinct primitive polynomials over GF(2), i.e., have no factors in common, $f(x)$=$f_1(x)f_2(x)$ leading to an equivalent LFSR having a length equal to $2m$.

Consider the following Theorem:

Theorem 1 *If $f_1(x)$ and $f_2(x)$ are two primitive polynomials over $GF(2)$ each with degree m and period $n = 2^m - 1$, then the product $f(x) = f_1(x)f_2(x)$ with degree $2m$ is irreducible over $GF(2)$ and has a period n.*

Proof *Since $f_1(x)$ and $f_2(x)$ are primitive polynomials over $GF(2)$, the smallest positive integer p for which each polynomial divides $x^p - 1$ is $p = n$. Since*

$x^n - 1 = \prod_i f_i(x)$; *$f_i(x)$'s are the minimal polynomial of the elements in $GF(2^m)$,*

the smallest positive integer q for which $f(x)$ divides $x^q - 1$ is $q = n$.
Finally, since $2^m - 1$ divides $2^{2m} - 1$, $f(x)$ is irreducible over $GF(2)$ and has a period $n = 2^m - 1$.

Consider a certain sequence $\{z\}$ in the set of Gold sequences that is generated by using the double LFSR configuration. This sequence will be the sum of two specific m-sequences $\{x\}$ and $\{y\}$ each of which originated from one of the two LFSR's. Knowledge of the first m bits (the initial contents) of each of the two m-sequences uniquely defines each of the sequences and in turn the resulting Gold sequence $\{z\}$. On the other hand, when considering the equivalent single LFSR configuration, the first $2m$ bits of each sequence, or at least their sum has to be known in order to uniquely define the Gold sequence $\{z\}$. This property comes into play at the receiver of such systems. The receiver is expected to use the single LFSR configuration since

it uses the received bits which are the sum of two m-sequences to generate a replica of the spreading sequence.

More insight on Gold sequences can be obtained by considering the De Brjun graph representation of the single LFSR configuration. Since the set of Gold sequences consists of $2^m + 1$ non-zero distinct sequences, a De Brjun graph will consist of $2^m + 1$ non-zero distinct subgraphs. Also, since there are $2^{2m} - 1$ possible non-zero distinct states of length $2m$, each subgraph will consist of $\frac{2^{2m}-1}{2^m+1} = 2^m - 1$ distinct states, implying that the period of each sequence is equal to $2^m - 1$. This argument is based on the assumption that each $2m$-bit state will not occur in more than one subgraph. This is indeed the case since each state will always have the same predecessor and the same successor [59]. Now, if a set of Gold sequences that is generated by using the double LFSR configuration is to be generated by using the single LFSR configuration, $2^m + 1$ valid $2m$-bit combinations out of the 2^{2m} possibilities have to be used as initial contents of the registers. $2^m - 1$ of these valid combinations correspond to the $2m$-bit subsequences obtained by fixing the initial contents of the upper LFSR in Fig. 4.22 to a non-zero sequence and then adding the first $2m$ bits of the resulting m-sequence to the first $2m$ bits of all possible $2^m - 1$ non-zero sequences generated by the lower LFSR. The last two valid combinations are the first $2m$ bits of the two original m-sequences obtained by setting, separately, the contents of each of the LFSR's to the all-zero sequence. These $2^m + 1$ possibilities generate all $2^m + 1$ subgraphs of the De Brjun graph. If the process is repeated with a different sequence at the upper LFSR, cyclically shifted versions of the same set of Gold sequences will be generated. The reason is that the new upper LFSR sequence is a cyclic shift of the original one used, so that the new $2m$-bit initial contents are a cyclic shift of an originally occurring state. In other words, this leads to one of the De Brjun subgraphs generated earlier. It is concluded that the set of Gold sequences is a subcode of a $(2^m - 1, 2m)$ cyclic code, call it $C^{\perp}$, where only one of the $2^m - 1$ cyclic shifts of each non-zero codeword is picked. These codewords are known as the cycle representative of $C^{\perp}$. Therefore, $2^m - 1$ distinct families of Gold sequences can be generated by using the two m-sequences $\{u\}$ and $\{v\}$. These families can not be employed in the same

system since they are cyclic shifts of each other. $C^{\perp}$ is a linear cyclic code that is a subcode of the 2nd order modified Reed-Muller code $R(2,m)^*$ of length $n = 2^m - 1$ and $k = 2m$ [60, 61]. It has $h^*(x)$, the reciprocal polynomial of $h(x) = \frac{x^n-1}{f_1(x)f_2(x)}$, as its generator polynomial. For $m \geq 3$, this code has the weight distribution in Table 4.5 below. This weight distribution is equivalent to the dual to a double-error-correcting BCH code with the same dimensions.

Weight w	Number of Codewords b_w
$2^{m-1}+2^{\frac{m-1}{2}}$	$(2^m-1)(2^{m-2}-2^{\frac{m-3}{2}})$
2^{m-1}	$(2^m-1)(2^{m-1}+1)$
$2^{m-1}-2^{\frac{m-1}{2}}$	$(2^m-1)(2^{m-2}+2^{\frac{m-3}{2}})$
0	1

Table 4.5: Weight distribution of the dual code $C^{\perp}$.

This weight distribution, together with (1) and the fact that the Gold set is a subcode of a linear cyclic code, can now be used to calculate the correlation functions of Gold sequences. $wt\{z\}$ in (1) is three valued with possible values

$$\{2^{m-1},\ 2^{m-1}+2^{\frac{m-1}{2}},\ 2^{m-1}-2^{\frac{m-1}{2}}\}.$$

By applying (1), the out-of-phase auto-correlation or the cross-correlation functions of Gold sequences is

$$\Theta_G \in \{-1,\ -t(m),\ t(m)-2\},$$

where

$$t(m) = 1 + 2^{\frac{m+1}{2}}.$$

This gives the following upper bound on Θ_G:

$$\Theta_G \leq t(m) = 1 + 2^{\frac{m+1}{2}}.$$

$C^{\perp}$ is dual to a $(2^m - 1, 2^m - 2m - 1)$ linear cyclic code, call it C, with a generator polynomial $f(x)=f_1(x)f_2(x)$ and parity check polynomial $h(x)$.

Now, the minimum weight of the code C and the number of minimum weight codewords are calculated. This will be accomplished by following the analysis suggested by Kasami [61, 62] and using the power-moment identities derived by Pless [63].

Consider a code C of length $2^m - 1$ generated by $f_1(x)f_2(x)$, where $f_1(x)$ and $f_2(x)$ are two different irreducible polynomials such that

$$f_1(\alpha) = 0$$

and

$$f_2(\alpha^{2^h+1}) = 0 \quad \text{for some integer } 0 < h < m,$$

and consider its dual code $C^{\perp}$. Let a_w and b_w denote the number of codewords of weight w in C and $C^{\perp}$, respectively. These codes satisfy the following symmetry properties:

For even w,

$$\begin{aligned} wa_w &= (2^m - w)a_{2^m-w} \\ wb_w &= (2^m - w)b_{2^m-w}, \end{aligned} \tag{4.6}$$

and

$$\begin{aligned} a_1 &= 0 \\ a_2 &= 0 \\ a_3 &= (2^{e-1} - 1)(\frac{2^m - 1}{3}), \end{aligned} \tag{4.7}$$

where

$$\begin{aligned} e &= \gcd(m, h) \\ &= 1 \qquad \text{for optimal Gold codes for odd } m \text{ by definition.} \end{aligned}$$

Since C contains the all-one codeword (1 1 1 . . . 1), $a_{2^m-w-1} = a_w$ or $a_{2^m-w} = a_{w-1}$.

Therefore (3) becomes

$$wa_w = (2^m - w)a_{w-1}. \tag{4.8}$$

Then

$$\begin{aligned} a_3 &= 0 \\ a_4 &= (2^{m-2} - 1)a_3 = 0. \end{aligned}$$

This is expected since the weight distribution of $C^{\perp}$ is equivalent to that of a dual to a double error correcting BCH code, i.e., $d_{min} \geq 5$, the designed minimum distance. In fact, C belongs to a class of codes where d_{min} equals the designed minimum distance leading to $d_{min} = 5$ in this case [64].

It was also shown in [62] that the extended code C_{ex}, obtained from C by adding an overall parity-check bit to each codeword, is invariant under the affine group of permutations, it consists of even weight codewords only, and its dual code is a subcode of a 2^{nd} order Reed-Muller code. Hence, the following power-moment identity specialized to the code C holds:
For even p,

$$I_p = \sum_{j \neq 0} (j - 2^{m-1})^p b_j.$$

Substituting the values of b_j given earlier, gives

$$I_p = (2^m - 1)2^{(m-1)(\frac{p}{2}+1)}.$$

In particular,

$$I_6 = (2^m - 1)2^{4(m-1)}. \tag{4.9}$$

In general, if $a_i = 0$; $1 \leq i \leq 4$ [61],

$$I_6 = 15 \cdot 2^{k-6}(2^{3m} - 2^{2m+1}) + 2^{k-2} \cdot 2^m - 2^{6m-6} + 6! \cdot 2^{k-6}(a_5 + a_6),$$

where, in this case, $k = 2m$.

Using (5)

$$a_6 = \frac{2^m - 6}{6} a_5. \tag{4.10}$$

Hence,

$$I_6 = 15(2^{5m-6} - 2^{4m-5}) + 2^{3m-2} - 2^{6m-6} + 5! \cdot 2^{3m-6} a_5 \tag{4.11}$$

Solving (6) and (8) gives

$$a_5 = \frac{2^m(2^{2m} - 11(2^m) + 26) - 16}{5!}. \tag{4.12}$$

Eqs. (7) and (9) also apply to double error correcting BCH codes for odd m. It follows that the number of codewords of weight 5 in C with a one in their first bit position is

$$\tilde{a}_5 = \frac{5a_5}{2^m - 1}.$$

Notice that the $(2^m - 1,\ 2^m - 2m - 1)$ code C with a generator polynomial $f(x) = f_1(x)f_2(x)$ consists of the codewords that belong to the intersection of the two $(2^m - 1,\ 2^m - m - 1)$ Hamming codes with generator polynomials $f_1(x)$ and $f_2(x)$. In a Hamming code, codewords of weight 5 having a one in their first bit position are expected to overlap. Therefore, codewords of weight 5 in C that exist in the two Hamming codes are expected to overlap.

So far we have considered Gold sequences for odd m. Most of the previous discussion, except for the weight enumeration, also applies to Gold sequences for even m. In general, for even m, subcodes of the 2nd order modified Reed-Muller codes are not guaranteed to have d_{min} equal to the designed minimum distance. The authors were able to generate some examples, and a similar conclusion was also reached by Kasami [65]. Eq. (4), which still applies for even m provided d is of the form $2^h + 1$, proves that a few codewords of weight 3 may exist. For example, for the set described in Case 1 of the Definition, $e = 2$ leading to

$$a_3 = \frac{2^m - 1}{3}.$$

Hence,

$$\tilde{a}_3 = 1.$$

Using Eq. (5) leads to

$$a_4 = (2^{m-2} - 1)\frac{2^m - 1}{3},$$

and therefore,

$$\tilde{a}_4 = (2^{m-2} - 1)\frac{4}{3}.$$

This case shows little improvement over Gold sequences for odd m at the expense of higher correlations. Later, it will be shown that, the small set of Kasami sequences, defined for even m, represent an optimal set in terms of both the minimum weight and the correlations. Also, for the set described in Case 2 of the Definition

$$\begin{aligned} e &= \gcd(m,\ h) \\ &= \gcd(m,\ \frac{m+2}{2}) \end{aligned}$$

Since $m = 0$ mod-4, and $\frac{m+2}{2}$ is always odd, $e = 1$. This implies that

$$a_3 = 0.$$

In conclusion, in addition to their higher cross-correlations, sequences obtained for $m = 0$ mod-4 do not reduce the minimum weight of the dual code. On the other hand; for even $m \neq 0$ mod-4, a reduction in the minimum weight is possible at the expense of higher cross-correlations. In general, LFSR's with odd length m are not only optimal in the sense of minimizing the cross-correlations, but they are also better behaved and easier to handle, when it comes to their weight enumeration, than those with even m.

4.2 Kasami Sequences

Kasami sequences evolved as the result of a study on weight distributions of linear cyclic codes, reported by Kasami between 1967-1969 [61, 62].

Let m be even. Let $f_1(x)$ be a primitive polynomial over the binary field GF(2) with degree m with α as a root, and let $f_2(x)$ be the irreducible minimal polynomial

of α^d where $d = 2^{\frac{m}{2}} + 1$. Let $\{u\}$ and $\{v\}$ represent the two m-sequences of periods $2^m - 1$ and $2^{\frac{m}{2}} - 1$ generated by $f_1(x)$ and $f_2(x)$, respectively. The set of Kasami sequences, $K[u, v]$, is generated by using the two m-sequences $\{u\}$ and $\{v\}$ in a fashion similar to the generation of Gold sequences. It consists of the long sequence $\{u\}$ and the sum of $\{u\}$ with all $2^{\frac{m}{2}} - 1$ cyclic shifts of the short sequence $\{v\}$. So

$$K[u, v] = \{u,\ u + T^p v; \quad p = 0, 1, ..., 2^{\frac{m}{2}} - 2\}.$$

The number of sequences in this set is $2^{\frac{m}{2}}$, each having a period $n = 2^m - 1$. In fact this set is known as the *small set* of Kasami sequences, to be distinguished from the *large set* of Kasami sequences to be described later in this section.

Consider the following Theorem:

Theorem 2 *If $f_1(x)$ is a primitive polynomial over $GF(2)$ with degree m and period $n = 2^m - 1$ and if $f_2(x)$ is an irreducible polynomial over $GF(2)$ with degree $\frac{m}{2}$ and period $2^{\frac{m}{2}} - 1$, then the product $f(x) = f_1(x)f_2(x)$ with degree $\frac{3m}{2}$ is reducible over $GF(2)$ and has a period n.*

Proof *Since $f_1(x)$ is a primitive polynomial over $GF(2)$, the smallest positive integer p for which $f_1(x)$ divides $x^p - 1$ is $p = n$. Since $f_2(x)$ is an irreducible polynomial over $GF(2)$ with period $2^{\frac{m}{2}} - 1$, the smallest positive integer q for which $f_2(x)$ divides $x^q - 1$ is $q = 2^{\frac{m}{2}} - 1$. Finally, since*

$x^n - 1 = \prod_i f_i(x)$; *$f_i(x)$'s are the minimal polynomial of the elements in $GF(2^m)$,*

the smallest positive integer r for which $f(x)$ divides $x^r - 1$ is $r = n$, i.e., $f(x)$ has a period n.

Now consider the De Brjun graph representation of the single LFSR configuration. Since the set of Kasami sequences consists of $2^{\frac{m}{2}}$ non-zero distinct sequences, a De Brjun graph will contain $2^{\frac{m}{2}}$ non-zero distinct subgraphs each of which consumes $2^m - 1$ distinct states of length $\frac{3m}{2}$ each. In total, these subgraphs will consume $(2^{\frac{m}{2}})(2^m - 1) = 2^{\frac{3m}{2}} - 2^{\frac{m}{2}}$ states leaving $2^{\frac{m}{2}} - 1$ states unused. These states correspond to the sequence obtained by setting the contents of the longer LFSR to the

all-zero sequence. This means that the De Brjun graph contains another subgraph with $2^{\frac{m}{2}} - 1$ *states which proves that* $f(x)$ *is reducible.*

The Kasami sequence generated by adding two m-sequences resulting from $f_1(x)$ and $f_2(x)$ can also be generated by a LFSR with a feedback pattern that corresponds to the polynomial

$$f(x) = \text{lcm}(f_1(x), f_2(x)) = f_1(x)f_2(x).$$

Following an analysis similar to that given for Gold sequences, we conclude that the set of Kasami sequences is a subcode of a $(2^m - 1, \frac{3m}{2})$ code, $C^{\perp}$, where only one of the $2^m - 1$ cyclic shifts of each non-zero codeword with period $2^m - 1$ is picked. This excludes the short m sequence. $C^{\perp}$ is a linear cyclic code that is a subcode of the 2^{nd} order modified Reed-Muller code $R(2,m)^*$ of length $n = 2^m - 1$ and $k = \frac{3m}{2}$, where $2\gcd(m, \frac{m}{2}) = \gcd(m, 2\frac{m}{2}) = m$ [61]. It has $h^*(x)$, the reciprocal polynomial of $h(x) = \frac{x^n-1}{f_1(x)f_2(x)}$, as its generator polynomial. For $m \geq 4$, this code has the weight distribution in Table 4.6

Weight	Number of Codewords
w	b_w
$2^{m-1}+2^{\frac{m}{2}-1}$	$(2^{m-1} - 2^{\frac{m}{2}-1})(2^{\frac{m}{2}} - 1)$
2^{m-1}	$2^m - 1$
$2^{m-1} - 2^{\frac{m}{2}-1}$	$(2^{m-1} + 2^{\frac{m}{2}-1})(2^{\frac{m}{2}} - 1)$
0	1

Table 4.6: Weight distribution of the dual code $C^{\perp}$.

This weight distribution, together with (1) and the fact that the Kasami set is a subcode of a linear cyclic code, can be used to calculate the correlation functions

of Kasami sequences. Hence,

$$\Theta_K \in \{-1,\ -s(m),\ s(m)-2\},$$

where

$$s(m) = 1 + 2^{\frac{m}{2}}.$$

This gives the following upper bound on Θ_K,

$$\Theta_K \leq s(m) = 1 + 2^{\frac{m}{2}}.$$

$C^{\perp}$ is dual to a $(2^m - 1,\ 2^m - \frac{3m}{2} - 1)$ linear cyclic code, C, with a generator polynomial $f(x)=f_1(x)f_2(x)$. Eq. (4) still applies to this code C, since the degree of $f_2(x)$ is a factor of the degree of $f_1(x)$. Hence, C has a minimum weight of 3 and the number of minimum weight codewords is

$$a_3 = (2^{e-1} - 1)(\frac{2^m - 1}{3}),$$

where

$$\begin{aligned} e &= \gcd(m,\ h) \\ &= \gcd(m,\ \frac{m}{2}) \\ &= \frac{m}{2}. \end{aligned}$$

therefore,

$$a_3 = (2^{\frac{m}{2}-1} - 1)(\frac{2^m - 1}{3}),$$

and by using (5)

$$a_4 = 2^{m-2}a_3.$$

The number of weight 3 codewords in C with a one in their first bit position is

$$\tilde{a}_3 = \frac{3a_3}{2^m - 1} = 2^{\frac{m}{2}-1} - 1.$$

Contrary to the case of Gold sequences, these codewords are not expected to overlap since codewords of weight 3 with a one in their first bit position in a Hamming code do not overlap.

In addition to the small set of Kasami sequences, there also exists a large set of Kasami sequences that contains both the set of Gold sequences and the small set of Kasami sequences as subsets. This leads to the minimum weight of the codewords in C to be at least 5. The large set of Kasami sequences does not possess any major improvements over the set of Gold sequences which makes it unnecessary to consider.

4.3 Conclusions

In this section, the families of Gold and Kasami sequences used in CDMA communication systems were considered. The following was concluded:

1. The set of Gold sequences consists of $2^m + 1$ sequences each having a period of $2^m - 1$. The sequences for odd m are better than those for $m = 0$ mod-4, in the sense of their correlations and the minimum weight of their dual code. For even $m \neq 0$ mod-4, an insignificant reduction in the minimum weight was possible at the expense of higher cross-correlations. For odd m, The correlations are bounded by:

$$\Theta_G \leq 2^{\frac{m+1}{2}} + 1.$$

   The dual code has a sufficiently large number of codewords of weight 5. These codewords are expected to overlap.

2. The small set of Kasami sequences is defined for even m. It consists of $2^{\frac{m}{2}}$ sequences each with a period of $2^m - 1$. This does not represent any disadvantage since m will usually be very large anyway, leading to a large number of sequences. The correlations of Kasami sequences are bounded by:

$$\Theta_K \leq 2^{\frac{m}{2}} + 1,$$

   which is less than that for Gold sequences. Also the dual codes of Kasami sequences have a sufficiently large number of codewords of weight 3 which do not overlap.

3. The small set of Kasami sequences represent the optimal set of the CDMA sequences considered in this correspondence for the purpose of implementing sequence acquisition methods that use bit estimation techniques.

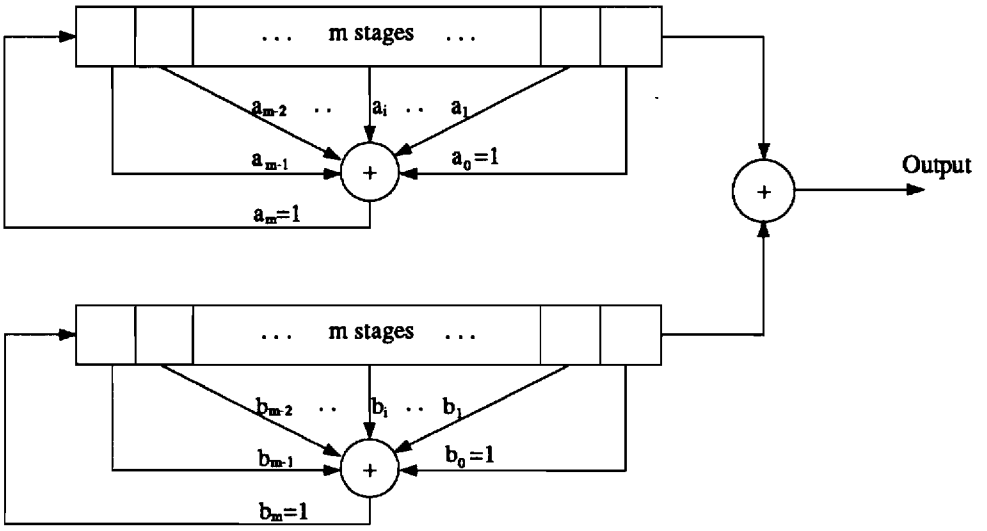

$$f_1(x) = a_0 + a_1 x + a_2 x^2 + \ldots . + a_{m-1} x^{m-1} + a_m x^m$$

$$f_2(x) = b_0 + b_1 x + b_2 x^2 + \ldots . + b_{m-1} x^{m-1} + b_m x^m$$

Figure 4.22: Gold-Sequence Generator Employing Two m-Stage LFSR's.

5 Sequence Acquisition Techniques for CDMA Systems Employing Kasami Sequences

5.1 Introduction

In Code Division Multiple Access (CDMA) systems, the process of synchronizing the locally generated PN sequence in a receiver to the incoming spread-spectrum signal is a major task. This process, known as sequence acquisition, is necessary for despreading the received signal, and it is desirable that acquisition be achieved as quickly as possible. This report addresses the issue of sequence acquisition for CDMA systems that use the small family of Kasami sequences in spreading their signals. During sequence acquisition, a receiver is assumed to have no information regarding the carrier phases or chip delays of the signals that are received from the multiple transmitters. Furthermore, the receiver does not know if the received signal contains an intended transmission, and if an intended transmission is present, it has no *a priori* information regarding the initial phase of the PN sequence. The only information that is available to the receiver is the structure of the PN sequence generator.

Numerous PN sequence acquisition techniques, under a variety of conditions and assumptions, have been proposed in the literature [66]-[67]. In all PN acquisition schemes, estimates are generated from the incoming PN sequence for a sufficient number of consecutive PN chips and loaded into a local shift register. The local shift register is then used to produce a supposedly synchronized replica of the employed PN sequence. The locally generated and a reference sequence are cross-correlated for an examination interval to verify the correctness of the phase estimate. In most cases, the reference sequence is the incoming sequence. If the phase estimate is deemed to be correct, then acquisition is declared. Otherwise, the receiver either generates another estimate of the initial sequence phase, or improves upon the existing one, and enters into another examination interval.

The simplest of acquisition technique is the serial or sliding correlator [68]. It

sequentially examines all possible sequence phases until acquisition is achieved. On average, half the phases are examined before reaching acquisition. Unfortunately, this can result in a long acquisition time for PN sequences having a long period.

Alternatives to the sliding correlator include the sequential estimation methods originated by Ward [69]. Ward introduced a technique, called rapid acquisition by sequential estimation (RASE), where the incoming symbols are hard quantized to generate an estimate of the current phase of the received PN sequence. These estimates are examined sequentially until acquisition is achieved. Variations of RASE exploit the algebraic properties of the employed PN sequence to achieve more rapid acquisition. These variations use (large) sets of codewords that are orthogonal to the employed PN sequence, have the minimum possible Hamming weight, and have a one in the first bit position. These codewords are used to define parity-check polynomials of the spreading code, and they are a subset of the dual to the spreading code [58, 54]. Ward and Yiu [70] have used a small number of such parity-check polynomials to check the validity of the phase estimate before attempting to correlate with the reference sequence, thereby eliminating an examination period for those estimates which are not error free. This technique is called recursion-aided rapid acquisition by sequential estimation RARASE.

Other variations of RASE use a large number of parity-check polynomials to generate multiple estimates of each chip in the initial phase estimate of the received PN sequence. These multiple estimates are combined in some way to generate an estimate of each chip. Pearce and Ristenbatt [71] and Kilgus [72] have analyzed this technique using threshold combining and majority logic (hard decision) combining, respectively. Stüber *et. al.* [73] have studied such acquisition techniques that use soft-decision combining techniques. Wright and Milstein [74] analyzed a version of RASE where previous estimates are improved on by using the chips that have arrived during an examination period.

This report differs from the above literature in two respects. First, all the above literature restricts attention to single-user spread-spectrum systems that employ m-sequences. In this report, we consider CDMA systems that employ Kasami

sequences. Second, the sequence acquisition schemes in the above literature have been analyzed under the assumption that the receiver has already achieved chip and carrier phase synchronization. This report assumes that the random chip delays and carrier phases are unknown. In addition, the proposed acquisition scheme can be employed in CDMA systems that use either receiver-oriented or transmitter-oriented channel access protocols [75]. This is due to the algebraic properties of Kasami sequences described in Section 5.2

The remainder of the Section is organized as follows. Section 5.2 provides a brief review of Gold and Kasami sequences and explains why Kasami sequences are preferred over Gold sequences for the proposed acquisition scheme. Section 5.3 analyzes the acquisition technique, and expressions are derived for the mean acquisition time. In Section 5.4, a two-branch diversity receiver is used to combat the deleterious effect of random chip delays. Section 5.6 presents the numerical results followed by some concluding remarks.

5.2 Gold and Kasami Sequences

CDMA systems require large sets of pseudonoise (PN) sequences with good randomness and correlation properties [55]. For a given m, there exists a small number of m-sequences and they have poor cross-correlation properties. However, it is easy to generate large families of Gold or Kasami sequences that have good correlation properties. A detailed discussion of properties of Gold and Kasami sequences can be found in [61]-[76]. The following properties are important for the analysis of the proposed acquisition scheme and have been obtained by the authors in Chapter 4:

1. The set of Gold sequences is dual to a $(2^m - 1, 2^m - 2m - 1)$ linear cyclic code, C. The sequences for odd m are better than those for $m = 0 \bmod 4$, in terms of their correlation properties and the minimum weight of the code C. For odd m, the minimum weight of C is 5 with $\frac{5}{2^m-1}\ \frac{2^m(2^{2m}-11(2^m)+26)-16}{5!}$ codewords of that weight with a one in their first bit position. These nonzero positions of these codewords are overlapping.

2. The set of Kasami sequences is defined for even m. The set of Kasami sequences is dual to a $(2^m - 1, 2^m - \frac{3m}{2} - 1)$ linear cyclic code, C which contain $2^{\frac{m}{2}-1} - 1$ codewords of weight 3 with a one in their first bit position. These nonzero positions of these codewords do not overlap. Furthermore, the parity-check polynomials that are defined from these codewords are the same for every Kasami sequence belonging to the same set of Kasami sequences.

It is desirable that the parity-check polynomials be obtained from non-overlapping codewords in the dual code so that the multiple estimates of each chip are uncorrelated. If the polynomials are obtained from codewords that overlap, then the received chips at these positions are used more than once, and the resulting chip estimates will be correlated. Correlation not only complicates the analysis, but also tends to increase the mean acquisition time. In this sense, Kasami sequences are better than Gold sequences for the proposed acquisition scheme.

5.3 Analysis of Mean Acquisition Time

Consider a direct-sequence code division multiple-access DS/CDMA system that uses binary phase-shift keying BPSK. At any receiver, the received signal after band-pass filtering has the following general form:

$$r(t) = \sum_{k=0}^{I} \sqrt{2S_k} d_k(t - \tau_k) \tilde{a}_k(t - \tau_k) \cos(w_c t + w_{dk} t + \phi_k) + n(t) \quad , \tag{5.13}$$

where

I = number of interfering users,

S_k = received signal power for user k,

$d_k(t)$ = $\sum_n d_{k,n} u_{T_b}(t - nT_b)$, where $\{d_{k,n}\}$ is the data sequence for user k, $d_{k,n} \in \{-1, +1\}$, T_b is the bit duration, and $u_{T_b}(t)$ is a unit amplitude rectangular pulse of duration T_b starting at $t = 0$,

$\tilde{a}_k(t)$ = $\sum_i \tilde{a}_{k,i} \psi(t - nT_c)$, where $\{\tilde{a}_{k,i}\}$ is the Kasami spreading sequence for user k, $a_{k,i} \in \{-1, +1\}$, T_c is the chip duration, and $\psi(t)$ is a

shaping function of duration T_c with $\int_0^{T_c} \psi^2(t)dt = 1$,

w_c = carrier frequency,

w_{dk} = Doppler shift for user k,

$n(t)$ = zero mean AWGN with two-sided power spectral density $\frac{N_o}{2}$ w/Hz,

τ_k and ϕ_k = random chip delay and carrier phase for user k.

The analysis proceeds under the assumption that the received signal power from any transmitter is the same, the shaping function is $\psi(t) = u_{T_c}(t)$, the effects of Doppler shift are ignored, and the data sequence of an intended transmission is set to +1 during the acquisition process. Under these conditions, the received signal is effectively

$$r(t) = \sum_{k=0}^{I} \sqrt{2S} a_k(t - \tau_k) \cos(w_c t + \phi_k) + n(t) \quad , \tag{5.14}$$

where $a_k(t - \tau_k)$ represents the spreading sequence modified by the data sequence; during acquisition $a_0(t - \tau_0) = \tilde{a}_0(t - \tau_0)$. The received signal is processed with the I-Q detector shown in Fig. 5.23. Defining $\mathcal{E}_c = ST_c$ and assuming that $T_c w_c \gg 1$ leads to the inphase and quadrature components

$$\begin{aligned} r_I^i &= \int_{iT_c}^{(i+1)T_c} r(t)\sqrt{\frac{2}{T_c}} \cos w_c t \, dt = \sqrt{\mathcal{E}_c} \sum_{k=0}^{I} A_k^i \cos\phi_k + n_I^i \\ r_Q^i &= \int_{iT_c}^{(i+1)T_c} r(t)\sqrt{\frac{2}{T_c}} \sin w_c t \, dt = \sqrt{\mathcal{E}_c} \sum_{k=0}^{I} A_k^i \sin\phi_k + n_Q^i \quad , \end{aligned}$$

where

$$\begin{aligned} A_k^i &= \frac{1}{T_c} \int_{iT_c}^{(i+1)T_c} a_k(t - \tau_k) \, dt \\ n_I^i &= \int_{iT_c}^{(i+1)T_c} n(t)\sqrt{\frac{2}{T_c}} \cos w_c t \, dt \\ n_Q^i &= \int_{iT_c}^{(i+1)T_c} n(t)\sqrt{\frac{2}{T_c}} \sin w_c t \, dt \quad . \end{aligned}$$

Suppose that $\tau_k = (J_k + \delta_k)T_c$, where J_k is an integer and δ_k is a random variable

uniformly distributed in the interval $(-\frac{1}{2}, \frac{1}{2}]$. Then

$$\begin{aligned} A_k^i &= \frac{1}{T_c}\int_{iT_c}^{(i+1)T_c} a_k(t - J_kT_c - \delta_kT_c)\,dt \\ &= (1-|\delta_k|)a_{k,i} + |\delta_k|a_{k,i-\mathrm{sgn}(\delta_k)} \qquad -\tfrac{1}{2} < \delta_k \le \tfrac{1}{2}, \end{aligned} \tag{5.15}$$

where $\mathrm{sgn}(x)$ is the sign of x. The inphase and quadrature noise components, n_I^i and n_Q^i, are uncorrelated zero-mean Gaussian random variables with variance $\frac{N_o}{2}$. In complex notation, the sampled output of the I-Q detector is

$$r_i = r_I^i + jr_Q^i = \sqrt{E_c}\sum_{k=0}^{I} A_k^i e^{j\phi_k} + n^i \ . \tag{5.16}$$

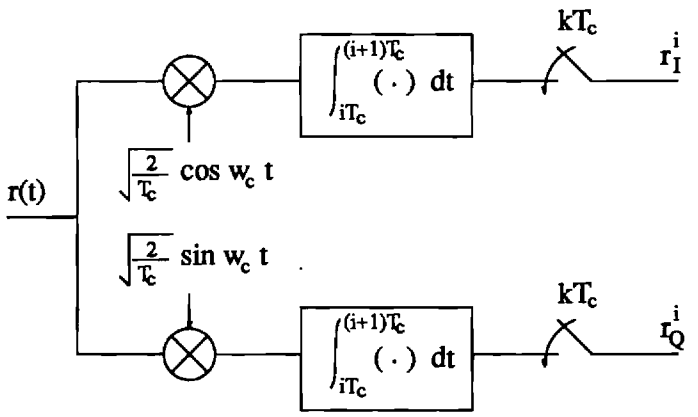

Figure 5.23: I-Q detector

To generate an estimate of the chip $a_{0,j}$, the receiver forms the product $r_{j+p}r_{j+q}^*$, such that $1 + \alpha^p + \alpha^q$ represent the i^{th} parity-check polynomial over the employed set of Kasami sequences, and generates the estimate[9]

$$\begin{aligned} U_i &= \frac{1}{\mathcal{E}_c}\Re\{r_p r_q^*\} \\ &= \sum_{k=0}^{I}\sum_{l=0}^{I} A_k^p A_l^q \cos(\phi_k - \phi_l) + \frac{1}{\sqrt{\mathcal{E}_c}}\sum_{k=0}^{I} A_k^p(n_I^q\cos\phi_k + n_Q^q\sin\phi_k) \\ &\quad + \frac{1}{\sqrt{\mathcal{E}_c}}\sum_{l=0}^{I} A_l^q(n_I^p\cos\phi_l + n_Q^p\sin\phi_l) + \frac{1}{\mathcal{E}_c}(n_I^p n_I^q + n_Q^p n_Q^q) \ . \end{aligned}$$

It is important to note that the random carrier phases $\{\phi_k\}$ must remain constant over an interval of $(q-p)T_c$ seconds. The receiver uses $\mathcal{N}$ parity check polynomials

[9]Without loss of generality, we choose $j = 0$ to simplify notation. Also, the normalization by $\mathcal{E}_c$ is not necessary at the receiver, but it streamlines the analysis.

to generate $\mathcal{N}$ such estimates. These estimates are then combined to form a final decision variable. There are a variety of combinations, but if the channel remains stationary over the acquisition interval, the following linear combination is known to give good results [77]

$$Z = \frac{1}{\mathcal{N}} \sum_{i=1}^{\mathcal{N}} U_i \quad .$$

Applying the central limit theorem, the distribution of the decision variable Z can be approximated as being Gaussian. The mean of Z is

$$\begin{aligned} \overline{Z} \;=\; \overline{U_i} \;&=\; \sum_{k=0}^{I}\sum_{l=0}^{I} \mathrm{E}[A_k^p A_l^q]\cos(\phi_k - \phi_l) \\ &=\; \mathrm{E}[A_0^p A_0^q] + \sum_{k=1}^{I} \mathrm{E}[A_k^p A_k^q] + \sum_{\substack{k=0 \\ k\neq l}}^{I}\sum_{l=0}^{I} \mathrm{E}[A_k^p A_l^q]\cos(\phi_k - \phi_l)\} \quad . \quad (5.17) \end{aligned}$$

The variance of Z is

$$\sigma_Z^2 = \frac{\sigma_U^2}{\mathcal{N}} = \frac{\mathrm{E}[U^2] - \overline{U}^2}{\mathcal{N}}$$

where

$$\mathrm{E}[U^2] \;=\; \frac{1}{4\mathcal{E}_c^2}\mathrm{E}[(r_p r_q^* + r_p^* r_q)^2] \;=\; \frac{1}{4\mathcal{E}_c^2}\left(\mathrm{E}[r_p^2 r_q^{*2}] + \mathrm{E}[r_q^2 r_p^{*2}] + 2\mathrm{E}[|r_p|^2|r_q|^2]\right) \quad .$$

Substituting r_p and r_q from (5.16), and using the fact that n_I^i and n_Q^i are independent and zero-mean, leads to

$$\mathrm{E}[r_p^2 r_q^{*2}] = \mathcal{E}_c^2 \sum_{k=0}^{I}\sum_{l=0}^{I}\sum_{\hat{k}=0}^{I}\sum_{\hat{l}=0}^{I} \mathrm{E}[A_k^p A_l^p A_{\hat{k}}^q A_{\hat{l}}^q]\exp\{j(\phi_k + \phi_l - \phi_{\hat{k}} - \phi_{\hat{l}})\} \quad ,$$

$$\mathrm{E}[r_p^{*2} r_q^2] = \mathcal{E}_c^2 \sum_{k=0}^{I}\sum_{l=0}^{I}\sum_{\hat{k}=0}^{I}\sum_{\hat{l}=0}^{I} \mathrm{E}[A_k^q A_l^q A_{\hat{k}}^p A_{\hat{l}}^p]\exp\{j(\phi_k + \phi_l - \phi_{\hat{k}} - \phi_{\hat{l}})\} \quad ,$$

and

$$\begin{aligned} \mathrm{E}[|r_p|^2|r_q|^2] \;=\; & \mathcal{E}_c^2 \sum_{k=0}^{I}\sum_{l=0}^{I}\sum_{\hat{k}=0}^{I}\sum_{\hat{l}=0}^{I} \mathrm{E}[A_k^p A_l^p A_{\hat{k}}^q A_{\hat{l}}^q]\exp\{j(\phi_k + \phi_{\hat{k}} - \phi_l - \phi_{\hat{l}})\} \\ & + 2\mathcal{E}_c \mathrm{E}[|n^q|^2] \sum_{k=0}^{I}\sum_{l=0}^{I} \mathrm{E}[A_k^p A_l^p]\exp\{j(\phi_k - \phi_l)\} + \mathrm{E}[|n^p|^2|n^q|^2] \quad . \end{aligned}$$

Finally, using $\mathrm{E}[|n^q|^2] = \mathrm{E}[|n^p|^2] = N_o$ gives the variance

$$\begin{aligned} \sigma_Z^2 \;=\; & \frac{1}{\mathcal{N}}\left\{ \sum_{k=0}^{I}\sum_{l=0}^{I}\sum_{\hat{k}=0}^{I}\sum_{\hat{l}=0}^{I} \mathrm{E}[A_k^p A_l^p A_{\hat{k}}^q A_{\hat{l}}^q]\exp\{j(\phi_k + \phi_l - \phi_{\hat{k}} - \phi_{\hat{l}})\} \right. \\ & \left. + \frac{1}{\mathcal{E}_c/N_o} \sum_{k=0}^{I}\sum_{l=0}^{I} \mathrm{E}[A_k^p A_l^p]\exp\{j(\phi_k - \phi_l)\} + \frac{1}{2(\mathcal{E}/N_o)^2} - \overline{U}^2 \right\} \quad . \quad (5.18) \end{aligned}$$

The mean and variance of Z depend on the set of random delays $\underline{\delta} = \{\delta_0, \delta_1, \cdots, \delta_I\}$, and are obtained by substituting (5.15) for A_k^i into (5.17) and (5.18).

1) Mean of Z

Considering the mean in Eq. (5.17), the first term is

$$\begin{aligned} \mathrm{E}[A_0^p A_0^q] &= \mathrm{E}\left[(1-|\delta_0|)^2 a_{0,p}a_{0,q} + |\delta_0|(1-|\delta_0|)\{a_{0,p}a_{0,q-1} + a_{0,p-1}a_{0,q}\} + |\delta_0|^2 a_{0,p-1}a_{0,q-1}\right] \\ &= \mathrm{E}\left[(1-|\delta_0|)^2 a_{0,0} + |\delta_0|(1-|\delta_0|)\{a_{0,p}a_{0,q-1} + a_{0,p-1}a_{0,q}\} + |\delta_0|^2 a_{0,-1}\right] \quad . \end{aligned}$$

Since $a_{0,q} = a_{0,0}a_{0,p}$ and $a_{0,p-1} = a_{0,-1}a_{0,q-1}$, it follows that $a_{0,p-1}a_{0,q} = a_{0,0}a_{0,-1}a_{0,p}a_{0,q-1}$. Therefore,

$$\mathrm{E}[A_0^p A_0^q] = (1-|\delta_0|)^2 a_{0,0} + |\delta_0|^2 a_{0,-1} + |\delta_0|(1-|\delta_0|)(1 + a_{0,0}a_{0,-1})\mathrm{E}[a_{0,p}a_{0,q-1}] \quad .$$

For the case when $a_{0,0} \neq a_{0,-1}$ the last term is zero, but for the case when $a_{0,0} = a_{0,-1}$ Appendix 5A shows that

$$\mathrm{E}[a_{0,p}a_{0,q-1}] = \begin{cases} +\Theta^0(1) & a_{0,0} = a_{0,-1} = +1 \\ -\Theta^0(1) & a_{0,0} = a_{0,-1} = -1 \end{cases} \quad ,$$

where $\Theta^k(n)$ is the autocorrelation of sequence k at delay n.

The expectation in the second term of (5.17) is

$$\mathrm{E}[A_k^p A_k^q] = (1-|\delta_k|)^2\mathrm{E}[a_{k,p}a_{k,q}] + (1-|\delta_k|)|\delta_k|\mathrm{E}[a_{k,p}a_{k,q-1} + a_{k,p-1}a_{k,q}] + |\delta_k|^2\mathrm{E}[a_{k,p-1}a_{k,q-1}] \quad .$$

It is shown in Appendix 5B that these expectations are all equal and that

$$\mathrm{E}[A_k^p A_k^q] = \mathrm{E}[a_{k,p}a_{k,q}] = \frac{\overline{\Theta}}{8} \quad ,$$

where $\overline{\Theta}$ is the average-out-of phase autocorrelation tabulated in Appendix 5H.

Finally, the expectation in the third term of (5.17) is

$$\begin{aligned} \mathrm{E}[A_k^p A_l^q] &= [(1-|\delta_k|)(1-|\delta_l|)\mathrm{E}[a_{k,p}a_{l,q}] + (1-|\delta_k|)|\delta_l|\mathrm{E}[a_{k,p}a_{l,q-1}] \\ &+ (1-|\delta_l|)|\delta_k|\mathrm{E}[a_{k,p-1}a_{l,q}] + |\delta_k||\delta_l|\mathrm{E}[a_{k,p-1}a_{l,q-1}] \quad . \end{aligned}$$

Appendix 5C shows that these expectations are equal to 0 and, therefore, $\mathrm{E}[A_k^p A_l^q] = 0$.

The above development shows that the mean in Eq. (5.17) is actually conditioned on $a_{0,0}$ and $a_{0,-1}$, and is a function of δ_0. To explicitly show these dependencies, we define the variable $\overline{Z}_{i,j}(\delta_0)$ as the mean $\overline{Z}$ conditioned on the chips $a_{0,0} = j$ and $a_{0,-1} = i$, and as a function of δ_0. Then

$$\begin{aligned}
\overline{Z}_{+1,+1}(\delta_0) &= \gamma_0 + 2\xi_0\Theta^0(1) + \frac{I\overline{\Theta}}{8} \\
\overline{Z}_{-1,-1}(\delta_0) &= -\gamma_0 - 2\xi_0\Theta^0(1) + \frac{I\overline{\Theta}}{8} \\
\overline{Z}_{-1,+1}(\delta_0) &= 1 - 2|\delta_0| + \frac{I\overline{\Theta}}{8} \\
\overline{Z}_{+1,-1}(\delta_0) &= -1 + 2|\delta_0| + \frac{I\overline{\Theta}}{8}
\end{aligned}$$

where

$$\begin{aligned}
\xi_i &= |\delta_i|(1 - |\delta_i|) \\
\gamma_i &= (1 - |\delta_i|)^2 + |\delta_i|^2
\end{aligned}$$

We note in passing that the terms involving the autocorrelation functions are very small compared to the terms that do not.

2) Variance of Z

The variance is more complicated, but can be obtained in a similar fashion. Let σ_1^2 denote the first term in (5.18)

$$\sigma_1^2 = \sum_{k=0}^{I}\sum_{l=0}^{I}\sum_{\hat{k}=0}^{I}\sum_{\hat{l}=0}^{I} \mathrm{E}[A_k^p A_l^p A_{\hat{k}}^q A_{\hat{l}}^q] e^{j(\phi_k + \phi_l - \phi_{\hat{k}} - \phi_{\hat{l}})}. \tag{5.19}$$

This four dimensional sum was opened up and equivalent terms were collected together. This lead to 17 terms each of which consisted of sums of one of the three forms; $\{A_k^{p^2} A_l^{q^2}, A_k^{p^2} A_l^q A_{\hat{k}}^q, A_k^p A_l^p A_{\hat{k}}^q A_{\hat{l}}^q\}$. The full expression is shown in Appendix 5D. Substituting A_k^i from Eq. 5.15 and using Appendices 5E,5F,5G, and 5H, leads to the following expression for σ_1^2:

$$\begin{aligned}
\sigma_1^2 &= 4\xi_0\gamma_0\Theta^0(1) + 4\xi_0^2 a_{0,0}a_{0,-1} + \sum_{k=0}^{I}\gamma_k^2 + 8I\xi_0(\overline{\Psi}^2 - \frac{1}{n}) \\
&+ \sum_{k=1}^{I}\{4\xi_k\gamma_k + \frac{\xi_k^2}{2} + \frac{1}{2}[(1 - |\delta_0|)^2 a_{0,0} + |\delta_0|^2 a_{0,-1}]\}\overline{\Theta}
\end{aligned}$$

$$+ \quad 2\sum_{k=1}^{I}\{\gamma_0\gamma_k + 2\xi_0\gamma_k\Theta^0(1) + 2\xi_k\gamma_0\overline{\Theta} + 4\xi_0\xi_k(\overline{\Psi}^2 - \frac{1}{n})\}\cos(2\phi_0 - 2\phi_k)$$

$$+ \quad \sum_{\substack{k=1 \\ k\neq l}}^{I}\sum_{l=1}^{I}\{\gamma_k\gamma_l + [2\xi_k\gamma_l + 2\xi_l\gamma_k]\overline{\Theta} + 4\xi_0\xi_k(\overline{\Psi}^2 - \frac{1}{n})\}\cos(2\phi_k - 2\phi_l) \qquad (5.20)$$

where $\overline{\Psi}$ represents the average cross-correlation tabulated in Appendix 5H.

Now, let σ_2^2 denote the second term in Eq. (5.18). Then

$$\begin{aligned}\sigma_2^2 = & \sum_{k=0}^{I}\sum_{l=0}^{I}\mathrm{E}[A_k^p A_l^p]e^{j(\phi_k-\phi_l)} \\ = & \quad \mathrm{E}[A_0^{p^2}] + \sum_{k=1}^{I}\mathrm{E}[A_k^{p^2}] + \sum_{\substack{k=0 \\ k\neq l}}^{I}\sum_{l=0}^{I}\mathrm{E}[A_k^p A_l^p]e^{j(\phi_k-\phi_l)} \quad . \end{aligned} \qquad (5.21)$$

Substituting A_k^i from Eq. (5.15) and simplifying results in

$$\begin{aligned}\mathrm{E}[A_0^{p^2}] &= \gamma_0 + 2\xi_0\Theta^0(1) \\ \mathrm{E}[A_k^{p^2}] &= \gamma_k + 2\xi_k\overline{\Theta} \\ \mathrm{E}[A_k^p A_l^p] &= \mathrm{E}[a_{k,p}a_{l,p}] = 0\end{aligned}$$

Hence,

$$\sigma_2^2 = \gamma_0 + 2\xi_0\Theta^0(1) + \sum_{k=1}^{I}\gamma_k + 2\xi_k\overline{\Theta} \quad . \qquad (5.22)$$

Substituting σ_1^2 and σ_2^2 obtained above into Eq. (5.18), gives the variance of Z conditioned on $a_{0,0}$ and $a_{0,-1}$ and as a function of the set of random delays $\underline{\delta}$. In the sequel, this variance will be denoted by $\sigma_Z(\underline{\delta})$.

5.3.1 Probability of Successful Tracking

In order to calculate the mean acquisition time, the probability of successful tracking is required. Successful tracking occurs when the $\frac{3m}{2}$ chips that are required to initialize the local shift register have been estimated correctly. Probability of successful tracking is determined by considering all possible $2^{\frac{3m}{2}}$ initial subsequences of the LFSR, the reason being that the means and variances of a chip estimate depend not only on the chip to be estimated, but also on the immediately preceding chip. Let P_a and P_b be the probability of estimating a particular chip correctly, given that it is preceded by

a chip of the opposite sign and the same sign, respectively. Using the results just derived

$$\begin{aligned} P_a &= 1 - Q\left(\frac{\overline{Z}_{+1,-1}(\delta_0)}{\sigma_Z(\underline{\delta})}\right) = 1 - Q\left(-\frac{\overline{Z}_{-1,+1}(\delta_0)}{\sigma_Z(\underline{\delta})}\right) \\ P_b &= 1 - Q\left(\frac{\overline{Z}_{-1,-1}(\delta_o)}{\sigma_Z(\underline{\delta})}\right) = 1 - Q\left(-\frac{\overline{Z}_{+1,+1}(\delta_0)}{\sigma_Z(\underline{\delta})}\right) \end{aligned}$$

To proceed further, some properties of Kasami sequences are required. Let

$$\begin{aligned} P_0 &= \frac{\text{number of zeros in the Kasami sequence}}{\text{length of the Kasami sequence}} \\ P_1 &= \frac{\text{number of ones in the Kasami sequence}}{\text{length of the Kasami sequence}} \\ P_{i|j} &= P[a_{0,-1} = i | a_{0,0} = j] \quad . \end{aligned}$$

As explained in Section , set 1 in Appendix 5H will be used as a reference for evaluating the performance of the acquisition scheme. For this set, $P_{0|1} + P_{1|0} = P_1$ and $P_{1|1} + P_{0|0} = P_0$.

Let n_a be the number of times that two adjacent chips have opposite signs in the subsequence of length $\frac{3m}{2}$. For a specific value of n_a, there exist $\binom{\frac{3m}{2}}{n_a}$ subsequences with n_a sign changes. Using the above sequence properties, it follows that the probability of n_a sign changes is

$$P_{n_a} = \binom{\frac{3m}{2}}{n_a} (P_1)^{n_a} (P_0)^{\frac{3m}{2} - n_a} \quad .$$

The probability of successful tracking, given n_a sign changes, is

$$P_{c|n_a} = (P_a)^{n_a} (P_b)^{\frac{3m}{2} - n_a} \quad .$$

Therefore, the probability of successful tracking conditioned on the set of random delays $\underline{\delta}$ is

$$P_{st|\underline{\delta}} = \sum_{n_a=0}^{\frac{3m}{2}} P_{c|n_a} P_{n_a} = (P_1 P_a + P_0 P_b)^{\frac{3m}{2}} \quad .$$

5.3.2 Minimum Span Calculation

To calculate the mean acquisition time, it is necessary to determine the smallest span of chips needed to obtain the $\mathcal{N}$ estimates. More precisely, we must determine the

largest exponent of α that is necessary to obtain $\mathcal{N}$ parity check trinomials of the form $1+\alpha^i+\alpha^{j_i}$ in the dual to the family of Kasami sequences, C. This quantity is denoted by $M(m,\mathcal{N})$ for a Kasami sequence of period $n=2^m-1$.

An analysis similar to that developed by Stüber *et. al.* [73] for hamming codes will be followed and then extended to the code C. It is important to remember that in a Hamming code there exists $2^{m-1}-1$ parity-check trinomials of the form $\{1+\alpha^i+\alpha^{j_i}, i=1,2,....,n-1\}$ that exhaust all possible positions with no overlaps. Also, the dual to the family of Kasami sequences contains $2^{\frac{m}{2}-1}-1$ of these trinomials. Now consider the set of such trinomials in a Hamming code and suppose the integers j_i are assigned at random so that the ordered $n-1$-tuple $(j_1,j_2,.....,j_{n-1})$ is a random permutation of $(1,2,...,n-1)$. In this model, let $\hat{\ell}$ and ℓ be the number of the j_i, $i\leq t$, that are less than or equal to t in a Hamming code and in code C, respectively. The random variable $\hat{\ell}$ has the hypergeometric distribution

$$\mathrm{P}[\hat{\ell}=s]=\frac{\binom{t}{s}\binom{n-1-t}{t-s}}{\binom{n-1}{t}}$$

with mean $t^2/(n-1)$ [73]. Since the dual to the family of Kasami sequences contains $2^{\frac{m}{2}-1}-1$ out of the $2^{m-1}-1$ trinomials in the Hamming code

$$\begin{aligned}\mathrm{E}[\ell] &= \frac{2^{\frac{m}{2}-1}-1}{2^{m-1}-1}\mathrm{E}[\hat{\ell}] \\ &= \frac{2^{\frac{m}{2}-1}-1}{2^{m-1}-1}\frac{t^2}{n-1} \quad .\end{aligned}$$

Identifying t with $M(m,\mathcal{N})$ and noting that the trinomials occur in pairs, results in the following estimate on the number of such relationships

$$\begin{aligned}\mathcal{N} &= \frac{\mathrm{E}[\hat{\ell}]}{2} \\ &= \frac{(2^{\frac{m}{2}-1}-1)M^2(m,\mathcal{N})}{(2^m-2)^2}\end{aligned}$$

or

$$M(m,\mathcal{N})=(2^m-2)\sqrt{\frac{\mathcal{N}}{2^{\frac{m}{2}-1}-1}} \quad . \tag{5.23}$$

The same result can by obtained by adopting a binomial rather than hypergeometric model. Some experimental work was done on Kasami sequences for m up to 16

and it was noted that the approximation yields surprisingly good agreement with the observed values for as low as $m = 10$. For example, Fig. 5.24 compares the approximation and observed values for $m = 12$. Note that, Eq. (5.23) only applies for $\mathcal{N} \leq 2^{\frac{m}{2}-1} - 1$, the maximum number of trinomials in one period of the sequence. For larger values of $\mathcal{N}$, one needs to add $(2^m - 2)$ chips for every full period covered by $\mathcal{N}$ and then use Eq. (5.23) to calculate the extra chips needed for the remaining fraction of a period.

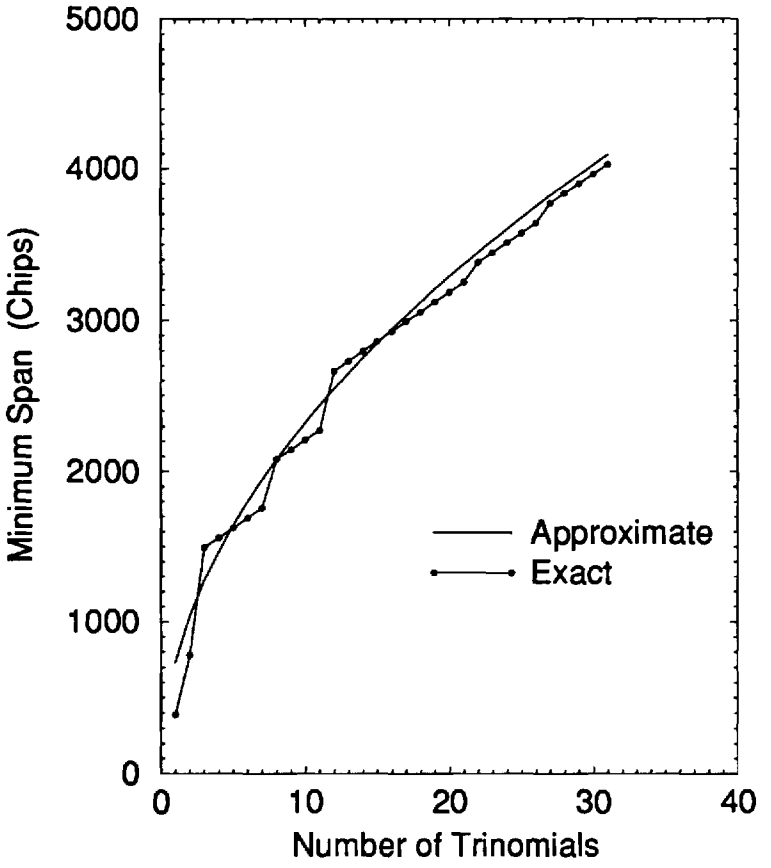

Figure 5.24: Comparison of approximate and exact values of $M(m,\mathcal{N})$ for Kasami sequences with $m = 12$.

5.3.3 Mean Acquisition Time

One possible acquisition process proceeds as follows. The receiver employs the equivalent LFSR of length $\frac{3m}{2}$. It first waits for $M(m,\mathcal{N})+1$ chips to generate an estimate of the first received chip using $\mathcal{N}$ trinomials. Following that, $\frac{3m}{2} - 1$ extra chips will

be needed to generate an estimate of the next $\frac{3m}{2} - 1$ chips. The chip estimates are then loaded to the LFSR and verified by correlating the locally generated sequence with the reference sequence for an examination interval of N_e chips. In this report, the reference sequence is taken as the estimate of the N_e-tuple subsequence directly following the initial phase estimate. This subsequence estimate is generated in a manner similar to that of the initial phase estimate. The reason for preferring the use of the estimate of the incoming sequence rather than the incoming sequence itself was motivated by the analysis of the false alarm and false dismissal distributions described in Section 5.5. It was observed that the bit error probability in the reference sequence represents a significant factor in evaluating the probabilities of false alarm and false dismissal. Since CDMA systems usually operate at low signal-to-noise ratios, the bit error probability in the estimated sequence is expected to be much less than that of the incoming sequence.

If the original estimate fails, a new estimate using the most recent $M(m, \mathcal{N}) + \frac{3m}{2}$ is formed and verified. This process continues until acquisition is declared. With this algorithm, the expected number of trials is equal to $\frac{1}{P_{st|\underline{\delta}}}$. Hence, the expected acquisition time is

$$\overline{T}_{acq|\underline{\delta}} = N_e \frac{1}{P_{st|\underline{\delta}}} + M(m, \mathcal{N}) + \frac{3m}{2} \quad .$$

An alternative acquisition algorithm that is expected to reduce the mean acquisition time is the energy retentive technique described by Wright and Milstein [74]. With this technique, the receiver waits for $M(m, 1) + \frac{3m}{2}$ chips to generate an estimate of the first $\frac{3m}{2}$ chips. This estimate is then examined for N_e chips. During the examination interval, other arriving chips are used to update the estimate. If the original estimate is determined to be incorrect, then the updated estimate is used. This process is repeated until acquisition is declared. The conditional mean acquisition time and the conditional acquisition time variance are:

$$\begin{aligned} \overline{T}_{acq|\underline{\delta}} &= \sum_{i=1}^{\infty} [M(m, 1) + \frac{3m}{2} + iN_e] P_i \\ \sigma^2_{acq|\underline{\delta}} &= \sum_{i=1}^{\infty} [M(m, 1) + \frac{3m}{2} + iN_e]^2 P_i \end{aligned}$$

where

$$\begin{aligned} P_i &= P[\text{No success for the first } (i-1) \text{ trials, Success at the } i^{\text{th}} \text{ trial}] \\ &= (1-P_1)(1-P_2)\cdots(1-P_{i-1})(P_{st|\underline{\delta},\mathcal{N}_i}) \\ \mathcal{N}_i &= \text{Number of checks available at the } i^{\text{th}} \text{ trial.} \end{aligned}$$

The mean and variance of the acquisition time are obtained by averaging $\overline{T}_{acq|\underline{\delta}}$ and $\sigma^2_{acq|\underline{\delta}}$ over all possible values of $\underline{\delta}$

$$\overline{T}_{acq} = \int_{-\frac{1}{2}}^{\frac{1}{2}} \overline{T}_{acq|\underline{\delta}} P(\underline{\delta}) d\underline{\delta} = \int_{-\frac{1}{2}}^{\frac{1}{2}} \overline{T}_{acq|\underline{\delta}} d\underline{\delta} \tag{5.24}$$

$$\sigma^2_{acq} = \int_{-\frac{1}{2}}^{\frac{1}{2}} \sigma_{acq|\underline{\delta}} d\underline{\delta} \ . \tag{5.25}$$

The above algorithm is also expected to improve the capture capability of the system when multiple signals intended for the same receiver arrive during acquisition. If a phase estimate does not lead to acquisition, then a new phase estimate is generated, so the original and newly arriving signals compete for the same receiver. If the first algorithm is used, then all signals have an equal chance of capturing the receiver and, usually, the strongest signal does. If the energy retentive algorithm is used, then energy build up during previous trials is expected to improve the chance that the first arriving signal captures the receiver [75].

5.4 Two-Branch Diversity Receiver

A significant problem with using the simple I-Q detector in Fig. 5.23 is that a very large mean acquisition time will result when $|\delta_0| \approx \frac{1}{2}$. One possible solution is to use the two-branch diversity receiver shown in Fig. 5.25. The samples generated by branch A are offset by $T_c/2$ from those generated by branch B. For this receiver, the probability of successful tracking given n_a sign changes is

$$P_{c|n_a} = P_{c|n_a,A} Pr[A|n_a] \ + \ P_{c|n_a,B} Pr[B|n_a] \ .$$

Then the probability of successful tracking conditioned on the set of random delays $\underline{\delta} = \{\delta_0, \delta_1, \cdots, \delta_I\}$, is

$$P_{st|\underline{\delta}} = \sum_{n_a=0}^{\frac{3m}{2}} P_{c|n_a} P_{n_a} \ .$$

In order to calculate Pr[A|n_a] and P[B|n_a], a rule for branch selection must be defined. One possible method is to compute the sum of the squares of the $\frac{3m}{2}$ chip estimates for branches A and B, denoted by X_A and X_B, respectively. The branch selection rule is

$$\begin{aligned} &\text{choose branch A,} \quad \text{if } X_A \geq X_B \\ &\text{choose branch B,} \quad \text{otherwise} \end{aligned}$$

Then,

$$\Pr[A] = \Pr[(X_A - X_B) \geq 0] = \Pr[D \geq 0] \ ,$$

where D is a random variable that is the difference between two non-central chi-square distributed random variables. Provided that $3m/2$ is large enough (and almost always it is) the central limit theorem can be applied and the distribution of $D = X_A - X_B$ can be approximated as being Gaussian, where the mean and variance of D can be obtained from the characteristic function of D in [78]

$$\overline{D} = \frac{3m}{2}\left(\sigma_{ZA}^2 - \sigma_{ZB}^2\right) + \sum_{i=1}^{\frac{3m}{2}} \overline{Z}_{Ai}^2 - \sum_{i=1}^{\frac{3m}{2}} \overline{Z}_{Bi}^2 \tag{5.26}$$

$$\sigma_D^2 = 3m\left(\sigma_{ZA}^4 + \sigma_{ZB}^4\right) + 4\sigma_{ZA}^2 \sum_{i=1}^{\frac{3m}{2}} \overline{Z}_{Ai}^2 + 4\sigma_{ZB}^2 \sum_{i=1}^{\frac{3m}{2}} \overline{Z}_{Bi}^2 \ , \tag{5.27}$$

where

$$\begin{aligned} \overline{Z}_{Ai} &= \overline{Z}_{i,i-1}\left(\delta_0 + \tfrac{1}{4}\right) \\ \overline{Z}_{Bi} &= \overline{Z}_{i,i-1}\left(\delta_0 - \tfrac{1}{4}\right) \\ \sigma_{ZA}^2 &= \sigma_Z^2\left(\delta_0 + \tfrac{1}{4}, \cdots, \delta_k + \tfrac{1}{4}\right) \\ \sigma_{ZB}^2 &= \sigma_Z^2\left(\delta_0 - \tfrac{1}{4}, \cdots, \delta_k - \tfrac{1}{4}\right) \end{aligned}$$

are defined in Eqs. (5.17) and (5.18), respectively. Note that $\overline{Z}_{Ii}$ depends on chips i and $(i-1)$. Following the notation of Section 5.3.1, the sums in Eq. (5.26) and (5.27) are

$$\begin{aligned} \sum_{i=1}^{\frac{3m}{2}} \overline{Z}_{Ai}^2 &= n_a \overline{Z}_{+1,-1}^2\left(\delta_0 + \frac{1}{4}\right) + \left(\frac{3m}{2} - n_a\right)\overline{Z}_{+1,+1}^2\left(\delta_0 + \frac{1}{4}\right) \\ \sum_{i=1}^{\frac{3m}{2}} \overline{Z}_{Bi}^2 &= n_a \overline{Z}_{+1,-1}^2\left(\delta_0 - \frac{1}{4}\right) + \left(\frac{3m}{2} - n_a\right)\overline{Z}_{+1,+1}^2\left(\delta_0 - \frac{1}{4}\right) \ . \end{aligned}$$

Finally, $\Pr[\mathrm{A}|n_a] = Q\left(-\frac{\overline{D}}{\sigma_D}\right)$ and $\Pr[\mathrm{B}|n_a] = 1 - \Pr[\mathrm{A}|n_a]$.

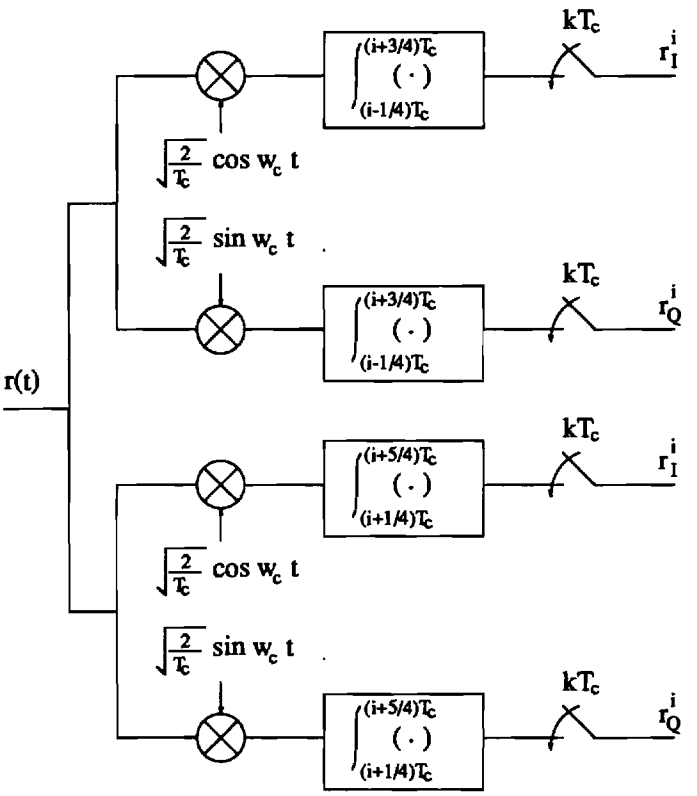

Figure 5.25: Two-branch I-Q detector

5.5 Other Performance Measures

Finite Acquisition Time: The mean acquisition time calculated above measures the performance of the proposed acquisition scheme for spread spectrum systems having no limit on the acquisition time. This is valid measure for systems with continuous data transmission. However, in packet radio networks, acquisition must be reached within a specified time interval T_s-chip with a high probability; otherwise communication is impossible. The probability of acquisition within a T_s-chip interval is obtained by evaluating the probability of generating a correct phase estimate using the $\mathcal{N}_s$ checks available during the T_s-chip interval. Hence,

$$P_{acq} = \Pr[\text{acquisition in } T_s \text{ seconds}] = P_{st|T_s} = P_{st|\mathcal{N}_s} \ .$$

False Dismissal and False Alarm: After a phase estimate is generated, it is loaded into the local sequence generator. The received sequence is compared chip-by-chip with the locally generated sequence for N_e chips, and the number of disagreements is counted. If the number of disagreements does not exceed a threshold i_{th}, the estimate is accepted; otherwise, it is rejected. This leads to two distinct possibilities;

1. A *False dismissal* occurs when the generated estimate is correct, but is rejected because the number of disagreements exceeds i_{th}. Let $P_i = Pr[i$ 1's in N_e chips $]$ $= Pr[i$ erroneous estimates out of $N_e]$, and let n_b be the number of sign changes in the N_e-tuple locally generated sequence that directly follows the initial phase. Similar to the analysis in Section 5.3.1,

$$P_{n_b} = \binom{N_e}{n_b}(P_1)^{n_b}(P_0)^{N_e-n_b} \quad .$$

It can also be shown that

$$\begin{aligned} P_{i|n_b} &= \sum_{j=\max(0,i-(N_e-n_b))}^{\min(i,n_b)} P_{i|n_b,j}P_j \\ &= \sum_{j=\max(0,i-(N_e-n_b))}^{\min(i,n_b)} \binom{n_b}{j}(1-P_b)^{i-j}P_b^{N_e-n_b-(i-j)}(1-P_a)^j P_a^{n_b-j} \quad . \end{aligned}$$

where j represent the number of errors that are preceded by a sign change, and n_b, P_a, and P_b are as defined in Section 5.3.1

Then,

$$P_{fd} = \sum_{n_a=0}^{\frac{3m}{2}} \sum_{n_b=0}^{N_e} \sum_{i=i_{th}+1}^{N_e} P_{i|n_b}P_{n_b}P_{n_a} \quad .$$

2. A *False alarm* occurs when the generated estimate is incorrect, but is accepted because the number of disagreements is less than i_{th}. In this case, the received sequence (with errors) is being added to another Kasami sequence. Since the set of Kasami sequences is a subset of a linear cyclic code, the sum leads to a third Kasami sequence modified by the same errors as the received sequence. This third Kasami sequence can have any of the three possible weights as desribed in Appendix 5H. On average $P_1 = P_0 = \frac{1}{2}$. Using these values

$$P_i = \binom{N_e}{i}(\frac{1}{2})^{N_e}$$

and hence,

$$P_{fa} = \sum_{n_a=0}^{\frac{3m}{2}} \sum_{i=0}^{i_{th}} \binom{N_e}{i} (\frac{1}{2})^{N_e} P_{n_a} = \sum_{i=0}^{i_{th}} \binom{N_e}{i} (\frac{1}{2})^{N_e} \quad .$$

This is similar to a result obtained by Ward [70].

5.6 Numerical Results

Appendix 5H shows that, the family of Kasami sequences is divided into 5 sets with different balance structures. While carrying out the analysis, it was noticed that the performance of the proposed acquisition scheme remains essentially unchanged when the set to which the sequence of interest belongs to was varied. In the following, the 0^{th} sequence is assumed to belong to set 1. Every other sequence can belong to any set with a probability that is proportional to the number of sequences in that set.

As expected, the two branch diversity receiver considered in Section IV outperforms the single branch receiver. Also, the energy retentive acquisition algorithm leads to a further reduction in mean acquisition time. Fig. 5.26 compares the mean acquisition time for these different cases. Also, shown is the performance of an ideal two-branch receiver where the best branch is always chosen.

The rest of the numerical results assume the use of the two-branch diversity receiver employing the energy retentive algorithm. Fig. 5.27 shows the mean acquisition time for 1, 11, and 64 simultaneous users. Figs. 5.28 and 5.29 show that the mean acquisition time increases with the length of the examination interval and the length of the spreading sequence. Fig. 5.30 plots the probability of acquisition. Finally, Fig. 5.31 shows the probabilities of false dismissal and false alarm at different chip energy-to-noise ratios. For each chip energy-to-noise ratio, the number of checks required to reach acquisition obtained from Fig. 5.27 is used to calculate the probability of false dismissal.

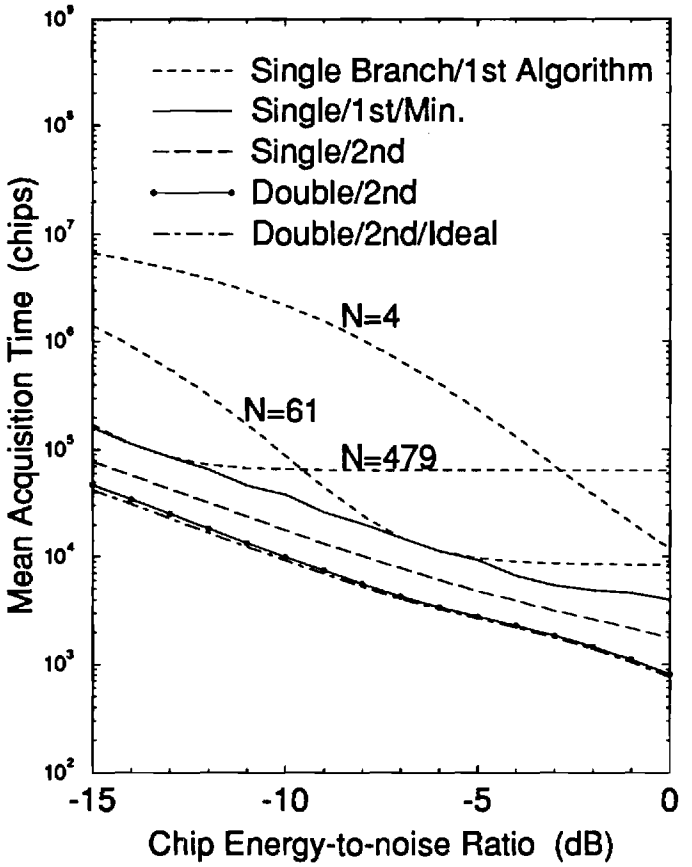

Figure 5.26: Comparison of mean acquisition time for the single-branch and two-branch receivers for the two acquisition schemes with a single user; m=12, N_e=50.

5.7 Appendices

Appendix 5A

$$\mathrm{E} = \mathrm{E}[a_{0,p}a_{0,q-1}|a_{0,0}, a_{0,-1}]$$

Case 1: $a_{0,0} = a_{0,-1} = +1$

$$\begin{aligned}
\mathrm{E} &= \mathrm{E}[a_{0,p}a_{0,q-1}|a_{0,0} = a_{0,-1} = 1] \\
&= \Pr[a_{0,p} = a_{0,q-1}|a_{0,0} = 1, a_{0,-1} = 1] - \Pr[a_{0,p} \neq a_{0,q-1}|a_{0,0} = 1, a_{0,-1} = 1] \\
&= \Pr[a_{0,p} = -1, a_{0,q-1} = -1|a_{0,0} = 1, a_{0,-1} = 1] + \Pr[a_{0,p} = 1, a_{0,q-1} = 1|a_{0,0} = 1, a_{0,-1} = 1] \\
&\quad -\Pr[a_{0,p} = -1, a_{0,q-1} = 1|a_{0,0} = 1, a_{0,-1} = 1] - \Pr[a_{0,p} = 1, a_{0,q-1} = -1|a_{0,0} = 1, a_{0,-1} = 1] \\
&= \Pr[a_{0,p} = -1, a_{0,p-1} = -1] + \Pr[a_{0,p} = 1, a_{0,p-1} = 1] \\
&\quad -\Pr[a_{0,p} = -1, a_{0,p-1} = 1] - \Pr[a_{0,p} = 1, a_{0,p-1} = -1]
\end{aligned}$$

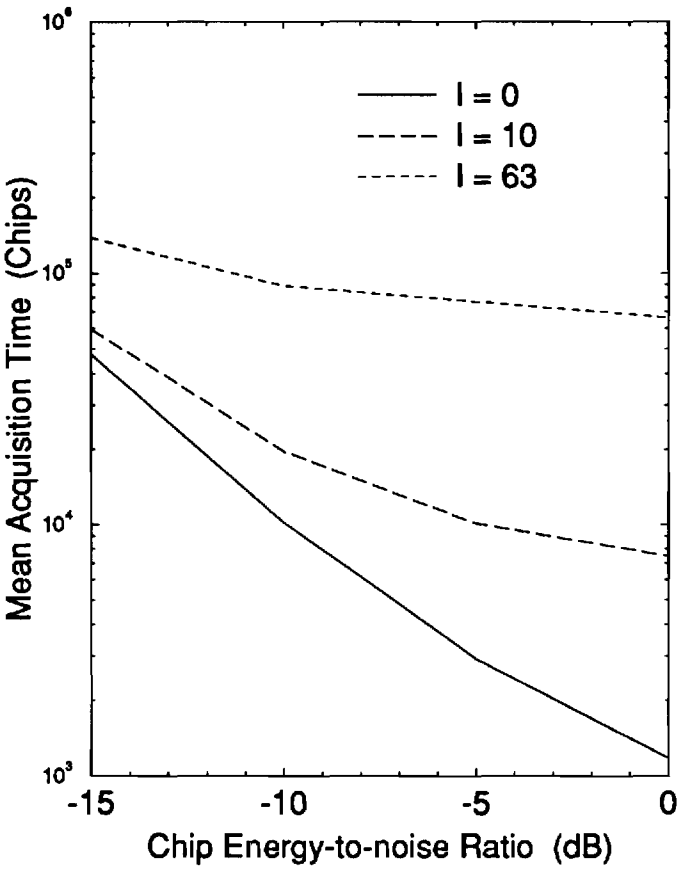

Figure 5.27: Mean acquisition time against the chip energy-to-noise ratio for various numbers of simultaneous users; $m = 12$, $N_e = 50$.

$$= \Pr[a_{0,p} = a_{0,p-1}] - \Pr[a_{0,p} \neq a_{0,p-1}]$$
$$= \Theta^0(1),$$

where $\Theta^k(n)$ represents the autocorrelation function of user k evaluated at delay n. $\Theta^0(1)$ is tabulated in Appendix 5H.

Case 2: $a_{0,0} = a_{0,-1} = -1$

$$\begin{aligned} E &= E[a_{0,p}a_{0,q-1}|a_{0,0} = a_{0,-1} = -1] \\ &= \Pr[a_{0,p} = a_{0,q-1}|a_{0,0} = -1, a_{0,-1} = -1] \\ &\quad -\Pr[a_{0,p} \neq a_{0,q-1}|a_{0,0} = -1, a_{0,-1} = -1] \\ &= \Pr[a_{0,p} = -1, a_{0,q-1} = -1|a_{0,0} = -1, a_{0,-1} = -1] \\ &\quad +\Pr[a_{0,p} = 1, a_{0,q-1} = 1|a_{0,0} = -1, a_{0,-1} = -1] \\ &\quad -\Pr[a_{0,p} = -1, a_{0,q-1} = 1|a_{0,0} = -1, a_{0,-1} = -1] \end{aligned}$$

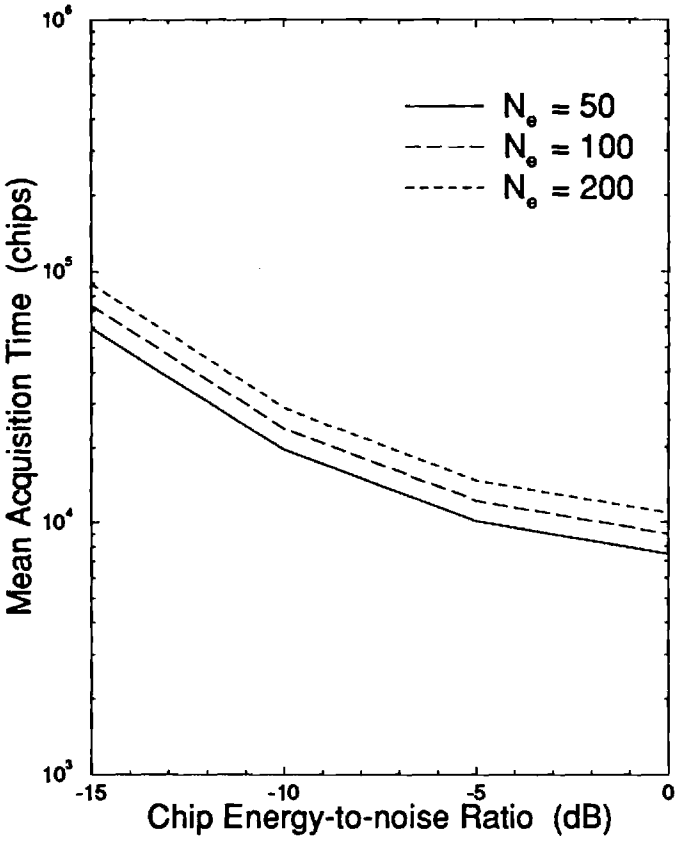

Figure 5.28: Mean acquisition time against the chip energy-to-noise ratio for various examination intervals; $m = 12$, $I = 10$.

$$
\begin{aligned}
& -\Pr[a_{0,p} = 1, a_{0,q-1} = -1 | a_{0,0} = -1, a_{0,-1} = -1] \\
= \; & \Pr[a_{0,p} = -1, a_{0,p-1} = 1] + \Pr[a_{0,p} = 1, a_{0,p-1} = -1] \\
& -\Pr[a_{0,p} = -1, a_{0,p-1} = -1] - \Pr[a_{0,p} = 1, a_{0,p-1} = 1] \\
= \; & \Pr[a_{0,p} \neq a_{0,p-1}] - \Pr[a_{0,p} = a_{0,p-1}] \\
= \; & -\Theta^0(1).
\end{aligned}
$$

Appendix 5B

$$\mathrm{E} = \mathrm{E}[a_{k,p} a_{k,q}] \;\; ; \;\; k \neq 0$$

Recall that $a_{k,i} = \tilde{a}_{k,i} d_{k,i}$, where $\{\tilde{a}_{k,i}\}$ is the Kasami spreading sequence for user k, and $\{d_{k,i}\}$ is the data sequence for user k. Then

$$\mathrm{E} \;=\; \Pr[a_{k,p} = a_{k,q}] - \Pr[a_{k,p} \neq a_{k,q}]$$

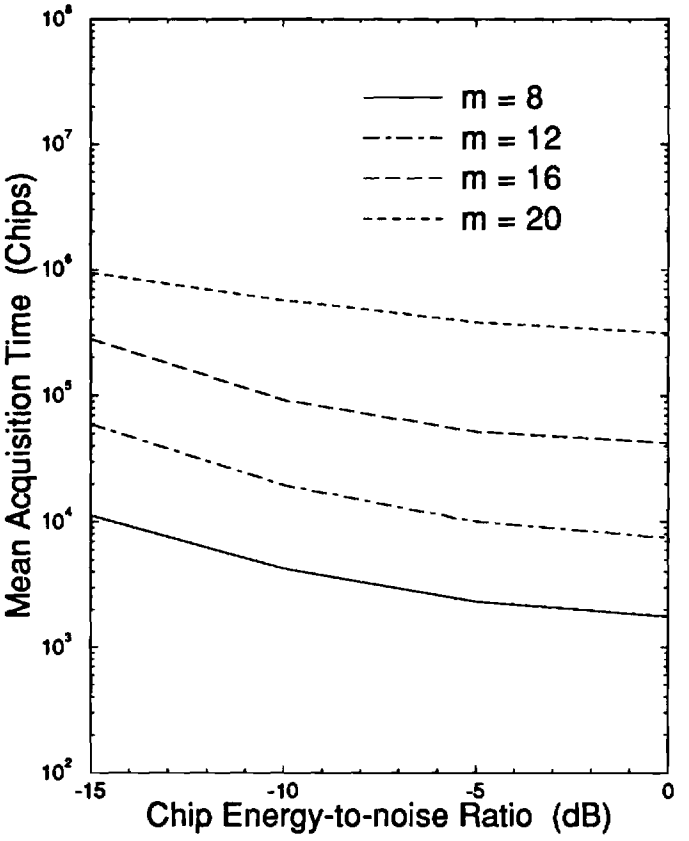

Figure 5.29: Mean acquisition time against the chip energy-to-noise ratio for various sequence lengths; $I = 10$, $\mathrm{N_e} = 50$.

$$
\begin{aligned}
= \; & \Pr[\tilde{a}_{k,p} = \tilde{a}_{k,q} | d_{k,p} = d_{k,q}] \Pr[d_{k,p} = d_{k,q}] + \Pr[\tilde{a}_{k,p} \neq \tilde{a}_{k,q} | d_{k,p} \neq d_{k,q}] \Pr[d_{k,p} \neq d_{k,q}] \\
& - \Pr[\tilde{a}_{k,p} \neq \tilde{a}_{k,q} | d_{k,p} = d_{k,q}] \Pr[d_{k,p} = d_{k,q}] - \Pr[\tilde{a}_{k,p} = \tilde{a}_{k,q} | d_{k,p} \neq d_{k,q}] \Pr[d_{k,p} \neq d_{k,q}]
\end{aligned}
$$

Since the spreading sequence and the data sequence are independent,

$$
\begin{aligned}
\mathrm{E} &= \Pr[\tilde{a}_{k,p} = \tilde{a}_{k,q}] \Pr[d_{k,p} = d_{k,q}] + \Pr[\tilde{a}_{k,p} \neq \tilde{a}_{k,q}] \Pr[d_{k,p} \neq d_{k,q}] \\
&- \Pr[\tilde{a}_{k,p} \neq \tilde{a}_{k,q}] \Pr[d_{k,p} = d_{k,q}] - \Pr[\tilde{a}_{k,p} = \tilde{a}_{k,q}] \Pr[d_{k,p} \neq d_{k,q}] \\
&= \Theta^k(v) \Pr[d_{k,p} = d_{k,q}] - \Theta^k(v) \Pr[d_{k,p} \neq d_{k,q}] \\
&= \Theta^k(v) \{ \Pr[d_{k,p} = d_{k,q}] - \Pr[d_{k,p} \neq d_{k,q}] \} \qquad \text{(5B.1)}
\end{aligned}
$$

where $v = q - p$.

Let G represent the processing gain of the system. If $G \leq v$, then at least one data bit transition occurs somewhere between chips p and q. Since the data bits are

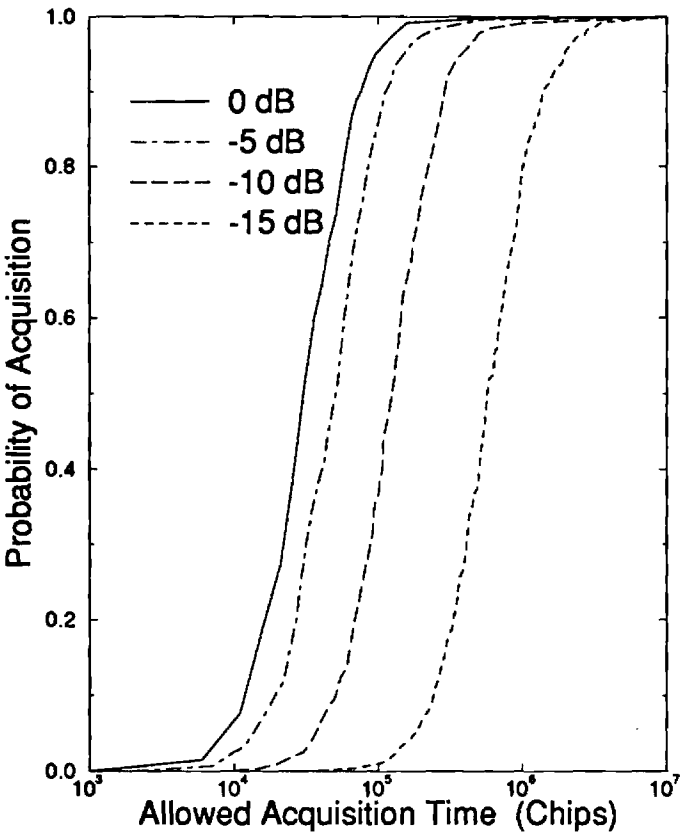

Figure 5.30: Probability of acquisition against the allowed acquistion time for various chip energy-to-noise ratiosl $I = 10$, $N_e = 50$.

independent and equi-probable

$$\Pr[d_{k,p} = d_{k,q}] = \Pr[d_{k,p} \neq d_{k,q}] = \tfrac{1}{2}$$

resulting in $E = 0$.

If $G > v$, then at most one data bit transition occurs between chips p and q. Therefore,

$$\begin{aligned} \Pr[d_{k,p} \neq d_{k,q}] &= \Pr[\text{bit transition} \bigcap \text{next bit is opposite in sign}] \\ &= \Pr[\text{bit transition}] \Pr[\text{next bit is opposite in sign}] \\ &= \frac{v}{G}\frac{1}{2} = \frac{v}{2G} \end{aligned}$$

since the bit transition can occur at the beginning of any chip during the data bit. Then, Eq. (5B.1) becomes

$$E = \Theta^k(v)\frac{G-v}{G} \quad . \tag{5B.2}$$

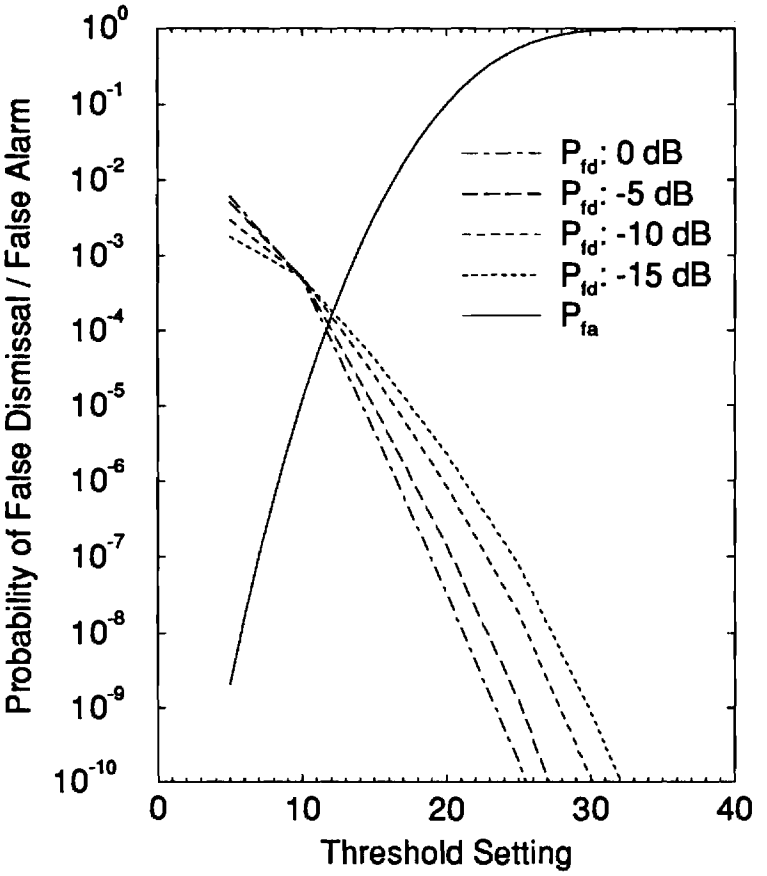

Figure 5.31: Probabilities of false dismissal and false alarm against the threshold setting for various chip energy-to-noise ratios; $I = 10$, $N_e = 50$.

Since the average value of $\Theta^k(v)$ over the ensemble of sequences is independent of v, Eq. (5B.2) becomes

$$E = \overline{\Theta}\frac{G - v}{G} \quad ,$$

where $\overline{\Theta}$ is the average out-of-phase autocorrelation tabulated in Appendix 5H.

In general, v is different for different trinomials. For short sequences, $G > v$ for most trinomials. This leads to E being a fraction of $\overline{\Theta}$. As the sequence lengths increase, more trinomials will be separated by $v > G$ leading to $E = 0$ for these trinomials and in general E getting smaller. Considering sequences of different lengths, it was concluded that $E = \frac{\overline{\Theta}}{8}$ represents a valid approximation.

Similarly, it can be shown that

$$E[a_{k,p}a_{k,q-1}] = E[a_{k,p-1}a_{k,q}] \approx E[a_{k,p-1}a_{k,q-1}] = \frac{\overline{\Theta}}{8} \quad ; \quad k \neq 0 \quad .$$

By substituting for $v = 1$ in Eq. (5B.2), it can be shown that

$$\mathrm{E}[a_{k,p}a_{k,p-1}] \approx \overline{\Theta} \;\; ; \;\; k \neq 0 \;\; .$$

Appendix 5C

$$\mathrm{E} = \mathrm{E}[a_{k,p}a_{l,q}] \;\; ; \;\; k,l = 0,1,...,I; \;\; k \neq l$$

$$\begin{aligned}
\mathrm{E} &= \Pr[a_{k,p} = a_{l,q}] - \Pr[a_{k,p} \neq a_{l,q}] \\
&= \Pr[\tilde{a}_{k,p} = \tilde{a}_{l,q} | d_{k,p} = d_{l,q}]\Pr[d_{k,p} = d_{l,q}] + \Pr[\tilde{a}_{k,p} \neq \tilde{a}_{l,q} | d_{k,p} \neq d_{l,q}]\Pr[d_{k,p} \neq d_{l,q}] \\
&\quad -\Pr[\tilde{a}_{k,p} \neq \tilde{a}_{l,q} | d_{k,p} = d_{l,q}]\Pr[d_{k,p} = d_{l,q}] - \Pr[\tilde{a}_{k,p} = \tilde{a}_{l,q} | d_{k,p} \neq d_{l,q}]\Pr[d_{k,p} \neq d_{l,q}] \\
&= \Pr[\tilde{a}_{k,p} = \tilde{a}_{l,q}]\Pr[d_{k,p} = d_{l,q}] + \Pr[\tilde{a}_{k,p} \neq \tilde{a}_{l,q}]\Pr[d_{k,p} \neq d_{l,q}] \\
&\quad -\Pr[\tilde{a}_{k,p} \neq \tilde{a}_{l,q}]\Pr[d_{k,p} = d_{l,q}] - \Pr[\tilde{a}_{k,p} = \tilde{a}_{l,q}]\Pr[d_{k,p} \neq d_{l,q}] \\
&= \Psi(v)\Pr[d_{k,p} = d_{l,q}] - \Psi(v)\Pr[d_{k,p} \neq d_{l,q}] \\
&= \Psi(v)\{\Pr[d_{k,p} = d_{l,q}] - \Pr[d_{k,p} \neq d_{l,q}]\}
\end{aligned}$$

where $\Psi(v)$ represents the cross-correlation function between any two Kasami sequence evaluated at delay v.

In this case, p and q do not necessarily represent the locations of two chips in a trinomial, because of the random bit delays. Therefore, $\tilde{a}_{k,p}$ and $\tilde{a}_{l,q}$ are any two randomly picked chips in any two sequences. Furthermore, the data bits of different users are independent and equi-probable, so that

$$\Pr[d_{k,p} = d_{l,q}] = \Pr[d_{k,p} \neq d_{l,q}] = \frac{1}{2}$$

and in turn, $\mathrm{E} = 0$.

In general,

$$\mathrm{E}[a_{k,i}a_{l,j}] = 0 \;\; ; \;\; k,l = 0,1,...,I; \;\; k \neq l$$

Appendix 5D

$$
\begin{aligned}
\sigma_1^2 &= \mathrm{E}[A_0^{p^2}A_0^{q^2} + 2\sum_{k=1}^{I} A_0^{p^2}A_k^{q^2}\cos(2\phi_0 - 2\phi_k) + \sum_{k=1}^{I} A_k^{p^2}A_k^{q^2} \\
&+ \sum_{\substack{k=1\\k\neq l}}^{I}\sum_{l=1}^{I} A_k^{p^2}A_l^{q^2}\cos(2\phi_k - 2\phi_l) + 4\sum_{k=1}^{I} A_0^{p^2}A_0^q A_k^q \cos(\phi_0 - \phi_k) \\
&+ 2\sum_{\substack{k=1\\k\neq l}}^{I}\sum_{l=1}^{I} A_0^{p^2}A_k^q A_l^q \cos(2\phi_0 - \phi_k - \phi_l) + 4\sum_{\substack{k=1\\k\neq l}}^{I}\sum_{l=1}^{I} A_0^p A_k^p A_l^{q^2}\cos(\phi_0 + \phi_k - 2\phi_l) \\
&+ 4\sum_{\substack{k=1\\k\neq l}}^{I}\sum_{l=1}^{I} A_k^{p^2}A_k^q A_l^q \cos(\phi_k - \phi_l) + 2\sum_{k=1}^{I}\sum_{\substack{l=1\\k\neq l\neq \hat{k}}}^{I}\sum_{\hat{k}=1}^{I} A_k^{p^2}A_l^q A_{\hat{k}}^q \cos(2\phi_k - \phi_l - \phi_{\hat{k}}) \\
&+ 4\sum_{k=1}^{I} A_0^p A_k^p A_k^{q^2}\cos(\phi_0 - \phi_k) + 4\sum_{k=1}^{I} A_0^p A_k^p A_0^q A_k^q \\
&+ 4\sum_{\substack{k=1\\k\neq l}}^{I}\sum_{l=1}^{I} A_0^p A_k^p A_0^q A_l^q \cos(\phi_k - \phi_l) + 8\sum_{\substack{k=1\\k\neq l}}^{I}\sum_{l=1}^{I} A_0^p A_l^p A_l^q A_k^q \cos(\phi_0 - \phi_k) \\
&+ 4\sum_{k=1}^{I}\sum_{\substack{l=1\\k\neq l\neq \hat{k}}}^{I}\sum_{\hat{k}=1}^{I} A_0^p A_k^p A_l^q A_{\hat{k}}^q \cos(\phi_0 + \phi_k - \phi_l - \phi_{\hat{k}}) + 2\sum_{\substack{k=1\\k\neq l}}^{I}\sum_{l=1}^{I} A_k^p A_l^p A_k^q A_l^q \\
&+ 4\sum_{k=1}^{I}\sum_{\substack{l=1\\k\neq l\neq \hat{k}}}^{I}\sum_{\hat{k}=1}^{I} A_k^p A_l^p A_k^q A_{\hat{k}}^q \cos(\phi_l - \phi_{\hat{k}}) + \sum_{k=1}^{I}\sum_{\substack{l=1\\k\neq l\neq \hat{k}\neq \hat{l}}}^{I}\sum_{\hat{k}=1}^{I}\sum_{\hat{l}=1}^{I} A_k^p A_l^p A_{\hat{k}}^q A_{\hat{l}}^q]
\end{aligned}
$$

Appendix 5E

$$\mathrm{E} = \mathrm{E}[a_{k,p-1}a_{k,p}a_{k,q-1}a_{k,q}] \;\; ; \;\; k \neq 0$$

Let $v+1$ be the separation between chips $p-1$ and q. If $G > v+1$, then at most one data transition occurs between chips $(p-1)$ and q. In this case, there exists two disjoint possibilities. They are

1. The data sequence does not change sign during the $(v+1)$ chips interval. This occurs with probability

$$
\begin{aligned}
\mathrm{P_d} &= \Pr[\text{no data bit transition}] \\
&\quad + \Pr[\text{data bit transition}]\Pr[\text{next bit same as previous bit}] \\
&= 1 - \frac{v+1}{G} + \frac{v+1}{G}\frac{1}{2} = 1 - \frac{v+1}{2G}
\end{aligned}
$$

In this case,

$$\begin{aligned} a_{k,p-1}a_{k,q-1} &= (\pm\tilde{a}_{k,p-1})(\pm\tilde{a}_{k,q-1}) = \tilde{a}_{k,-1} \\ a_{k,p}a_{k,q} &= (\pm\tilde{a}_{k,p})(\pm\tilde{a}_{k,q}) = \tilde{a}_{k,0} \end{aligned}$$

Hence,

$$a_{k,p-1}a_{k,p}a_{k,q-1}, a_{k,q} = \tilde{a}_{k,-1}\tilde{a}_{k,0}$$

2. The data sequence changes sign during the $(v+1)$ chips interval. This occurs with probability

$$\begin{aligned} \mathrm{P}_{\overline{\mathrm{d}}} &= \Pr[\text{data bit transition}]\Pr[\text{next bit opposite in sign to previous bit}] \\ &= \frac{v+1}{G}\frac{1}{2} = \frac{v+1}{2G}. \end{aligned}$$

In this case, the data bit transition can occur at any of three locations:

(a) At chip p with probability $\mathrm{P}_1 = \frac{1}{v+1}$, leading to

$$\begin{aligned} a_{k,p-1}a_{k,q-1} &= (\pm\tilde{a}_{k,p-1})(\mp\tilde{a}_{k,q-1}) = -\tilde{a}_{k,-1} \\ a_{k,p}a_{k,q} &= (\pm\tilde{a}_{k,p})(\pm\tilde{a}_{k,q}) = \tilde{a}_{k,0} \end{aligned}$$

Hence,

$$a_{k,p-1}a_{k,p}a_{k,q-1}, a_{k,q} = -\tilde{a}_{k,-1}\tilde{a}_{k,0}$$

(b) From chip $p+1$ to chip $q-1$ with probability $\mathrm{P}_2 = \frac{v-1}{v+1}$, leading to

$$\begin{aligned} a_{k,p-1}a_{k,q-1} &= (\pm\tilde{a}_{k,p-1})(\mp\tilde{a}_{k,q-1}) = -\tilde{a}_{k,-1} \\ a_{k,p}a_{k,q} &= (\pm\tilde{a}_{k,p})(\mp\tilde{a}_{k,q}) = -\tilde{a}_{k,0} \end{aligned}$$

Hence,

$$a_{k,p-1}a_{k,p}a_{k,q-1}, a_{k,q} = \tilde{a}_{k,-1}\tilde{a}_{k,0}$$

(c) At chip q with probability $\mathrm{P}_3 = \frac{1}{v+1}$, leading to

$$\begin{aligned} a_{k,p-1}a_{k,q-1} &= (\pm\tilde{a}_{k,p-1})(\pm\tilde{a}_{k,q-1}) = \tilde{a}_{k,-1} \\ a_{k,p}a_{k,q} &= (\pm\tilde{a}_{k,p})(\mp\tilde{a}_{k,q}) = -\tilde{a}_{k,0} \end{aligned}$$

Hence,

$$a_{k,p-1}a_{k,p}a_{k,q-1}, a_{k,q} = -\tilde{a}_{k,-1}\tilde{a}_{k,0}$$

Combining the above results gives

$$a_{k,p-1}a_{k,p}a_{k,q-1}a_{k,q} = \begin{cases} \tilde{a}_{k,-1}\tilde{a}_{k,0} & \text{with probability } \frac{G-1}{G} \\ -\tilde{a}_{k,-1}\tilde{a}_{k,0} & \text{with probability } \frac{1}{G} \end{cases}$$

Since $\frac{1}{G}$ is very small compared to $\frac{G-1}{G}$,

$$a_{k,p-1}a_{k,p}a_{k,q-1}a_{k,q} \approx \tilde{a}_{k,-1}\tilde{a}_{k,0}$$

Taking the expectation over the ensemble of spreading sequences and using the fact that the transmissions are asynchronous results in

$$\mathrm{E}[a_{k,p-1}a_{k,p}a_{k,q-1}a_{k,q}] = \overline{\Theta} \quad .$$

Now, if $G \leq v+1$, analysis similar to Appendix 5B and to the 2nd part of this Appendix leads to $\mathrm{E} \approx 0$. Hence, the approximation $\mathrm{E} = \frac{\overline{\Theta}}{8}$ applies.

Appendix 5F

$$\mathrm{E} = \mathrm{E}[a_{k,p-1}a_{k,p}a_{l,q-1}a_{l,q}] \;\; ; \;\; k,l = 0,1,...,I; \;\; k \neq l$$

Let $W = XY$, where $\mathrm{X} = a_{k,p-1}a_{l,q-1}$ and $\mathrm{Y} = a_{k,p}, a_{l,q}$. Then,

$$\begin{aligned}
\mathrm{E} &= \Pr[X=Y] - \Pr[X \neq Y] \\
&= \Pr[X=1,Y=1] + \Pr[X=-1,Y=-1] - \Pr[X=1,Y=-1] - \Pr[X=-1,Y=1] \\
&= \Pr[X=1,(d_{kl}=1,\tilde{a}_{k,p}=\tilde{a}_{l,q})] + \Pr[X=1,(d_{kl}=-1,\tilde{a}_{k,p}\neq\tilde{a}_{l,q})] \\
&\quad +\Pr[X=-1,(d_{kl}=1,\tilde{a}_{k,p}\neq\tilde{a}_{l,q})] + \Pr[X=-1,(d_{kl}=-1,\tilde{a}_{k,p}=\tilde{a}_{l,q})] \\
&\quad -\Pr[X=1,(d_{kl}=1,\tilde{a}_{k,p}\neq\tilde{a}_{l,q})] - \Pr[X=1,(d_{kl}=-1,\tilde{a}_{k,p}=\tilde{a}_{l,q})] \\
&\quad -\Pr[X=-1,(d_{kl}=1,\tilde{a}_{k,p}=\tilde{a}_{l,q})] - \Pr[X=-1,(d_{kl}=-1,\tilde{a}_{k,p}\neq\tilde{a}_{l,q})] \\
&= \frac{(A-1)}{n}\frac{1}{2}\frac{A}{n} + \frac{(D-1)}{n}\frac{1}{2}\frac{D}{n} + \frac{(D-1)}{n}\frac{1}{2}\frac{D}{n} + \frac{(A-1)}{n}\frac{1}{2}\frac{A}{n} \\
&\quad -\frac{A}{n}\frac{1}{2}\frac{D}{n} - \frac{D}{n}\frac{1}{2}\frac{A}{n} - \frac{D}{n}\frac{1}{2}\frac{A}{n} - \frac{A}{n}\frac{1}{2}\frac{D}{n} \\
&= \frac{(A-D)^2}{n^2} - \frac{A+D}{n^2} = \overline{\Psi}^2 - \frac{1}{n} \quad .
\end{aligned}$$

where A and D represent the number of agreements and disagreements between the two sequences, respectively, and $\overline{\Psi}$ represent the average cross-correlation between two Kasami sequences tabulated in Appendix 5H.

In general,

$$\mathrm{E}[a_{k,i}a_{k,j}a_{l,i}a_{l,j}] = \overline{\Psi}^2 - \frac{1}{n} \;\; ; \;\; k,l = 0,1,...,I; \;\; k \neq l$$

Appendix 5G

$$\mathrm{E} = \mathrm{E}[a_{k,p-1}a_{k,p}a_{\hat{k},q}a_{\hat{l},q}] \;\; ; \;\; k,\hat{k},\hat{l} = 0,1,...,I; k \neq \hat{k} \neq \hat{l}$$

Let $W = XY$, where X = $a_{k,p-1}a_{\hat{k},q}$ and Y = $a_{k,p}, a_{\hat{l},q}$. Then,

$$\begin{aligned}
\mathrm{E} &= \Pr[X = Y] - \Pr[X \neq Y] \\
&= \Pr[X = 1, Y = 1] + \Pr[X = -1, Y = -1] - \Pr[X = 1, Y = -1] - \Pr[X = -1, Y = 1] \\
&= \Pr[X = 1]\Pr[Y = 1] + \Pr[X = -1]\Pr[Y = -1] \\
&\quad -\Pr[X = 1]\Pr[Y = -1] - \Pr[X = -1]\Pr[Y = 1] \\
&= \Pr[X = 1]^2 + \Pr[X = -1]^2 - 2\Pr[X = 1]\Pr[X = -1] \;\; .
\end{aligned}$$

This term is the square of the expectation evaluated in Appendix 5C which is equal to 0. Hence, E = 0 .

In general,

$$\mathrm{E}[a_{k,i}a_{k,j}a_{\hat{k},\mu}a_{\hat{l},\nu}] = 0 \;\; ; \;\; k,\hat{k},\hat{l} = 0,1,...,I; \;\; k \neq \hat{k} \neq \hat{l}$$

Similarly, it can be shown that,

$$\mathrm{E}[a_{k,i}a_{l,j}a_{\hat{k},\mu}a_{\hat{l},\nu}] = 0 \;\; ; \;\; k,l,\hat{k},\hat{l} = 0,1,...,I; \;\; k \neq l \neq \hat{k} \neq \hat{l}.$$

Appendix 5H

In dealing with Kasami sequences, knowledge of the distributions of any 2 consecutive bits in every sequence was found to be essential in calculating the mean, the variance and hence the performance measures of the proposed acquisition scheme. In the following, the frequencies of such occurrences in Kasami sequences will be calculated.

The family of Kasami sequences of different lengths,$n = 2^m - 1$, are first generated and then the frequencies of occurrences of all possible 2 consecutive bits in

every sequence are counted. By doing so, it was observed that the family can be divided into five different sets. The first two of these sets correspond to the subfamily of Kasami sequences with Hamming weight $W1 = 2^{m-1} + 2^{\frac{m}{2}-1}$, while the second two sets correspond to the subfamily of Kasami sequences with Hamming weight $W2 = 2^{m-1} - 2^{\frac{m}{2}-1}$. The fifth set consists of only the long m-sequence used in generating the sequences with Hamming weight $W3 = 2^{m-1}$. The number of sequences, the 2-consecutive-bit frequencies, and $\Theta^0(1)$ for each set is shown in the Table below, where b_{ij} = number of occurrences of the 2-tuple ij in the sequence. In addition, $\overline{\Theta}$ and $\overline{\Psi}$ are given. These results were checked for all values up to $m = 16$. The probabilities $P_{i|j}$ are given by

$$P_{i|j} = \frac{b_{ij}}{\text{number of j's in the sequence}}$$

These results were checked for all values up to $m = 16$. The probabilities $P_{i|j}$ are given by $\frac{b_{ij}}{\text{number of j's in the sequence}}$.

Set No.	No. Sequences	b_{01}	b_{11}	b_{00}	b_{10}	$\Theta^0(1)$	$\overline{\Theta}$	$\overline{\Psi}$
1	$2^{\frac{m}{2}-2} - 1$	$\frac{W1}{2}$	$\frac{W1}{2}$	$n - W1 - \frac{W1}{2}$	$\frac{W1}{2}$	$\frac{n-2W1}{n}$	2^{-m}	2^{-m}
2	$2^{\frac{m}{2}-2}$	$\frac{W2}{2}$	$W1 - \frac{W2}{2}$	$n - W1 - \frac{W2}{2}$	$\frac{W2}{2}$	$\frac{n-2W2}{n}$	2^{-m}	2^{-m}
3	$2^{\frac{m}{2}-2}$	$\frac{W2}{2}$	$\frac{W2}{2}$	$n - W2 - \frac{W2}{2}$	$\frac{W2}{2}$	$\frac{n-2W2}{n}$	-2^{-m}	-2^{-m}
4	$2^{\frac{m}{2}-2}$	$\frac{W1}{2}$	$W2 - \frac{W1}{2}$	$n - W2 - \frac{W1}{2}$	$\frac{W1}{2}$	$\frac{n-2W1}{n}$	-2^{-m}	-2^{-m}
5	1	$\frac{W3}{2}$	$\frac{W3}{2}$	$\frac{W3}{2} - 1$	$\frac{W3}{2}$	$\frac{-1}{n}$	-2^{-m}	-2^{-m}

References

[1] Y. Yao and A. Sheikh, "Outage Probability Analysis for Microcell Mobile Radio Systems with Cochannel Interferers in Rician/Rayleigh Fading Enviornment," *Electronics Letters*, pp. 864–866, 1990.

[2] R. Prasad and A. Kegel, "Improved Assessment of Interference Limits in Cellular Radio Performance," *IEEE Vehicular Technology Conference*, pp. vol. 40, pp. 412–419, May 1991.

[3] S. Nanda and D. J. Goodman, *Third Generation Wireless Information Networks.* Kluwer Academic Publishers, 1992.

[4] P. Harley, "Short Distance Attenuation Measurements at 900 MHz and 1.8 GHz Using Low Antenna Heights for Microcells," *IEEE Journal on Selected Areas in Communications*, Vol. 7, pp. 5–11, January 1989.

[5] B. Eklundh, "Channel Utilization and Blocking Probability in a Cellular Mobile Telephone System with Directed Retry," *IEEE Trans. on communications*, Vol. COM-34, pp. 329–337, April 1986.

[6] H. Panzer and R. Beck, "Adaptive Resource Allocation in Metropolitan Area Cellular Mobile Radio Systems," in 40^{th} *IEEE Vehicular Technology Conference*, Orlando, FL, pp. 638–645, May 1990.

[7] D. Everitt and D. Manfield, "Performance Analysis of Cellular Mobile Communication Systems with Dynamic Channel Assignment," *IEEE Journal on Selected Areas in Communications*, Vol. 7, pp. 1172–1179, October 1989.

[8] P. Raymond, "Performance Analysis of Cellular Networks," *IEEE Transactions on Communications*, Vol. 39, pp. 1787–1793, December 1991.

[9] K. N. Sivarajan, R. J. McEliece, and J. W. Ketchum, "Dynamic Channel Assignment in Cellular Radio," in *IEEE Vehicular Technology Conference*, pp. 631–637, 1990.

[10] Y. Akaiwa, "A Conceptual Design of Microcellular Radio Communication System," in *IEEE Vehicular Technology Conference*, pp. 156–160, 1990.

[11] W. Gosling, "A Simple Mathematical Model of Co-channel and Adjacent Channel Interference in Land Mobile Radio," *IEEE Transactions on Vehicular Technology*, Vol. 28, pp. 361–364, November 1980.

[12] R. C. French, "The Effect of Fading and Shadowing on Channel Reuse in Mobile Radio," *IEEE Trans. on Vehicular Tech.*, Vol. VT-28, pp. 171–181, August 1979.

[13] R. Prasad and J. C. Arnbak, "Comments on Analysis for Spectrum Efficiency in Single Cell Trunked and Cellular Mobile Radio," *IEEE Transactions on Vehicular Technology*, Vol. 37, pp. 220–222, November 1988.

[14] R. Muammar and S. C. Gupta, "Cochannel interference in high-capacity mobile radio systems," *IEEE Trans. on communications*, Vol. COM-30, pp. 1973–1978, August 1982.

[15] G. Labedz, K. Felix, V. Lev, and D. Schaeffer, "Handover Control Issues in Very High Capacity Cellular Systems Using Small Cells," in *International Conference on Digital Land Mobile Radio Communications*, p. , 1987.

[16] K. G. Cornett and S. B. Wicker, "Bit Error Rate Estimation Techniques for Digital Land Mobile Radios," in *IEEE Vehicular Technology Conference*, pp. 543–548, 1991.

[17] E. A. Frech and C. L. Mesquida, "Cellular Models and Hand-off Criteria," in *IEEE Vehicular Technology Conference*, pp. 128–135, 1989.

[18] O. Grimlund and B. Gudmundson, "Handoff Strategies in Microcellular Systems," in *IEEE Vehicular Technology Conference*, pp. 505–510, 1991.

[19] M. Gudmundson, "Analysis of Handover Algorithms," in *1991 Vehicular Technology Conference*, pp. 537–541, 1991.

[20] A. Murase, I. C. Symington, and E. Green, "Handover Criterion for Macro and Microcellular Systems," in *IEEE Vehicular Technology Conference*, pp. 524–530, 1991.

[21] S. T. S. Chia and R. J. Warburton, "Handover Criteria For City Microcellular Systems," in *1990 Vehicular Technology Conference*, pp. 276–281, 1990.

[22] W. R. Mende, "Evaluation of a Proposed Handover Algorithm For the GSM Cellular System," in *IEEE Vehicular Technology Conference*, pp. 264–269, 1990.

[23] ETSI – European Telecommunications Standards Institute, *GSM Reccomendation 05.08.* January 1991.

[24] EIA/TIA Interim Standard, *Cellular System Dual Mode Mobile Station- Base Station Compatibility Standard.* January 1990.

[25] W. Jakes, *Microwave Mobile Communication.* John Wiley and Sons, 1974.

[26] W. Lee, *Mobile Communications Engineering.* McGraw Hill, 1982.

[27] J. G. Proakis, *Digital Communications, 2nd ed.* McGraw-Hill,Inc., 1989.

[28] Okumura, "Field Strength and its Variability in VHF and UHF Land Mobile Radio Service," *Rev. of the ECL*, Vol. 16, pp. 825–873, 1968.

[29] S. Mockford, A. M. D. Turkmani, and J. D. Parsons, "Local Mean Signal Variability in Rural Areas at 900 Mhz," in *IEEE Vehicular Technology Conference*, pp. 610–615, 1990.

[30] P. E. Mogensen, P. Eggers, C. Jensen, and J. B. Andersen, "Urban Area Radio Propagation Measurements at 955 and 1845 Mhz for Small and Micro Cells," in *IEEE Global Telecommunications Conference*, pp. 1297–1301, 1991.

[31] R. Prasad and A. Kegel, "Spectrum Efficiency of Microcellular Systems," *Electronic Letters*, pp. vol. 27, pp. 423–5, February 1991.

[32] R. Muammar, "Co-channel Interference in Microcellular Mobile Radio System," in *IEEE Vehicular Technology Conference*, pp. 198–203, 1991.

[33] R. Bultitude and G. Bedal, "Propagation Characteristics on Microcellular Urban Mobile Radio Channels at 910MHz," *IEEE Journal on Selected Areas in Communications*, Vol. SAC-7, pp. 31–39, January 1989.

[34] E. Green, "Path Loss and Signal Variability Analysis For Microcells," in *5th International Conference on Mobile Radio and Personal Communications*, pp. 38–42, 1989.

[35] U. Dersch and W. R. Braun, "A Physical Mobile Radio Channel Model," in *41st IEEE Vehicular Technology Conference*, pp. 289–294, 1991.

[36] U. Charash, "Reception through Nakagami Fading Multipath Channels with Random Delays," *IEEE Transactions on Communications*, Vol. 27, pp. 657–670, April 1979.

[37] D. C. Cox, "Cochannel Interference Considerations in Frequency Reuse Small-Coverage-Area Radio Systems," *IEEE Transactions on Communications*, Vol. 30, pp. 135–142, January 1982.

[38] Y. Yeh and S. C. Schwartz, "Outage Probability in Mobile Telephony Due to Multiple Log-Normal Interferers," *IEEE Trans. on communications*, Vol. COM-32, pp. 380–388, April 1984.

[39] R. C. French, "Error Rate Predictions and Measurements in the Mobile Radio Data Channel," *IEEE Trans. on Vehicular Tech.*, Vol. VT-27, pp. 214–220, August 1978.

[40] J.-P. M. Linnartz, "Exact Analysis of the Outage Probability in Multiple- User Mobile Radio," *IEEE Journal on Selected Areas in Communications*, pp. vol. 40, pp. 20–23, January 1992.

[41] R. Prasad and A. Kegel, "Improved Assesment of Interference Limits in Cellular Radio Performance," *IEEE Trans. on Vehicular Technology*, pp. 412–9, vol. 40, no. 2, May 1991.

[42] G. L. Stüber and L. Yiin, "Downlink Outage Predictions for Cellular Radio Systems," *IEEE Trans. on Vehicular Tech.*, Vol. 40, pp. 521–531, August 1991.

[43] J. Parsons, *The Mobile Radio Propagation Channel.* John Wiley and Sons, 1992.

[44] S. Mockford and A. M. D. Turkmani, "Penetration Loss Into Buildings at 900 Mhz," in *IEE Colloquim on Propagation Factors and Interference Modeling for Mobile Radio Systems*, pp. 1/1–1/4, 1988.

[45] E. Moriyama, T. Iwama, and T. Saruwatari, "Experimental Investigation of 1.5 GHz, 2.3 GHz, and 2.6 GHz Band Land Mobile Radio Propogation in Urban and Rural Area," in *IEEE Vehicular Technology Conference*, pp. 311–315, 1989.

[46] J. Parsons and I. M.F., "Cochannel Interference in High Capacity Mobile Radio Systems," *IEE Proc part F.*, pp. 385–391, 1983.

[47] R. Prasad and A. Kegel, "Spectrum Efficiency of Microcellular Systems," *IEEE Vehicular Technology Conference*, pp. 357–361, June 1991.

[48] A. A. Abu-Dayya and N. C. Beaulieu, "Outage Probabilities of Cellular Mobile Radio Systems with Multiple Nakagami Interfers," Tech. Rep., Queen's University, Ontario, Canada, 1990.

[49] K. Sowerby and A. G. Williamson, "Outage Probabilities in Mobile Radio Systems Suffering Cochannel Interference," *IEEE Journal on Selected Areas in Communications*, pp. 516–522, 1992.

[50] A. Safak and R. Prasad, "Effects of Correlated Shadowing Signals on Channel Reuse in Mobile Radio Systems," *IEEE Trans. on Vehicular Tech.*, Vol. VT-40, pp. 708–713, November 1991.

[51] S. C. Schwartz and Y. Yeh, "On the Distribution and Moments of Power Sums with Log-Normal Components," *Bell System Technical Journal*, Vol. 61, pp. 1441–1462, September 1982.

[52] R. Gold, "Optimum Binary Sequences for Spread-Spectrum Multiplexing," *IEEE Trans. on Information Theory*, pp. 619–621, October 1967.

[53] R. Gold, "Maximal Recursive Sequences With 3-Valued Recursive Crosscorrelation Functions," *IEEE Trans. on Information Theory*, pp. 154–156, January 1968.

[54] D. V. Sarwate and M. B. Pursley, "Applications of Coding Theory to Spread-Spectrum Multiple Access satellite Communications," in *Proc. IEEE Canadian Communications and Power Conf.*, Montreal, Canada, pp. 72 – 75, October 1976.

[55] D. V. Sarwate and M. B. Pursley, "Crosscorrelation Properties of Pseudorandom and Ralated Sequences," in *Proc. IEEE*, pp. 593 – 619, May 1980.

[56] J. J. Komo and C. C. Yuan, "Evaluation of Code Division Multiple Access Systems," in *IEEE Southeastcon*, Columbia, SC, pp. 849–853, April 1989.

[57] M. K. Simon, J. K. Omura, R. A. Scholtz, and B. K. Levitt, *Spread Spectrum Communications.* Vol. I, Computer Science Press, 1985.

[58] S. W. Golomb, *Shift Register Sequences.* Holden-Day, San Francisco, CA, 1967.

[59] N. Zierler, "Linear Reccuring Sequences," *J. Soc. Indust. Appl. Math.*, Vol. 7, pp. 31–48, March 1959.

[60] F. J. MacWilliams and N. J. Sloane, *The Theory of Error-Correcting Codes.* North-Holland Pub. Co., 1977.

[61] T. Kasami, "Weight Distribution of Bose-Chaudhuri-Hocquenghem Codes," in *Combinatorial Mathematics and its Applications*, University of North Carolina Press, Chapel Hill, NC, pp. 335–357, 1967.

[62] S. L. T. Kasami and W. Peterson, "Some Results on Cyclic Codes which Are Invariant under the Affine Group and Their Applications," *Informations and Control*, Vol. 11, pp. 475–496, 1968.

[63] V. Pless, "Power Moment Identities on Weight Distributions in Error Correcting Codes," *Informations and Control*, Vol. 6, pp. 147–152, 1963.

[64] S. L. T. Kasami, "Some Results on the Minimum Weight of Primitive BCH Codes," *IEEE Trans. on Information Theory*, Vol. 18, pp. 824–825, November 1972.

[65] N. T. T. Kasami, "Some Remarks on BCH Bounds and Minimum Weights of Binary Primitive BCH Codes," *IEEE Trans. on Information Theory*, Vol. 15, pp. 408–413, May 1969.

[66] M. J. Bouvier, Jr., "Spread Spectrum Acquisition Strategies," in *IEEE International conference on Communications*, Denver,CO, pp. 76.6.1–76.6.5, June 1981.

[67] A. Polydoros and C. Weber, "A Unified Approach to Serial Search Spread Spectrum Code Acquisition-Part II: A Matched Filter Receiver," *IEEE Trans. on communications*, Vol. 32, pp. 542–549, May 1984.

[68] G. F. Sage, "Serial Synchronization of Pseudonoise Systems," *IEEE Trans. on communications*, Vol. 12, pp. 123–127, December 1964.

[69] R. B. Ward, "Acquisition of Pseudonoise Signals by Sequential Estimation," *IEEE Transactions on Communication Technology*, Vol. 13, pp. 475–483, December 1965.

[70] R. B. Ward and K. P. Yiu, "Acquisition of Pseudonoise Signals by Recursion-Aided Sequential Estimation," *IEEE Trans. on communications*, Vol. 25, pp. 784–794, August 1977.

[71] H. M. Pearce and M. P. Ristenbatt, "The Threshold Decoding Estimator for Synchronization with Binary Linear Recursive Sequences," in *IEEE International conference on Communications*, Montreal, Canada, pp. 43.26–43.30, June 1971.

[72] C. C. Kilgus, "Pseudonoise Acquisition Using Majority Logic Decoding," *IEEE Trans. on communications*, Vol. 21, pp. 772–774, June 1973.

[73] G. L. Stüber and I. F. Blake, "Sequence Acquisition Using Bit Estimation Techniques," *Information Sciences*, Vol. 32, pp. 217–229, 1984.

[74] D. A. Wright and L. B. Milstein, "Energy Retentive Rapid Acquisition Techniques for Direct Sequence Spread Spectrum," in *IEEE Global Telecommunications Conference*, New Orleans, LA, pp. 16.2.1–16.2.6, December 1985.

[75] M. B. Pursley, "The Role of Spread-Spectrum in Packet Radio Network," in *Proceedings IEEE*, pp. 116 – 134, January 1987.

[76] G. Stüber, "Personal and Mobile Radio," Final Report for BellSouth Ent. E21-H03, Georgia Tech, June 1992.

[77] I. F. Blake and J. W. Mark, "Code Division for Spread Spectrum Multiple Access," Final Report for WRI Project No. 808-01-04, University of Waterloo, March 1982.

[78] J. K. Omura and T. Kailath, "Some Useful Probability Distributions," Technical report No. 7050-6, Stanford University, September 1965.